

**University of Alberta**

**DESIGN OF NEW FLUORESCENT REPORTERS FOR  
LIVE CELL IMAGING**

by

Carine Lafaille



A thesis submitted to the Faculty of Graduate Studies and Research  
in partial fulfillment of the requirements for the degree of

Master of Science

Department of Chemistry

Edmonton, Alberta

Fall 2007



Library and  
Archives Canada

Bibliothèque et  
Archives Canada

Published Heritage  
Branch

Direction du  
Patrimoine de l'édition

395 Wellington Street  
Ottawa ON K1A 0N4  
Canada

395, rue Wellington  
Ottawa ON K1A 0N4  
Canada

*Your file* *Votre référence*  
*ISBN: 978-0-494-33290-0*  
*Our file* *Notre référence*  
*ISBN: 978-0-494-33290-0*

**NOTICE:**

The author has granted a non-exclusive license allowing Library and Archives Canada to reproduce, publish, archive, preserve, conserve, communicate to the public by telecommunication or on the Internet, loan, distribute and sell theses worldwide, for commercial or non-commercial purposes, in microform, paper, electronic and/or any other formats.

The author retains copyright ownership and moral rights in this thesis. Neither the thesis nor substantial extracts from it may be printed or otherwise reproduced without the author's permission.

**AVIS:**

L'auteur a accordé une licence non exclusive permettant à la Bibliothèque et Archives Canada de reproduire, publier, archiver, sauvegarder, conserver, transmettre au public par télécommunication ou par l'Internet, prêter, distribuer et vendre des thèses partout dans le monde, à des fins commerciales ou autres, sur support microforme, papier, électronique et/ou autres formats.

L'auteur conserve la propriété du droit d'auteur et des droits moraux qui protègent cette thèse. Ni la thèse ni des extraits substantiels de celle-ci ne doivent être imprimés ou autrement reproduits sans son autorisation.

---

In compliance with the Canadian Privacy Act some supporting forms may have been removed from this thesis.

Conformément à la loi canadienne sur la protection de la vie privée, quelques formulaires secondaires ont été enlevés de cette thèse.

While these forms may be included in the document page count, their removal does not represent any loss of content from the thesis.

Bien que ces formulaires aient inclus dans la pagination, il n'y aura aucun contenu manquant.

  
**Canada**

If we knew what it was we were doing, it would not be called research, would it?

*Albert Einstein*

## ABSTRACT

Recently, live cell imaging with fluorescent probes has emerged as a powerful technique in molecular and cell biology. Here we describe progress towards the development of two new fluorescence-based probes. First, a fluorescent reagent for localization of the mitotic checkpoint protein hBub1 was developed. A single chain variable fragment antibody (ScFv) against hBub1 was constructed starting from a hybridoma. Sequencing of the construct enabled positive identification of the antibody chain types. Unfortunately, the antibody appeared deleterious to HeLa cells as shown by an expression timeline. Second, a new bioorthogonal protein labelling system based on the covalent modification of the glutamic acid 166 to asparagine mutant of a TEM1  $\beta$ -lactamase, with  $\beta$ -lactam substrates, was developed. Bacterial cell expression, purification and refolding of the mutant protein yielded an active protein. Labelling of the mutant protein with Bocillin FL was demonstrated in vitro but attempted labelling of cell-surface displayed protein was found unsuccessful.

## **ACKNOWLEDGEMENTS**

I am deeply grateful to my supervisor, Dr. Robert Campbell, for his invaluable guidance and advices throughout my graduate studies. I wish to thank all the members of the Campbell group for their support and sharing of experience and knowledge.

I am forever grateful to my friends, Mickael De Oliveira Neves for helping me through preparatory classes, Sonia Brun, my ENSCM “binôme”, and all the “Montpellierfiotes” for making my years at the ENSCM an unforgettable and rewarding experience. I am grateful to Evelyn McClure for her moral support and patience and to everyone who participated in making my studying in Canada an extraordinary experience.

I also thank my brothers, Guy and Thomas, for putting up with me. Finally I owe the most thanks to my parents for their constant support and encouragements throughout the years.

# TABLE OF CONTENTS

CHAPTER 1: INTRODUCTION.....	1
1.1    FLUORESCENCE IMAGING OF CELLS .....	2
1.1.1    Fixed cells imaging.....	3
1.1.2    Genetically encoded labels for live cell imaging.....	5
1.1.3    Bioorthogonal chemical labelling.....	7
1.1.4    Beta-lactamase as a catalytic reporter .....	10
1.2    FLUORESCENCE MICROSCOPY .....	13
1.2.1    Introduction .....	13
1.2.2    Epi-fluorescence .....	15
1.2.3    Confocal microscopy.....	17
1.3    OBJECTIVE OF THE THESIS .....	18
CHAPTER 2: CONSTRUCTION OF A SINGLE CHAIN VARIABLE FRAGMENT FOR DETECTION OF HBUB1 .....	19
2.1    INTRODUCTION.....	20
2.2    MATERIAL AND METHODS .....	24
2.2.1    General procedures and materials.....	24
2.2.2    Anti-hBub1 ScFv gene design.....	26
2.2.3    Construction of anti-hBub1 ScFv bacterial and mammalian expression vectors ..	27
2.2.4    Anti-hBub1 ScFv modelization.....	28
2.2.5    Protein expression and purification .....	28
2.2.6    ScFv-anti-hBub1 and hBub1 expression and imaging in HeLa cells .....	29

2.3	RESULTS AND DISCUSSION.....	30
2.3.1	anti-hBub1 ScFv gene design.....	30
2.3.2	Construction of anti-hBub1 ScFv bacterial and mammalian expression vectors ..	32
2.3.3	Characterization of anti-hBub1 ScFv .....	35
2.3.4	Expression and purification of ScFv-anti hBub1.....	37
2.3.5	Expression of ECFP- anti-hBub1 ScFv ± NLS and EYFP-hBub1 in mammalian cells	39
2.4	DISCUSSION AND CONCLUSIONS .....	42
CHAPTER 3: DESIGN OF A BETA-LACTAMASE BASED LABELLING SYSTEM.....		43
3.1	INTRODUCTION.....	44
3.2	MATERIAL AND METHODS .....	48
3.2.1	General material and methods .....	48
3.2.2	Cloning and site-directed mutagenesis of TEM1 beta-lactamase.....	48
3.2.3	Expression, purification and mass spectrometry characterization of WT and mutant $\beta$ -lactamases .....	49
3.2.4	Preliminary kinetic characterization of WT and E166N $\beta$ -lactamases.....	51
3.2.5	Characterization of the binding of E166N $\beta$ -lactamase to $\beta$ -lactam substrates.....	52
3.2.6	Expression and display of $\beta$ -lactamase on HeLa cell surface.....	54
3.2.7	Labelling of HeLa cells with Bocillin FL.....	54
3.3	RESULTS.....	55
3.3.1	Cloning and site-directed mutagenesis of TEM1 beta-lactamase.....	55
3.3.2	Expression, purification and mass spectrometry characterization of WT and mutant $\beta$ -lactamases .....	57

3.3.3	Preliminary kinetic characterization of WT and E166N $\beta$ -lactamases.....	59
3.3.4	Characterization of the binding of E166N $\beta$ -lactamase to $\beta$ -lactam substrates by gel displacement assay .....	64
3.3.5	Characterization of the binding of E166N $\beta$ -lactamase to $\beta$ -lactam substrates by Ni-NTA fast purification of the reacted enzyme .....	66
3.3.6	Expression and display of $\beta$ -lactamase on HeLa cell membrane .....	67
3.3.7	Tentative labelling of HeLa cells with Bocillin FL .....	69
3.4	DISCUSSION AND CONCLUSIONS .....	70
CHAPTER 4: CONCLUSIONS AND FUTURE DIRECTIONS .....		73
4.1	SCFV FOR DETECTION OF HBUB1 .....	74
4.2	$\beta$ -LACTAMASE BASED LABELLING STRATEGY .....	75
BIBLIOGRAPHY .....		77
APPENDIX A : THEORETICAL TREATMENT OF ENZYME KINETICS .....		89
A.1	RATE EQUATION FOR A SIMPLE ENZYME MECHANISM .....	90
A.2	IRREVERSIBLE INACTIVATION OF THE MUTANT $\beta$ -LACTAMASE.....	92
APPENDIX B : PRIMERS FOR HEAVY AND LIGHT CHAIN AMPLIFICATION AND CLONING .....		94
APPENDIX C : MALDI AND ESI MASS SPECTRA OF WT AND E166N BETA-LACTAMASE.....		100



## LIST OF TABLES

<b>Table 1</b>	Protein concentrations and total protein after refolding .....	58
<b>Table 2</b>	Kinetic parameters for interaction between WT $\beta$ -lactamase and CENTA or nitrocefin .....	62
<b>Table 3</b>	Kinetic parameters for interaction between E166N $\beta$ -lactamase and CENTA.. ..	63

## LIST OF FIGURES

<b>Figure 1</b>	Strategies for labelling of proteins of interest (POI) in cells.....	3
<b>Figure 2</b>	Schematic representation of a genetically encoded FP label for live cell imaging .....	6
<b>Figure 3</b>	Labelling of a fusion protein containing the tetracysteine motif with biarsenical compounds.....	9
<b>Figure 4</b>	$\beta$ -lactamase based catalytic reporter system .....	10
<b>Figure 5</b>	General catalytic pathway of active-site serine $\beta$ -lactamase.....	11
<b>Figure 6</b>	General mechanism of hydrolysis of $\beta$ -lactams with $\beta$ -lactamase .....	12
<b>Figure 7</b>	Jablonski energy diagram and excitation and emission spectral profiles.....	14
<b>Figure 8</b>	Fluorescence microscope set up and fluorescence filter spectral profiles.....	15
<b>Figure 9</b>	Diagram of an inverted epi-fluorescence microscope .....	16
<b>Figure 10</b>	Diagram of a confocal fluorescent microscope. ....	17
<b>Figure 11</b>	Schematic picture describing a full length antibody and various recombinant formats .....	22
<b>Figure 12</b>	Effect of linker length on ScFv structure.....	23
<b>Figure 13</b>	Flow chart of the formation of the anti-hBub1 ScFv.....	31
<b>Figure 14</b>	Fluorescence screening of the starting, intermediate and final constructs of the ScFv-Anti hBub1 into pBAD436.....	32
<b>Figure 15</b>	Xho1 digestion pattern of pECFP-Nuc with inserted anti-hBub1 ScFv.....	34
<b>Figure 16</b>	Nucleotides and deduced amino acid sequences of anti-hBub1 ScFv.....	36

<b>Figure 17</b> Three dimensional predicted structure of anti-hBub1 ScFv.....	37
<b>Figure 18</b> SDS-PAGE and Western Blot of anti-hBub1 ScFv purified by Ni-NTA chromatography .....	38
<b>Figure 19</b> Effect of overexpression of ECFP in HeLa cell nucleus on FRET measurements.....	40
<b>Figure 20</b> Pictures of mCherry-PDGFR-TM and ECFP-ScFv expressing HeLa cells ...	41
<b>Figure 21</b> Acyl-enzyme intermediate of TEM1 $\beta$ -lactamase .....	44
<b>Figure 22</b> Structure of the $\beta$ -lactamase substrates used and of their hydrolysis products.. .....	46
<b>Figure 23</b> Ligation of ketones with hydrazides.....	47
<b>Figure 24</b> Flow Chart of the QuickChange® method.....	55
<b>Figure 25</b> Alignment of TEM1 $\beta$ -lactamase, WT $\beta$ -lactamase, and E166N $\beta$ -lactamase sequences .....	56
<b>Figure 26</b> E166N $\beta$ -lactamase purification.....	58
<b>Figure 27</b> Hydrolysis of nitrocefin.....	59
<b>Figure 28</b> Kinetics of nitrocefin hydrolysis with WT $\beta$ -lactamase .....	60
<b>Figure 29</b> Kinetics of CENTA hydrolysis with WT and E166N $\beta$ -lactamase.....	61
<b>Figure 30</b> Michaelis-Menten plot for WT $\beta$ -lactamase .....	62
<b>Figure 31</b> Comparison of CENTA hydrolysis by WT and E166N $\beta$ -lactamases.....	64
<b>Figure 32</b> Gel displacement assay of $\beta$ -lactamase with Bocillin FL. ....	65
<b>Figure 33</b> Relative fluorescence of Bocillin FL-reacted $\beta$ -lactamases purified with Ni-NTA .....	66

<b>Figure 34</b> HeLa cells transfected with pDisplay-mCherry .....	68
<b>Figure 35</b> HeLa cells displaying membrane-anchored mCherry, WT $\beta$ -lactamase and E166N $\beta$ -lactamase.....	69
<b>Figure 36</b> Interaction between a serine $\beta$ -lactamase and a substrate .....	90
<b>Figure 37</b> Scheme of irreversible inactivation of a mutant enzyme by a substrate .....	92
<b>Figure 38</b> Scheme of reversible inactivation of a mutant enzyme with a substrate.....	93

## LIST OF ABBREVIATIONS

Ab	Antibody
AGT	O <sup>6</sup> -alkylguanine-DNA-alkyltransferase
bp	Base pairs
BiFC	Bimolecular fluorescence complementation
cDNA	Complementary DNA - DNA synthesized from a mature mRNA template
CDR	Complementary determining region
CFP	Cyan fluorescent protein
C <sub>H</sub> /C <sub>L</sub>	Heavy/light domain of the constant region of an antibody
CIAP	Calf intestinal alkaline phosphatase
DMEM	Dulbecco's modified Eagle's medium
DMSO	Dimethyl sulfoxide
DNA	Deoxyribonucleic acid
dsFv	Disulfide-stabilized variable fragment
DTT	Dithiothreitol, strong reducing agent
E166N	Glutamic acid 166 to asparagine mutant (also Glu166Asn)
<i>E. Coli</i>	Escherichia coli
ECFP	Enhanced cyan fluorescent protein
ELISA	Enzyme-linked immunosorbent assay
ESI	Electrospray ionization

ER	Endoplasmic Reticulum, cell component
EYFP	Enhanced yellow fluorescent protein
Fab	Fragment antigen binding, region of an antibody
Fc	Fragment crystallisable region, constant region of an antibody
FLIP	Fluorescence loss in photobleaching
FP	Fluorescent protein
FRAP	Fluorescence recovery after photobleaching
FRET	Förster (or fluorescence) resonance energy transfer
Fv	Variable fragment of an antibody
GFP	Green fluorescent protein
HA	Hemagglutinin A epitope tag
HBSS	Hanks balanced salt solution containing no calcium chloride, magnesium chloride, magnesium sulfate nor Phenol Red
hBub1	Human budding uninhibited by benzimidazoles 1
HeLa	Immortal cell line derived from Henrietta Lacks cervical cancer cells
Ig	Immunoglobulin
IPTG	Isopropyl $\beta$ -D-1-thiogalactopyranoside
LB	Luria-Bertini media
mAb	Monoclonal antibody
MALDI	Matrix-assisted laser desorption/ionization
Ni-NTA	Ni <sup>2+</sup> -nitrilotriacetate

NLS	Nuclear localization sequence
OD	Optical density
PBS	Phosphate buffered saline buffer
PCR	Polymerase chain reaction
PDGFR-TM	Platelet-derived growth factor receptor transmembrane domain
PVDF	Polyvinylidene difluoride membrane
TTBS	0.1% Tween20 Tris-buffered saline buffer
RNA/mRNA	Ribonucleic acid/messenger ribonucleic acid
rpm	Revolutions per minute
ScFv	Single chain variable fragment
SDS	Sodium dodecyl sulfate
SDS-PAGE	Sodium dodecyl sulfate polyacrylamide gel electrophoresis
TOF	Time of flight
UV	Ultraviolet light
V <sub>H</sub>	Heavy chain of an antibody variable domain
V <sub>L</sub>	Light chain of an antibody variable domain
WT	Wild-type protein
YFP	Yellow fluorescent protein

**CHAPTER 1:**  
**INTRODUCTION**



Over the last decade, the direct visualization and quantification of biological molecules and activities in live cells has emerged as the single most powerful strategy for investigation of complex cellular processes. Accordingly, the ability to track, both spatially and temporally, biomolecules in live cells has become an essential and widespread analytical tool used in cell biology and biomedical sciences. In particular, fluorescent probes are powerful tools for real-time live cell imaging. An ideal fluorescent probe should demonstrate high sensitivity and flexibility while perturbing the cell as little as possible.

An overview of the various classes of fluorescent probes currently used for cell imaging will be presented in the following sections. These classes of probes include: labelled antibodies (immunolabels); small organic fluorescent dyes; fluorescent proteins; bioorthogonal chemical labelling systems; and catalytic reporters. The characteristics, advantages and limitations of these probes in fixed or live cell imaging will be highlighted. Furthermore, live cell fluorescence imaging relies as much on the development of fluorescent probes as on fluorescent microscopy techniques, and so the instrumentation currently used will also be introduced.

## **1.1 FLUORESCENCE IMAGING OF CELLS**

Fluorescence has long been a method of choice for the visualization of specific molecules, cells, tissues, or organisms in cell biology. Initially, small organic dyes attached to antibodies were used for fluorescent detection and imaging of a protein of interest [1] (Figure 1A). Fluorophores directly targeting nucleic acids, organelles and ions in live cells are also widely used. However, in the past decade the majority of the new approaches to imaging in live cells and in organisms have been based on fluorescent proteins (FPs) such as the *Aequorea* green FP (GFP) [2, 3] (Figure 1B). A recent and exciting development in live cell imaging is the specific and covalent labelling of fusion proteins with fluorophores [4] using hybrid systems (Figure 1C, Figure 1D).

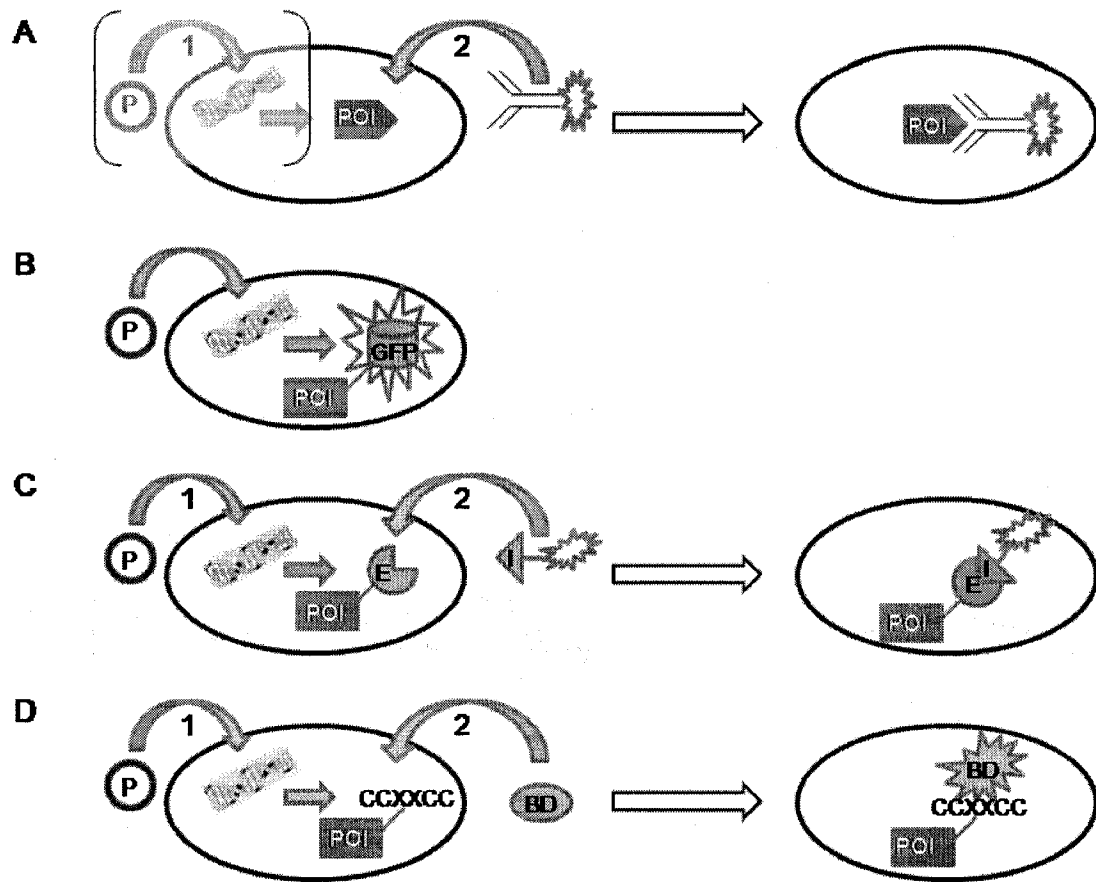


**Figure 1** Strategies for labelling of proteins of interest (POI) in cells. *A.* Immunolabelling, with a dye conjugated antibody, of the endogenous POI (2), or of the genetically tagged POI (1 & 2). *B.* Direct genetic labelling of the POI by fusion to GFP. *C.* Creation of an enzyme (E) fusion protein (1) and covalent labelling (2) with a dye conjugated inhibitor (I). *D.* Creation of a fusion protein displaying a tetracysteine motif (CCXXCC) (1) and labelling with a biarsenical dye (BD) (2). P: plasmid.

### 1.1.1 Fixed cells imaging

Today, fixed cell imaging is widely used for imaging of endogenous proteins and is done without previous genetic modification of the cell. Fixed cells are mostly imaged with labelled antibodies or small organic dyes.

Immunolabelling is the most common technique for fluorescent detection of endogenous proteins and is usually performed with a primary antibody followed by signal amplification with a secondary antibody conjugated to a small organic dye [2]. It is also possible to use a primary antibody directly conjugated to a fluorophore.

Antibodies, either polyclonal or monoclonal, are useful tools in the detection of epitopes of various sizes. Polyclonal antiserum from an animal can be highly sensitive but contains a heterogeneous population of antibodies, difficult to reproduce in subsequent immunization. This problem was overcome in 1975, with the first system for production of a unique monoclonal antibody [5]. Hybridomas resulting from the fusion of an antibody secreting plasma cell with a myeloma cell generate the desired monoclonal antibody in large quantity. For immunolabelling, the availability of a high-quality and specific antibody against the target epitope is fundamental to accurate detection. Antibodies recognizing virtually any epitope can be produced, and therefore can be relevant to the detection of a variety of biomolecules [6]. However, in the case where such an antibody is not directly available, use of a recombinantly expressed epitope tag such as a His-tag or Hemagglutinin A [7] is valuable, although the detected protein is then no longer endogenous (Figure 1A).

An apparent drawback of antibody targeting of intracellular proteins is that it requires cell fixation to stabilize and immobilize cellular antigens and permeabilization to make the interior of the cell accessible to the antibodies. These treatments necessitate cell death and thus valuable information regarding the spatiotemporal dynamics of proteins is not experimentally accessible with immunolabeling. The size of the fluorophore-antibody complex, usually more than 200kDa, and the possible oligomerization of the target protein due to antibodies multivalency are other shortcomings of immunofluorescence.

For immunolabelling, the antibodies are chemically conjugated to a variety of dyes [1]. Hundreds of small organic fluorophores covering the visible through near-infrared spectrum, used for conjugation to antibodies or not, are commercially available [8]. Generally, those small organic dyes have a better access to intracellular and extravascular compartments, but lack any specificity of their own for a particular biomolecule and thus usually need to be targeted (i.e. by conjugation to an antibody).

Nevertheless, some fluorophores can directly target nucleic acids, organelles and ions in living cells, such as the nuclear and chromosome counterstain DAPI [9]. Such dyes can covalently bind to macromolecules and can be used either in fixed or live cells. Furthermore, many organic fluorescent dyes present the additional advantage of being

very sensitive to their environment and being able to change their fluorescent characteristics upon binding. For example,  $\text{Ca}^{2+}$  indicators such as Fura-2 [10] can increase their fluorescence up to 40-fold when binding to calcium [11].

The immunolabeling approach to imaging of intracellular protein localization is extremely useful and widespread, but is not without its limitations. Most importantly, spatiotemporal information is not experimentally accessible. That is, a timelapse movie of a fixed cell contains no more biological information than a single snapshot. Moreover, these labels usually yield nonspecific background signals due to a common characteristic, the presence of fluorescence whether bound or not to the intended target. These limitations have given rise to efforts to develop alternative non-invasive and site specific protein labelling in living cells.

### **1.1.2 Genetically encoded labels for live cell imaging**

Whereas fixed cell imaging is limited to static information, live cell imaging enables access to the time dimension. Live cell imaging is widely performed through the use of genetically encoded labels such as FPs, which enable visualisation of cellular events and tracking of proteins in their normal environment (Figure 1B). The development of such fluorescent reporters relied on the advances in molecular biology and especially in recombinant DNA technology.

Although it was first discovered in 1962 [12], it has only been since the cloning of its gene in 1992 [13] that the green FP (GFP) from the jellyfish *Aequorea Victoria*, has emerged as a well established and widely used genetically encoded label. Visible fluorescence is observed when the gene encoding GFP is expressed either alone or in fusion to a gene encoding a protein of interest (Figure 2). In the past decade, extensive engineering of FPs, with particular emphasis on GFP, into mutants with improved properties (decreased oligomerization, increased brightness, better folding efficiency, greater photostability, etc.) [14] and diversified spectra has provided a wide variety of tools for non-invasive imaging in living cells and organisms [2, 3].

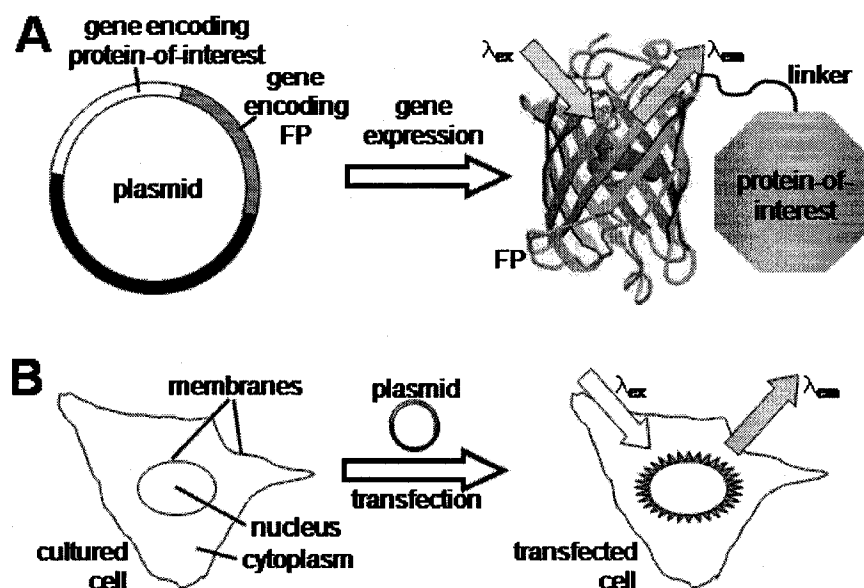


**Figure 2** Schematic representation of a genetically encoded FP label for live cell imaging. *A.* The plasmid containing the FP gene in frame with the protein-of-interest gene allows expression of the FP-fusion protein. *B.* Transfection of the plasmid in mammalian cells enables live cell labelling. [Image credit: Robert E. Campbell]

In parallel with the development of improved FPs has come the development of a wide variety of techniques by which FPs can be employed for imaging of molecular dynamics and interactions in living cells. For example, FPs are used for imaging of protein trafficking and diffusion with techniques including fluorescence loss in photobleaching (FLIP), fluorescence recovery after photobleaching (FRAP), and FP photoactivation. This latter technique relies on one of a number of recently developed ‘photoswitchable’ FPs in which a non-fluorescent FP is switched to a fluorescent FP with UV light [2, 15]. To study molecular interactions in living cells, Förster (or fluorescence) resonance energy transfer (FRET) [16] and bimolecular fluorescence complementation (BiFC) [17] are commonly employed methods.

Genetic fusion of a FP to a protein of interest presents some key advantages relative to the use of simple organic dye fluorophores. In particular, precise targeting to subcellular compartment is possible with FPs but not with organic dyes. In addition, response to a great variety of events or signals can be detected using designed FP-based sensors.

Finally, transfection and transgenic techniques make for easy exogenous DNA delivery to cells or organisms (Figure 2B) and photodynamic toxicity is rarely caused.

Despite extensive protein engineering [14, 18], FPs face limitations as sensors for biological processes, such as the restriction to the fluorescence as the only useful property, their limited spectral range, the noticeable absence of near-infrared FPs [14], and the need of oxygen for the formation of the chromophore [19, 20]. An important limitation of FPs relative to small molecule dye fluorophores is their relatively large size (~27 kDa for a monomer) which may perturb the normal function and/or localization of the protein of interest [21, 22]. Another concern is the non-physiological concentrations of the overexpressed fusion protein compared to its native copies. Finally, FPs only allow tagging of proteins and are of no use for the imaging of other classes of biomolecules such as nucleic acids, lipids, glycans and secondary metabolites.

Although fluorescent fusion proteins are extremely useful for live cell imaging, smaller probes with faster rates of labelling and ability to be imaged through fluorescence or another property are highly desirable. Alternative labelling technologies may be able to overcome some of the limitations of FPs without sacrificing the advantages.

### **1.1.3 Bioorthogonal chemical labelling**

In recent years, hybrid systems combining the abilities and convenience of genetically encoded labels and the flexibility of small molecule labels have been developed [23]. In these systems, synthetic probes such as organic fluorophores are covalently targeted to genetically specified proteins (Figure 1C and Figure 1D). These methods have enabled several interesting live cell imaging applications including determination of protein age, visualization of protein synthesis and turnover [24, 25], and rapid chromophore-assisted light inactivation of selected proteins [26, 27], both inside and on the surface of living cells [4, 28, 29].

This approach allows proteins to be equipped with properties that cannot be genetically encoded and may also enable the use of a single fusion protein for studying a variety of

the protein's properties due to the wide selection of small labels. To be practical, the labelling reaction must be both broadly applicable, allowing the attachment of chemically diverse compounds, and highly specific, allowing for labelling to take place both *in vitro* and *in vivo*. Furthermore, modification of the probe must be possible and should not affect its reactivity towards the tag, enabling binding of a large variety of molecules [29]. *In vivo* site-specific protein labelling is performed by genetically fusing a protein of interest with either a protein or peptide tag that will undergo a specific reaction with a small molecule probe. The small molecule probe consisting of a cell-permeable, non-toxic tag-binding compound coupled to a fluorophore or other functional group is added to live cells. The probe enters the cells and covalently binds to the tag fusion.

*In vivo* chemical labelling of proteins usually relies on fusion of either a peptide sequence or a protein sequence to the protein of interest. Currently used approaches include intein-based labelling, modification of the tag by a third protein, reversible and specific binding, and irreversible and specific covalent modification [4, 29, 30].

The prototypical system for small molecule labelling of a protein using a peptide targeting sequence is the biarsenical-tetracysteine system (Figure 1D). In this system, a small tetracysteine tag, such as CCPGCC, is genetically fused to the protein of interest and site specifically labelled with a membrane-permeable biarsenical dye [31, 32] (Figure 3). Blue xanthone derivative (CHoXAsH), green fluorescein derivative (FlAsH), red rhodamine derivative (ReAsH) and Nile Red biarsenical derivatives are currently available [33, 34].

The biarsenical-tetracysteine technique presents the advantages of a small size tag, the ability to give electron microscopy as well as fluorescence images, a dramatic increase in fluorescence upon binding and the stability of the biarsenical-tetracysteine complex. However, to minimize arsenic acute toxicity to the cells and to decrease non-specific binding by outcompeting endogenous cysteine-rich proteins, dithiol antidotes such as 1,2-ethanedithiol (EDT) have to be added [31]. Other limitations of the system include the necessity for the tetracysteines to be in their reduced form, and the presence of a background staining. Finally, since the tetracysteine motif binds directly to the

fluorophore, the development of chemically diverse biarsenical probes may be challenging.

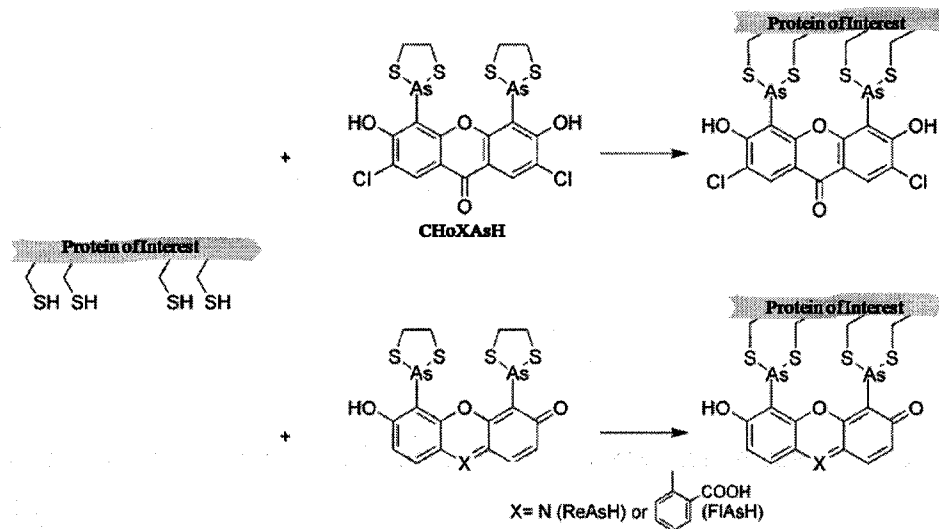


**Figure 3** Labelling of a fusion protein containing the tetracysteine motif with biarsenical compounds. Reaction with 3 different biarsenical reagents, CHoXAsH, ReAsH and FIAsH, is presented.

In the case of small molecule labelling using a protein targeting sequence, an enzyme-substrate or enzyme-inhibitor combination is usually used. For an enzyme-inhibitor combination, a synthetic inhibitor-fluorophore labelling reagent must be designed and synthesized. The label will thus be covalently coupled to the fusion protein through the enzyme-inhibitor reaction (Figure 1C), provided that the fluorophore does not interfere with the labelling reaction. It is also possible to employ a protein-label combination if the product of the normal specific reaction is a stable protein-small-molecule adduct [23]. For example, the labelling of O<sup>6</sup>-alkylguanine-DNA alkyltransferase (AGT) fusion proteins relies on the irreversible alkylation of a cysteine of AGT with O<sup>6</sup>-benzylguanine derivatives [35].

While FPs and the above mentioned hybrid systems allow for the labelling of proteins and imaging of their intracellular localization, they do not provide any signal amplification. The lack of signal amplification limits the sensitivity of these molecules when used as reporters of gene expression. Fortunately, alternative hybrid systems for



detection of small numbers (i.e. dozens to hundreds) of protein molecules in live cells have been developed and one of these will be described in the next section.

#### 1.1.4 Beta-lactamase as a catalytic reporter

Catalytic reporters, which define another class of imaging tools, rely on the expression of a recombinant enzyme and the addition of an exogenous substrate. Traditionally, several such catalytic reporters have been used, including  $\beta$ -galactosidase [36] and chloramphenicol acetyltransferase [37]. In recent years a new enzyme,  $\beta$ -lactamase, has emerged as the preferred catalytic reporter due to its great versatility [38] (Figure 4).

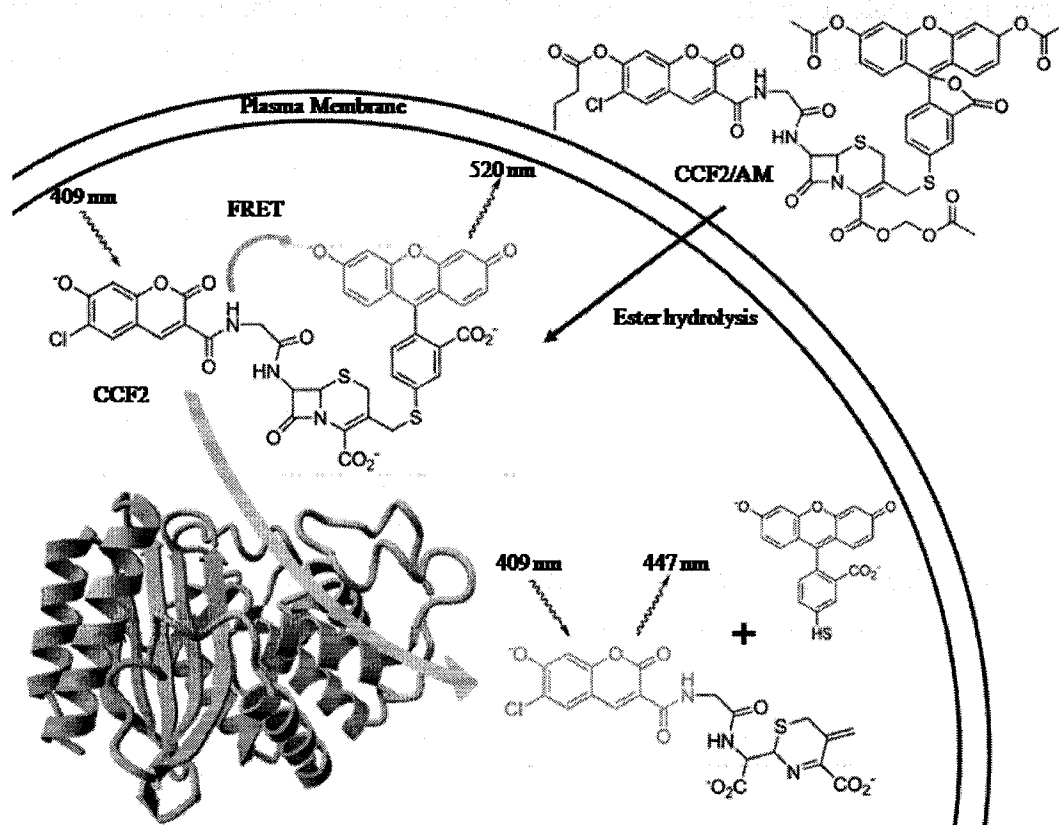


**Figure 4**  $\beta$ -lactamase based catalytic reporter system. The membrane permeable prosubstrate acetoxymethyl ester of coumarin cephalosporin fluorescein (CCF2/AM) forms the fluorogenic  $\beta$ -lactamase substrate CCF2 after cleavage by intracellular esterases. In absence of  $\beta$ -lactamase, CCF2 fluoresces green under violet excitation, due to intramolecular FRET between the coumarin donor and the fluorescein acceptor. In presence of  $\beta$ -lactamase, CCF2 is hydrolysed, the fluorescein fragment is released and the intramolecular FRET is disrupted leading to increase in the coumarin blue fluorescence.

$\beta$ -Lactamases are the main cause of bacterial resistance to  $\beta$ -lactam antibiotics, due to their ability to hydrolyze and inactivate these antibiotics [39, 40]. In particular, class A  $\beta$ -lactamases [41, 42] are the most widespread enzymes and efficiently catalyze the irreversible hydrolysis of the amide bond of the four-membered  $\beta$ -lactam ring of penicillins and cephalosporins, yielding a biologically inactive product [43, 44]. TEM1  $\beta$ -lactamase, a class A active-site serine  $\beta$ -lactamase of 29 kDa, has a well known three-dimensional structure [45-48] and its catalytic mechanism has been extensively studied and probed by site directed mutagenesis.

The catalysis of the hydrolysis of the antibiotic with a  $\beta$ -lactamase proceeds in two steps, acylation and deacylation. In the first step, an acyl-enzyme intermediate is formed by nucleophilic attack of an active-site serine residue (Ser70) at the carbonyl oxygen of the  $\beta$ -lactam. In the second step, the intermediate is hydrolyzed by a water molecule to release the inactivated antibiotic and regenerate the enzyme for the next turnover (Figure 5) [49].

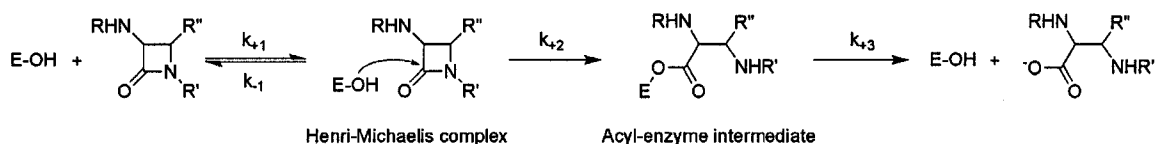


**Figure 5** General catalytic pathway of active-site serine  $\beta$ -lactamase. Usually, both acylation ( $k_{+2}$ ) and deacylation of the acyl-enzyme ( $k_{+3}$ ) are rapid, resulting in high turnover numbers.

General base catalysis is believed to increase the nucleophilicity of Ser70 during the acylation step, and to help deprotonate the hydrolytic water prior to the rupture of the acyl-enzyme intermediate. The role of Glu166 as a proton abstractor in the deacylation step has been widely accepted since it was first proposed in 1987 [50]. However, it is unresolved whether the conserved Glu166, Lys73 or some other residue plays the role of general base in the acylation step [44, 51]. In one hypothesis, Glu166 alone acts as the general base [51-54] during acylation. In a second hypothesis, Lys73 and Glu166 share the role [48]. As mentioned above, for the deacylation step, there exists a consensus that the conserved residue in the class A  $\beta$ -lactamases, Glu166 activates a water molecule for

attack on the carbonyl carbon of the acyl-enzyme and ensures delivery of the abstracted proton back to the O of Ser70 (Figure 6C).

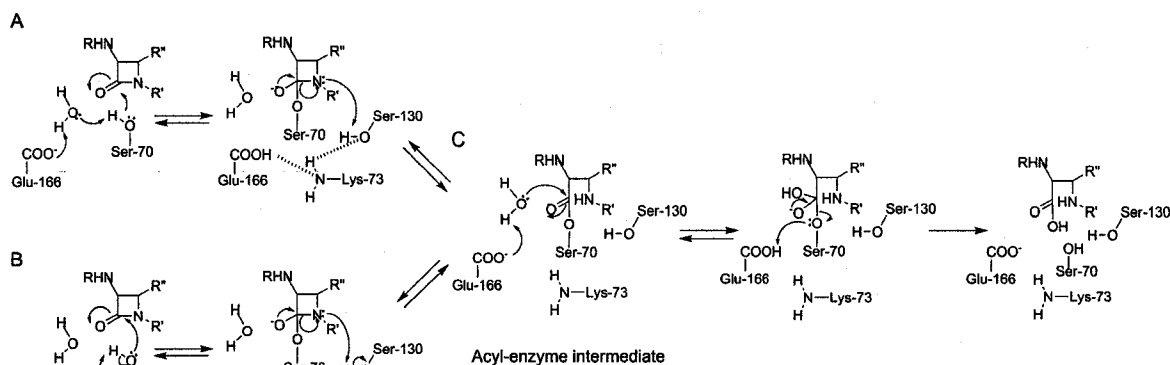


**Figure 6** General mechanism of hydrolysis of  $\beta$ -lactams with  $\beta$ -lactamase. *A.* Representation of hypothesis 1 for the acylation step where Glu166 acts as general base. *B.* Description of hypothesis 2 with Lys73 as general base. *C.* Illustration of the widely accepted mechanism of deacylation.

For the acylation step, a less widely accepted hypothesis suggests that the water molecule might act as a relay in the transfer of the proton between Ser70 and the carboxylate of Glu166. The activated O of Ser70 can then attack the  $\beta$ -lactam carbonyl carbon and the proton is donated back to the leaving nitrogen atom through a network of hydrogen bonds (Figure 6A). Other proposals for the acylation mechanism assign an active kinetic role to Lys73 or Ser130 (Figure 6B).

Lately,  $\beta$ -lactamase has emerged as a catalytic reporter for detecting and imaging biological processes and interactions *in vivo* [38].  $\beta$ -Lactamase was first used as a fusion protein to monitor protein expression via ampicillin resistance [55], and its applications as a reporter have since expanded and range from gene expression monitoring [56] to protein-protein interaction detection [57, 58] and ribozyme activity imaging [59, 60], for example.

For the successful implementation of  $\beta$ -lactamase assays, high sensitivity of the enzyme detection is critical and in this regard, chromogenic  $\beta$ -lactamase substrates such as

nitrocefin and CENTA [61, 62] have been surpassed by superior fluorogenic substrates. Fluorogenic substrates that can be used in cells, such as CCF2 the first reported substrate of that kind [56] (Figure 4), are particularly interesting and various such fluorogenic substrates have since been developed, including near-infrared substrates [63-65].

$\beta$ -Lactamase presents several advantages for the development of a reporter, including the absence of endogenous activity in mammalian cells, the facility of expression in eukaryotic cells without noticeable toxicity [44, 66], as well as the retention of activity in fusion to other proteins [55]. Furthermore, the enzyme hydrolyses substrates containing a  $\beta$ -lactam ring in a unique manner, and a large variety of specific  $\beta$ -lactamase substrates containing an appropriate label can potentially be synthesized. Finally, in the case of a catalytic reporter such as  $\beta$ -lactamase, the signal is amplified to produce robust fluorescence, even in the presence of only a small amount of the enzyme.

## **1.2 FLUORESCENCE MICROSCOPY**

In parallel to the development of new fluorescent reporters, an increasing number of imaging methods have been developed for the visualization and quantification of fluorescence in live cells. Fluorescence microscopy is rapidly and continually evolving and is today an essential tool of investigation in medical and biological sciences.

### **1.2.1 Introduction**

Certain organic molecules are fluorescent; that is, they absorb photons of light at a particular wavelength and emit photons at a longer wavelength after a brief interval. The emission phenomenon is due to relaxation to the ground state of an electronically excited molecule, as shown in the Jablonski diagram (Figure 7A). In the middle of the nineteenth century, Sir George G. Stokes first observed fluorescence and named it [67]. The Stokes shift was later defined as the difference between the emission and the excitation light wavelengths (Figure 7B).

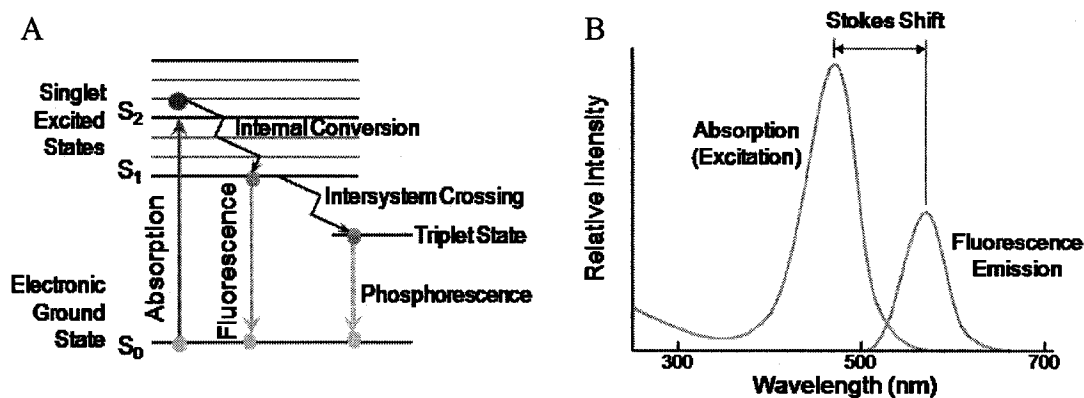


**Figure 7** Jablonski energy diagram and excitation and emission spectral profiles. *A.* The Jablonski diagram illustrates the singlet ground state  $S_0$ , the first and second singlet excited states  $S_1$  and  $S_2$  and the triplet excited state as a stack of horizontal lines, and vibrational energy levels as thin parallel lines. Transitions between states are represented by straight arrows for absorption or emission of a photon or stair case arrows for internal conversion or non-radiative relaxation processes. When a fluorophore absorbs energy, it is usually excited to a higher vibrational energy level in  $S_1$  or  $S_2$  before relaxing to the lowest energy level. *B.* The excitation and emission spectral profiles of a typical fluorophore illustrate the Stokes shift phenomenon.

Fluorescence microscopy allows the high-resolution imaging of fluorescent molecules, and relies on the use of fluorescence microscopes that were first designed in the early twentieth century but not fully exploited until late in the twentieth century. The fluorescence microscope allows irradiation of the sample with the excitation light and permits visualisation of the emitted light alone after separation of the emitted from the excited light using appropriate bandpass filters and a dichroic mirror (Figure 8A). These microscopes enable the highly sensitive detection of fluorescent molecules since the emission of photons is occurring against a dark background. To obtain maximum fluorescence intensity the fluorochrome is excited at the wavelength corresponding to the peak of the excitation curve and emission detection is performed close to the maximum of emission wavelength. When a broad spectrum lamp is used as the light source, the excitation wavelength is determined by the identity of the excitation bandpass filter (Figure 8). Alternatively a laser can be used for fluorescence excitation.

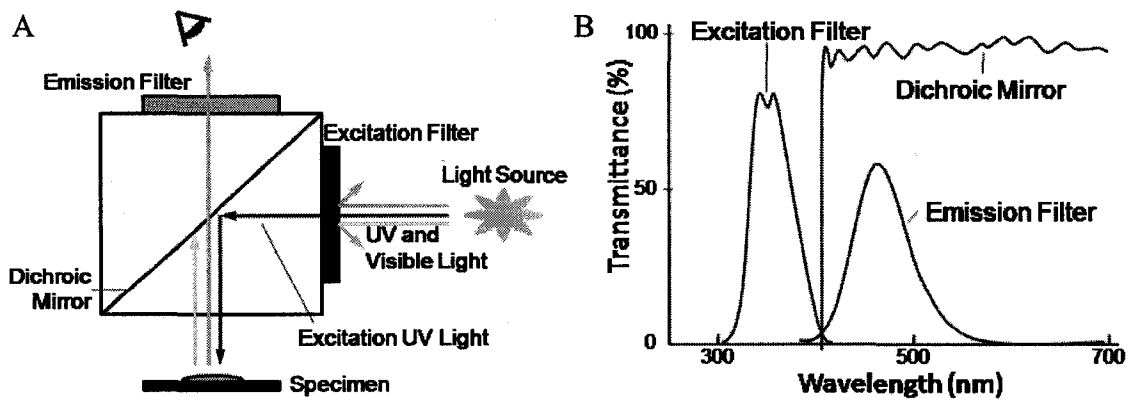


**Figure 8** Fluorescence microscope set up and fluorescence filter spectral profiles. *A.* Basic set up of a fluorescence microscope. *B.* Spectral profiles of the fluorescence filters that would be used for a fluorophore with the hypothetical characteristics  $\lambda_{\text{exc}} = 350 \text{ nm}$ ,  $\lambda_{\text{em}} = 490 \text{ nm}$ .

Fluorescence microscopy presents several advantages over optical microscopy techniques based on transmitted light. The use of fluorochromes allows a high degree of specificity in identification of molecules, cellular components and cells. In addition, fluorescence microscopes present a high sensitivity and can even be used for single molecule detection in certain configurations. Furthermore, with the use of multiple fluorophores, different target molecules can be highlighted. However, fluorescence microscopes are limited in their spatial resolution by the diffraction limit of light.

Fluorescence microscopy includes a variety of specific techniques. Two common techniques, epi-fluorescence and confocal microscopy, will be described in more detail in the following sections.

### 1.2.2 Epi-fluorescence

Epi-fluorescence (short for episcopic fluorescence), or incident light fluorescence, a method of choice for many applications, is currently used in most fluorescence microscopes and is more efficient than traditional microscopy in which transmitted light and two separate lenses are used. It is a fluorescence microscope optical set-up in which the objective lens is used both to focus the excitation light on the specimen and collect

fluorescent light from the specimen. In the case of an inverted epi-fluorescence microscope, the specimen is illuminated from below (Figure 9).

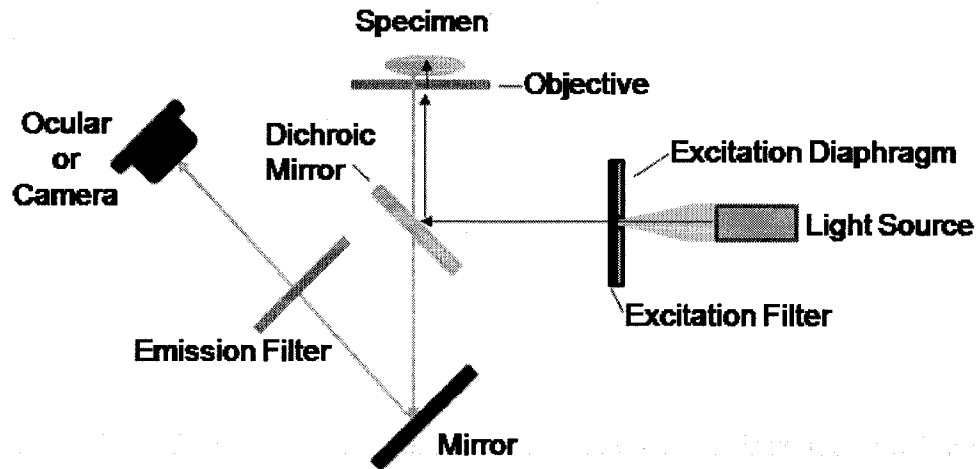


**Figure 9** Diagram of an inverted epi-fluorescence microscope. The ultraviolet light of a mercury or xenon lamp comes into the microscope and goes through the excitation filter which selects the light of the correct exciting wavelength. The light then hits a dichroic mirror and is reflected up to the specimen, where it excites fluorescent molecules. The fluorescent emitted light, collected by an objective lens, passes through the dichroic mirror. The emission filter subsequently lets the light of the emitted wavelength through to the detection system, where it forms the image.

Dichroic mirrors or beam splitters that reflect a range of wavelengths while allowing higher wavelengths to pass through (Figure 8) are central to the principle of epi-fluorescence. An epi-fluorescence microscope requires a complete fluorescence filter set which is composed of an excitation filter, a dichroic mirror and an emission filter (Figure 8B).

One advantage of epi-fluorescence is the relative simplicity of the instrumentation and thus this technique is often combined with other fluorescence microscopy techniques, such as confocal microscopy, in the same instrument.

### 1.2.3 Confocal microscopy

Confocal microscopy is currently a very popular imaging technique that offers several advantages over conventional microscopy, including control of the field depth, elimination of out-of-focus information and the ability to collect serial optical sections from thick specimens for a three-dimensional view of the sample. Confocal microscopy was originally developed by Marvin Minsky and patented in 1957. However, the method went largely unnoticed by researchers until developments in computer and laser technology in the late 1970's and 1980's led to growing interest [68]. In conventional widefield microscopy, the entire specimen is flooded in light and fluorescence from fluorophores outside of the focal plane decreases the resolution of features lying in the objective focal plane. The key point of confocal microscopy is the use of spatial filtering to remove out-of-focus light in samples thicker than the focal plane. A focused beam of light, usually from a laser, is used for point illumination of the specimen. Detection only of the light within the focal plane is accomplished by using a pinhole in an optically conjugate plane in front of the detector (Figure 10). To obtain a two-dimensional image, lateral scanning under computer control, detection of each resulting light signal from the specimen by a photomultiplier tube, and digital construction of an image are performed using specialized software.

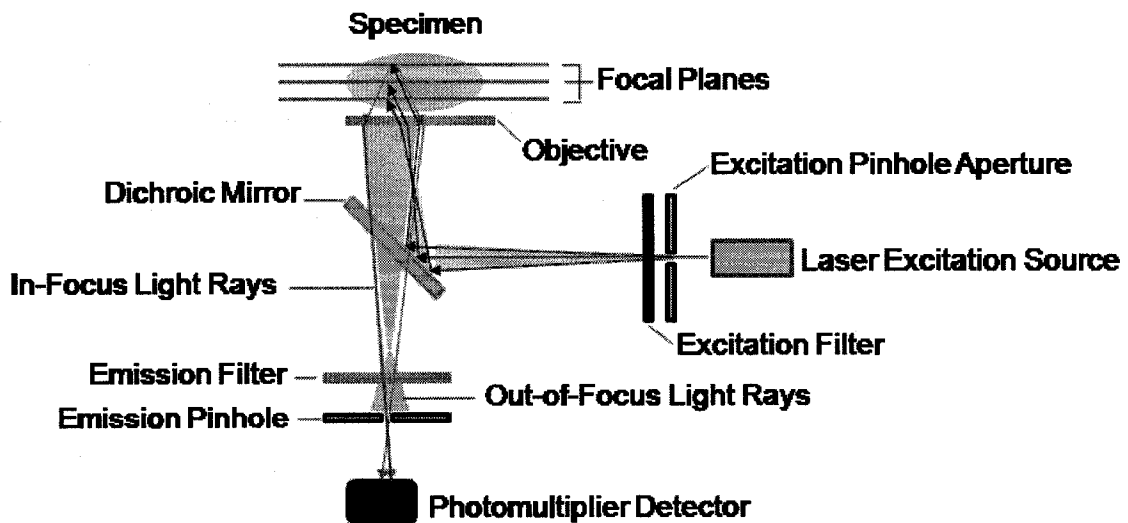


Figure 10 Diagram of a confocal fluorescent microscope.



Due to their complexity, modern confocal microscopes are completely integrated electronic systems where optical microscope, electronic detectors, computer and laser systems combined with wavelength selection devices and a beam scanning assembly collaborate closely.

### **1.3 OBJECTIVE OF THE THESIS**

The research related in this thesis has for objective the design of two very different fluorescent probes, for live cell imaging. The first reporter described, is a single chain variable fragment ScFv against hBub1, which can be genetically fused to a fluorescent protein, for example. It is intended for detection of the human protein hBub1, in live cells and *in vivo*. The second reporter, based on a mutant  $\beta$ -lactamase, is a hybrid system and is intended as a more general labelling strategy. This labelling system should allow introduction of a wide variety of labels into recombinant proteins expressed in live cells.

**CHAPTER 2:**  
**CONSTRUCTION OF A SINGLE CHAIN VARIABLE**  
**FRAGMENT FOR DETECTION OF HBUB1**

## 2.1 INTRODUCTION

The hBub1 (human budding uninhibited by benzimidazoles 1) gene was first identified in 1997 [69] and its complete nucleotide sequence determined soon afterwards [70]. The hBub1 gene encodes a 1085 amino acids protein with a calculated molecular mass of 122 kDa [69, 70]. The protein is composed of several domains that are highly conserved among mitotic checkpoint proteins, including a kinetochore localization and protein binding domain, a C-terminal kinase domain, and a nuclear localization signal [70, 71]. The hBub1 protein is a serine/threonine protein kinase involved in the mitotic checkpoint. The mitotic spindle checkpoint is an intracellular signalling pathway that detects the presence of unaligned chromosomes at the spindle equator in metaphase and delays anaphase [72]. In mammalian cells, disruption of this checkpoint system has been demonstrated to cause aneuploidy in cancer cells [71, 73]. Studies of hBub1 in cells have shown that its level increases in mitosis and that it localizes to the kinetochores in early prophase, and remains localized throughout mitosis until late anaphase [71]. Further investigation showed that it is required for cells to arrest in mitosis in the presence of spindle defects that were induced by microtubule inhibitors [71]. Mutations of the hBub1 gene in a subset of several cancers including human colon cancer [71], adult T-cell leukemia/lymphoma [74] and lymphoblastic leukemia [75], indicate that alteration of the gene is involved in various human cancers. Furthermore, increased expression of the human Bub1 gene is closely linked to abnormal cell proliferation in malignant conditions such as salivary gland tumors [76], breast cancers with chromosomal instability [77], and gastric cancers [78]. Recently, an additional role of hBub1 in preserving centromeric cohesion in mitosis has been reported [79, 80].

It is established that hBub1 has an important role during mitosis, ensuring normal cell division, and that its mutation or over expression is linked to various human cancers. However, the roles and interactions of hBub1 inside cells are complex and have not been totally elucidated. Therefore, detection, imaging and targeting of hBub1 in vivo is of great importance to fully clarify its functions in normal and cancerous cells as well as for potential drug targeting. Various tools have been used to investigate hBub1 in vitro and

in vivo, including polyclonal or monoclonal antibody, FP fusion and RNA interference [71, 80, 81].

A new versatile tool for convenient and sensitive detection, imaging or targeting of hBub1 in vivo would be of great interest to a large number of researchers, including our collaborator Dr. Gordon Chan in the Department of Oncology, University of Alberta. Such a tool should specifically target hBub1, be adaptable to different applications via easy manipulations (e.g. fusion with cytotoxic molecules or proteins for therapeutic goals or with genetically encoded fluorescent labels for detection purposes), give rise to no or a limited harmful immune response and finally, allow for easy production in large quantity.

Polyclonal and monoclonal antibodies (mAb) are powerful reagents for the detection of epitopes of various sizes (see 1.1.1). A wide variety of mAbs is used extensively in research and has even been developed for human diagnostic and therapeutic applications. As of the time of writing, there are nearly 500 mAb-based therapies in various stages of development [82]. However, mAbs present a major drawback that derives from the need for a labour intensive creation, maintenance and storage process of the hybridomas. Furthermore, when used for therapeutic applications, murine monoclonal antibodies usually cause an adverse immune response in patients.

In the past two decades, genetic and molecular techniques have enabled the production of a variety of antibody formats. The different antibody fragments include the antigen-binding Fab, the variable fragment Fv and the single chain variable fragment ScFv (Figure 11). The smallest antibody fragment necessary for complete antigen binding is the Fv fragment, composed of only one light variable ( $V_L$ ) and one heavy variable ( $V_H$ ) domain. In 1972, long before the use of recombinant DNA techniques were applied to Fv engineering, the first reported Fv fragments were prepared by pepsin digestion of a mouse antibody [83]. In a Fv fragment, the two domains can be associated non covalently [84], connected by a peptide linker (ScFv) [85, 86], a disulfide bond (dsFv) [87], or by both (sc-dsFv) [88]. By far the most popular of the four formats is the ScFv fragment.

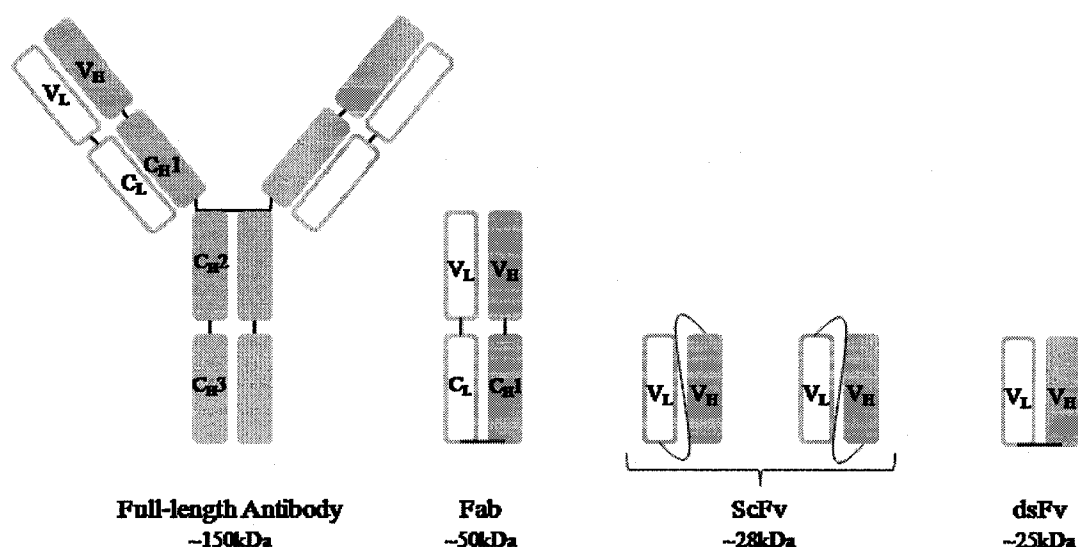


**Figure 11** Schematic picture describing a full length antibody and various recombinant formats: Fab, ScFv and dsFv. Fab (fragment antigen binding) is a structurally independent unit containing the antigen-binding site formed of the four domains V<sub>H</sub>, C<sub>H1</sub>, V<sub>L</sub> and C<sub>L</sub> while ScFv and dsFv only contain two domains; V<sub>H</sub> and V<sub>L</sub> linked respectively by a covalent linker or a disulfide bond.

The ScFv antibody fragments are usually quite stable and present a monomeric binding affinity similar to the parental monoclonal antibody (which has two equivalent binding sites) as demonstrated in a number of cases (e.g. [85, 87]). For simplified genetic manipulations they are encoded by a single gene, consisting of the gene segments coding for the V<sub>L</sub> and V<sub>H</sub> of an antibody, which can be obtained from different sources including hybridomas [89].

An important feature of the ScFv is its linker, which joins the C-terminal of one domain to the N-terminal of the other domain. The chain coupling can be done in two orientations, V<sub>H</sub>-linker-V<sub>L</sub> or V<sub>L</sub>-linker-V<sub>H</sub>, with the latter being the more common. The order of the domains can affect expression efficiency [90] and the required size of the linker, since the distance between the C-terminus of V<sub>L</sub> and the N-terminus of V<sub>H</sub> is greater than between the C-terminus of V<sub>H</sub> and the N-terminus of V<sub>L</sub> in an antibody [91]. A variety of linkers with different sequences and lengths have been used [85, 92, 93] and the most widely used linker is the flexible (Gly<sub>4</sub>Ser)<sub>3</sub>, a 15 amino acid peptide [94]. It has been shown that the size of the linker influences the multimeric size of a ScFv (Figure

12), with predominantly monomeric ScFv for a linker between 15 and 25 amino acids [95]. With shorter linkers, between 5-12 residues, antibody dimers (diabodies) are formed while with linkers of less than 3 residues, trimers (triabodies) are obtained [96, 97].

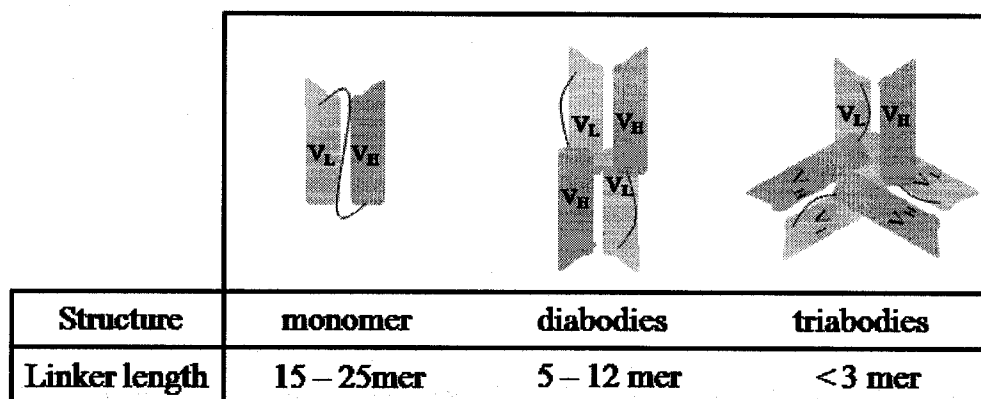


**Figure 12** Effect of linker length on ScFv structure. Monomers, bivalent dimers (diabodies) and trivalent trimers (triabodies) are formed with linkers 15 to 25 mer, 5 to 12 mer and less than 3 mer respectively.

With an approximate size of 27-30 kDa, ScFv fragments are relatively small compared to the original antibodies (~150 kDa). Due to this small size, the ScFv fragments have many applications in medicine [98-100] and have also great potential in biotechnology [101]. The size of the fragment plays an important role, especially in therapeutic applications, where it allows for improved pharmacokinetics properties with better target tissue penetration and clearance [102]. Another advantage of the ScFv fragments is the ease with which they can be manipulated to adapt to a variety of applications. Multifunctional ScFv can be coupled with various functional properties such as enzymes for prodrug therapy [103], toxins, drugs or radioisotopes for cancer targeting [100, 104], viruses for gene therapy [105], and more.

A further application of ScFv fragments is the intracellular expression in eukaryotic host cells. Intracellular antibodies (intrabodies) can be directed to various compartments including the cytoplasm, the endoplasmic reticulum, the nucleus and mitochondrias [106, 107] by incorporating the right signal sequence. The intrabodies are able to bind to and inactivate their target protein in their respective compartment, making them useful for

basic research applications, and potentially for the treatment of viral infections, or for cancer therapy [108]. Presumably, intrabody-based human therapies would be a version of gene therapy and thus will not be practical for several decades, if ever.

In this chapter, the engineering of a single chain variable fragment ScFv against hBub1, starting from a hybridoma is described. The expression, in vitro and in vivo, and the characterization of the putative anti-hBub1 ScFv are reported.

## **2.2 MATERIAL AND METHODS**

### **2.2.1 General procedures and materials**

The hybridomas producing anti-hBub1 antibody were provided by Dr. Hendzel from the Department of Oncology, University of Alberta. The pEYFP-hBub1 plasmid was provided by Dr. Chan from the Department of Oncology & Cross Cancer Institute, University of Alberta. The pBAD436 vector was a gift from Zihao Cheng of the Department of Chemistry, University of Alberta.

All synthetic DNA oligonucleotides used for cloning and mutation were purchased from Integrated DNA Technologies or Sigma-Genosys Canada. PCR amplifications were done in the buffers supplied by the manufacturers using either Taq DNA polymerase (Invitrogen) or Pfu DNA polymerase (Fermentas). Restriction and other modifying enzymes were purchased from Invitrogen, New England Biolabs or Promega. Fast digestions were done using FastDigest<sup>TM</sup> restriction enzymes (Fermentas). PCR and restriction digest products were analysed by agarose gel electrophoresis and routinely purified using either the QIAquick Gel extraction kit (Qiagen) or the DNA extraction kit (Fermentas) according to the manufacturer's protocols. Plasmid DNA was routinely purified using QIAprep Spin Miniprep Kit (Qiagen) according to the manufacturer's protocol. DNA sequence confirmation was performed by dye terminator cycle sequencing using the DYEnamic ET kit (Amersham Biosciences) and analyzed by the University of Alberta Molecular Biology Service Unit (MBSU). All DNA for mammalian

cell transfection was purified using a Plasmid Midi kit (Qiagen) following the manufacturer's protocol.

Protein purity was assessed using sodium dodecyl sulfate polyacrylamide gel electrophoresis (SDS-PAGE) with Coomassie blue staining as described by Laemmli [109] unless stated otherwise. PageRuler Prestained Protein Ladder Plus (Fermentas) was used as molecular weight marker for SDS-PAGE. Protein concentrations were determined by using UV absorbance at 280 nm in combination with the Beer-Lambert law  $A_{280\text{nm}} = \epsilon_{280\text{nm}} \times c \times l$  (with ' $\epsilon$ ' the molar absorptivity in  $\text{M}^{-1}\cdot\text{cm}^{-1}$ , ' $c$ ' the concentration in M and ' $l$ ' the path length of the sample in cm). DNA concentration and purity were determined by measuring the absorbance at 260 nm and 280 nm. Absorbance at 260 nm and 280 nm were measured using a DU 800 UV/Visible spectrophotometer (Beckman).

HeLa cells (ATCC) were cultured in Dulbecco's modified Eagle's medium (DMEM, Invitrogen) supplemented with 10 % fetal bovine serum (Sigma) at 37 °C in a humidified atmosphere containing 5 % CO<sub>2</sub>. Cells were placed in 35 mm imaging dishes, where they were transfected with 4 µg of plasmid DNA mixed with 10 µg of polyethyleneimine (linear, MW ~25000 g•mol<sup>-1</sup>; Polysciences) in 0.5 mL of OptiMEM medium (Invitrogen). Medium is changed to DMEM supplemented with serum after 1 h. The cells were imaged approximately 14-24 h later (unless stated otherwise), after exchanging the medium for Hanks balanced salt solution containing no calcium chloride, magnesium chloride, magnesium sulfate nor Phenol Red (HBSS; Invitrogen). The same protocol was followed for cotransfection, in which case 2 µg of 2 different plasmid DNA were used.

When mitotic cells were required, HeLa cells were synchronized using a double thymidine block (early S-phase block). Around  $1 \times 10^5$  cells were seeded in 35 mm dishes and blocked with 2 mM thymidine 24 h later (Block 1). Cells were released by washing with HBSS and transfected with the plasmid DNA respectively 15-16 h and 22 h after Block 1. Another block/release cycle was started 24 h after the first block. Cells were imaged in mitosis 8 to 10 h after the second release.



HeLa cells were imaged as described previously [110]. An epi-fluorescence inverted microscope Zeiss Axiovert 200M coupled with a xenon arc lamp and a monochrome Retiga 2000R 12-bit cooled CCD camera (QImaging) was used. A Lambda 10-3 controller (Sutter) controlled the external excitation filter wheel, excitation shutter and emission filter wheel. The motorized reflector turret encloses the dichroic mirrors. The QED InVivo software package (Media Cybernetics) was used for automated computer control of all microscope hardware and for image analysis.

### **2.2.2 Anti-hBub1 ScFv gene design**

The first strand cDNA synthesis of anti-hBub1 antibody was performed using the SuperScript III CellsDirect cDNA Synthesis System (Invitrogen), according to the manufacturer's protocol, starting directly from  $1-2 \times 10^5$  cells of frozen anti-hBub1 antibody producing hybridoma.

The generated first strand cDNA was used directly as PCR template for light and heavy chain amplification. The cDNA was amplified through two rounds of PCR using two sets of primers, LSLB and CLLF mixes then LB and CLLF mixes, to yield the light ( $V_L$ ) chain DNA. The cDNA was amplified in a similar manner with CLHB and Not-HF mixes to yield the heavy ( $V_H$ ) chain DNA. All five primers sets are listed in Appendix B and are adapted from the one described by Krebber [111] and Coloma *et al* [112].

To discriminate through the list of primers and select the ones annealing specifically to the anti-hBub1 antibody, the obtained  $V_L$  and  $V_H$  were individually PCR amplified with each possible primers of the sets. The PCR reactions were then analysed and the primers necessary to the amplification determined.

### 2.2.3 Construction of anti-hBub1 ScFv bacterial and mammalian expression vectors

**Bacterial Expression Construct.** The necessary primers for PCR amplification of the  $V_L$  and  $V_H$  DNA and insertion in pBAD436 (based on pBAD His/B; Invitrogen), LB-pBAD and LF-pBAD mixes and HF-pBAD and HB-pBAD mixes are listed in Appendix B.

The  $V_L$  and  $V_H$  DNA were PCR amplified with these primers encoding for Xho1 and Sac1 sites ( $V_L$ ) and Pst1 and EcoR1 site ( $V_H$ ). The amplified light variable chain ( $V_L$ ) DNA was digested with Xho1 and Sac1 restriction enzymes and ligated into a similarly cut pBAD436 vector. After transformation, several colonies were grown overnight, for expression, in LB containing ampicillin (0.1 mg/mL) and arabinose (0.2 %). The cells were lysed with B-PERII (Pierce), and the obtained supernatant screened for CFP and YFP fluorescence with a Safire<sup>2</sup> monochromator-based fluorescence microplate reader (Tecan). Samples were excited at 430 nm and 500 nm and the corresponding emission spectra were recorded. The colonies producing only YFP were identified, sequenced and used in the following step after sequence confirmation. The amplified heavy variable chain ( $V_H$ ) DNA was digested with Pst1 and EcoR1, and ligated into similarly digested  $V_L$  DNA-containing construct. The colonies obtained after transformation were screened in the way described above. The colonies producing neither CFP nor YFP were selected and sequenced.

**Mammalian Expression Construct.** The mammalian cell expression construct for nuclear targeting of an ECFP fusion protein was based on the pECFP-Nuc vector (Clontech). To create the ECFP-anti-hBub1 ScFv-NLS mammalian expression plasmid, the gene encoding ScFv-Anti-hBub1 was PCR amplified with 5' primers encoding a Kozak sequence (CGCCACCATGG) and a Nhe1 restriction site and a 3' primer encoding a Nhe1 site. The pECFP-Nuc vector was digested with Nhe1 restriction enzyme and treated with Calf Intestinal Alkaline Phosphatase (CIAP) to prevent vector religation. The PCR product was digested with the same enzyme, purified and ligated into the cut vector. After transformation, several 4 mL LB media cultures supplemented with kanamycin (25  $\mu$ g/mL) were inoculated with a single colony, allowed to grow overnight (37 °C and 225 rpm) and used for DNA preparation. The obtained constructs were fast digested with

Xho1 and the insert orientation determined through their Xho1 digestion pattern. The constructs containing the insert in the right orientation were then sequenced.

To create the pECFP-ScFv plasmid, an identical procedure was used after removing the nuclear localization sequence (NLS) from the pECFP-Nuc vector by BamH1 and BglII digestion, and self-ligation. The pECFP vectors lacking the NLS sequence were identified by double digestion with Nhe and BglII. To identify the pECFP vectors containing the ScFv-Anti-hBub1 insert in the right orientation, a fast double digestion with Xho1 and Xba1 was performed. The constructs were sequenced after positive identification.

#### **2.2.4 Anti-hBub1 ScFv modelization**

The obtained anti-hBub1 ScFv gene was fully sequenced and translated. Individual V<sub>L</sub> and V<sub>H</sub> sequences were aligned with a compilation of various known antibody V<sub>L</sub> and V<sub>H</sub> sequences provided on AAAAA, AHO's Amazing Atlas of Antibody Anatomy at <http://www.bioc.unizh.ch/antibody> [113]. Similarity and identity with some antibody V<sub>H</sub> and V<sub>L</sub> chains was determined. The alignment, similarity and identity determination were performed with macros obtained on AAAAA server. The three-dimensional structure of the ScFv-anti-hBub1 was predicted by homology modelling using the Swiss-Model server [114, 115], and the crystal structure of the single-chain Fv fragment 1696 (PDB ID 1SVZ) as template [116].

#### **2.2.5 Protein expression and purification**

*E. coli* strain LMG194 was transformed with the pBAD436 expression vector containing the gene of interest, for preparation of the anti-hBub1 ScFv protein in sufficient quantity for purification and preliminary characterization. A single colony was used to inoculate a 4 mL culture that was allowed to grow overnight (37 °C and 225 rpm) before being diluted into 1 litre of LB media containing ampicillin (0.1 mg/ml). The culture was grown at 37 °C until OD reached 0.5 and arabinose (0.2 %) was then added. The culture was

allowed to grow overnight at 25 °C before cells were harvested by centrifugation and lysed by a French press.

Proteins were purified by Ni<sup>2+</sup>-nitrilotriacetate (Ni-NTA) agarose gravity-flow chromatography (Qiagen) under native conditions. The protein was eluted with a Ni-NTA elution buffer containing 250 mM imidazole. Alternatively, protein purification with Ni-NTA chromatography (Amersham) was carried out under native conditions. In that case, elution was performed using a gradient of imidazole (20-500 mM over 40 min).

Protein purity was first estimated by SDS-PAGE electrophoresis. Further protein purity assessment was performed by Western Blot. The SDS-PAGE gel was transferred to a polyvinylidene difluoride (PVDF) membrane (Millipore) at 300 mA for 1 h. The membrane was washed with Tris-Buffered Saline with 0.1 % Tween 20 buffer (TTBS) and blocked overnight at 4 °C with 5 % non fat dry milk in TTBS. The membrane was washed briefly with TTBS, incubated with an anti-His6-peroxidase antibody (Roche) at 1:500 dilution in TTBS for 1 h at room temperature, and washed again three times with TTBS for 15 min. The membrane was incubated for 5 min with the SuperSignal West Femto Maximum Sensitivity Substrate (Pierce) for chemiluminescent detection and exposed 10 minutes to a Kodak BioMax Light Film (Kodak). The film was then developed.

### **2.2.6 ScFv-anti-hBub1 and hBub1 expression and imaging in HeLa cells**

HeLa cells were transfected with pECFP-Nuc-ScFv, pECFP-ScFv and pEYFP-hBub1 vectors and imaged. ECFP fluorescence was imaged with 436/20 nm and 480/40 nm bandpass filters for excitation and emission respectively while EYFP was imaged with 500/20 nm and 535/30 nm bandpass filters.

Anti-hBub1-ScFv-ECFP and EYFP-hBub1-expressing cells were also imaged in mitosis, after synchronization (see 2.2.1). In that case, HeLa cells were cotransfected with various combinations of pECFP-ScFv, pEYFP-hBub1 and pDisplay-mCherry (see 3.2.2 and 3.3.1

for vector description) and imaged as described above. mCherry was imaged with 535/50 nm and 610/75 nm bandpass filters for excitation and emission respectively.

Finally, HeLa cells were cotransfected with pDisplay-mCherry and pECFP-ScFv and imaged at different time after transfection. Fluorescence as well as cell morphology was recorded.

## 2.3 RESULTS AND DISCUSSION

### 2.3.1 anti-hBub1 ScFv gene design

The preparation of the anti-hBub1 ScFv starting from an anti-hBub1 producing hybridoma followed the procedure described in Figure 13. The SuperScript III CellsDirect cDNA Synthesis System (Invitrogen) was used to make mRNA and cDNA starting with anti-hBub1 producing hybridomas. The cDNA was then used as starting point to obtain the variable light ( $V_L$ ) and heavy ( $V_H$ ) chains. The PCR amplification of the murine light chain,  $V_L$ , was first attempted using 5' end primers annealing to the framework region 1 (LB primer set, based on Krebber *et al.* [111]) and failed. The same amplification was then attempted using a leader sequence primer set, LB LS mix, based on the set described by Coloma *et al.* [112]. The obtained fragment was then used as template for amplification with the framework region 1 annealing primer set. A previously published set of 3' end primers that anneal to the  $C_L$  constant portion of the antibody was used in all 3 cases (CL-LF primer set, based on Krebber *et al.*) [111]. The PCR amplification of the murine heavy chain,  $V_H$ , was performed using 5' end primers annealing to the framework region 1 and 3' end primers annealing to the  $C_H$  constant region, respectively CLHB and Not-HF primer sets based on [111]. PCR amplifications yielded sharp bands at the predicted sizes of ~ 450 bp and ~ 375 bp for  $V_L$ , respectively with or without the leader sequence (LS), and of ~ 400 bp for  $V_H$ .

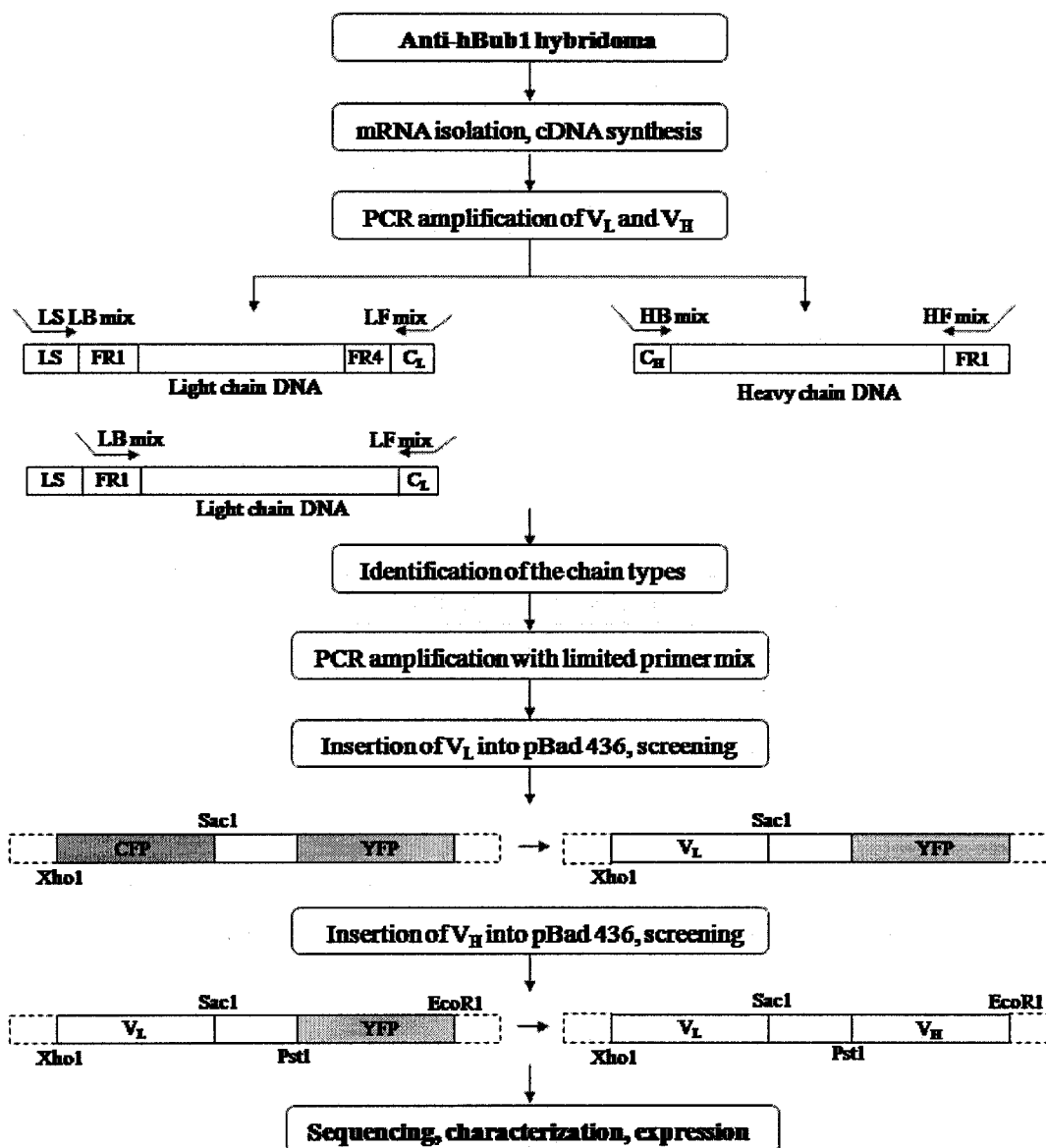


**Figure 13** Flow chart of the formation of the anti-hBub1 ScFv.

To determine the primers that are necessary for the amplification of this particular ScFv, individual PCR amplifications of V<sub>L</sub> and V<sub>H</sub> DNA with every primer were carried out and analysed. It was determined that V<sub>L</sub> could be amplified with LB1 and LB4 in combination with LF1 and LF5 and that V<sub>H</sub> could be amplified with HB5, HB6 and HB10 in combination with HF4. These primers were used for amplification and insertion of the V<sub>L</sub> and V<sub>H</sub> chains in the expression vector, pBAD436.

### 2.3.2 Construction of anti-hBub1 ScFv bacterial and mammalian expression vectors

The pBAD436 vector is based on the pBAD His/B vector (Invitrogen) and contains CFP and YFP separated by an 84 bp linker, allowing for easy screening of the ligation constructs (Figure 13). The amplification of the  $V_L$  and  $V_H$  chains with the selected primers yielded DNA fragments of the expected sizes (~400 bp). After digestion of the  $V_L$  fragment, insertion in the pBAD vector, transformation of *E. Coli* with the constructs, colonies were grown and lysed. The cell lysate supernatants were screened for CFP and YFP fluorescence by excitation at 430 nm and 500 nm respectively. A construct was found to have only YFP present after screening (Figure 14) and sequencing, and was kept for further manipulation. The same process was repeated with  $V_H$ , and 3 colonies were found to express a non-fluorescent protein (Figure 14) and thus to potentially contain the desired construct. Sequencing of the constructs indicated successful cloning of both fragments in the original vector in one case.

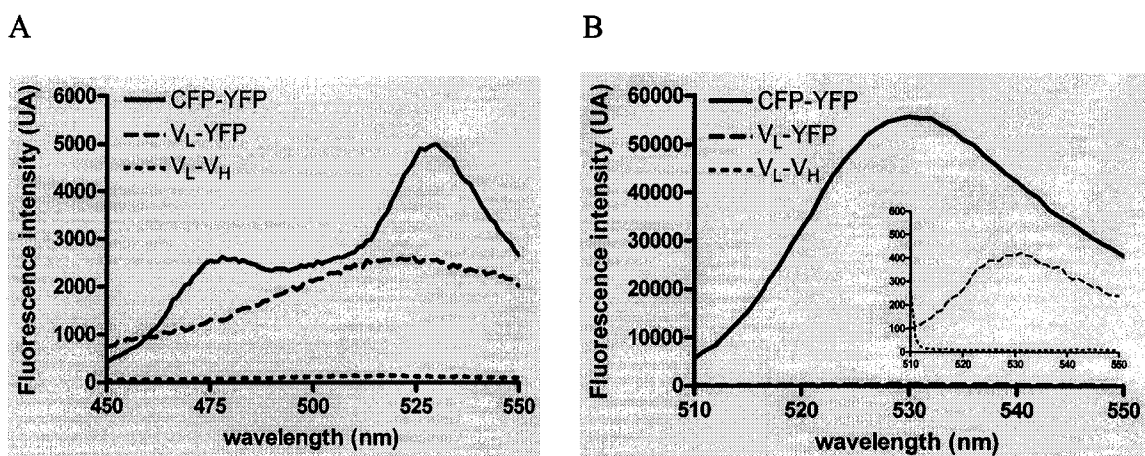


**Figure 14** Fluorescence screening of the starting, intermediate and final constructs of the ScFv-Anti hBub1 into pBAD436. *A.* Fluorescence emission spectra, upon excitation at 430 nm, of the protein expressed by the original construct, CFP-YFP (emission ~475 nm of CFP and ~530 nm of YFP caused by FRET), the  $V_L$  construct,  $V_L$ -YFP (slight excitation of YFP), and the ScFv construct,  $V_L$ - $V_H$  (no fluorescence). *B.* Fluorescence emission spectra, upon excitation at 500 nm, of the proteins CFP-YFP and  $V_L$ -YFP (emission ~530 nm of YFP) and  $V_L$ - $V_H$  (no fluorescence).

It is worth mentioning that the two-steps insertion method used allowed screening against non coding  $V_L$  chain. Any chain containing a frameshift or stop codon should be expressed in colonies presenting no fluorescence and thus discarded as background. Furthermore, analysis indicated that the  $V_L$  and  $V_H$  chain sequences were plausible and contained no atypical amino acids for murine domains, frameshifts, stop codons or obvious deletions.

In the resulting construct, the  $V_L$  and  $V_H$  chain were separated by a 28 amino acid linker, GAQKKGTGTGNPATGKGTGTGQEGTSAE, which was present in the original pBAD436 construct. The 28 amino acid linker should promote formation of a monomer ScFv, since it was shown that a linker of more than 15 mer decreases the percentage of dimer (see section 2.1).

For mammalian expression of the anti-hBub1 ScFv as a fusion to a fluorescent protein, the commercial pECFP-Nuc vector (Clontech) was chosen. The pECFP-Nuc vector contains the nuclear localization signal (NLS) of the simian virus 40 large T-antigen fused at the C-terminus of the enhanced cyan FP (ECFP) gene. The NLS (DPKKKRKV) of the simian virus 40 large T-antigen has been shown to induced transport to the nucleus [117, 118]. To increase the efficiency of relocation of the fused protein to the cell nucleus, three repeats of the sequence are included in the vector [119].

The anti-hBub1 ScFv gene was amplified with primers encoding the Kozak consensus translation initiation sequence [120]. The Kozak sequence, CGCCACCATGG, was added at the N-terminus of the gene to replace the one removed by cloning in the Nhe1 site and allowed for enhanced expression of the gene in mammalian cells. The anti-hBub1 ScFv gene was inserted at the N-terminus of the ECFP gene using a Nhe1 restriction site. After ligation and transformation, 5 colonies were obtained and screened. The insert orientation was determined using the Xho1 digestion pattern (Figure 15). Following digestion, two of the colonies showed the pattern expected for a sense orientation of the insert and three colonies showed the pattern expected for an antisense insertion. Sequencing confirmed the sense insertion.



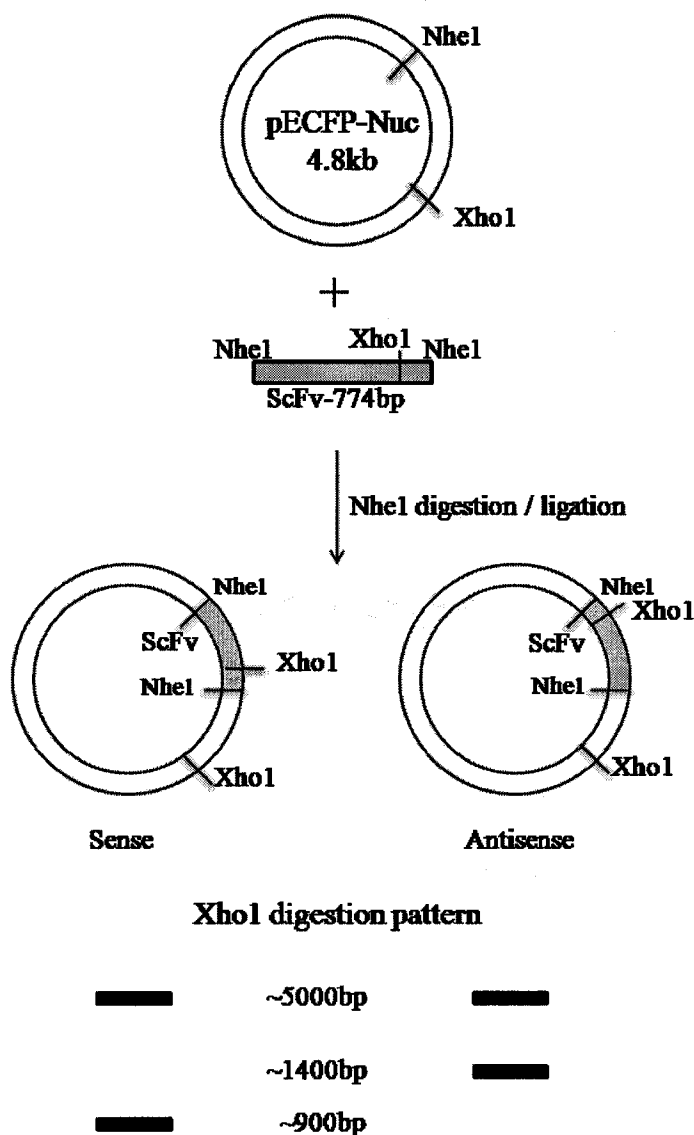


**Figure 15** XhoI digestion pattern of pECFP-Nuc with inserted anti-hBub1 ScFv. The original vector, pECFP-Nuc contains a NheI site (592 bp) and an XhoI site (1344 bp). The insert anti-hBub1 ScFv is 774 bp and contains NheI sites at the extremities, and an XhoI site (629 bp). The orientation of the insert between the NheI sites can be determined by XhoI digestion.

The NLS gene was removed from the pECFP-Nuc plasmid by BamHI and BglII digestion. The 2 enzymes have a different recognition sites but an identical 5'- overhang, GATC. After digestion, the vector can be self-ligated and the obtained vector tested for the absence of the NLS gene by double digestion with NheI and BglII. The absence of a

low molecular weight band (~750 bp) indicated the destruction of the BglIII site i.e. the successful removal of the NLS.

To obtain the pECFP-ScFv, a procedure identical to the one used for pECFP-ScFv-Nuc, was performed starting from the pECFP vector. To test for the insert orientation, an XhoI/XbaI double digestion was performed. The expected results are very similar to the one described in Figure 15. The XhoI site at 1344 bp was removed with the NLS, and the XbaI site at 1436 bp is used instead. After ligation and transformation, 6 colonies were tested, and 3 of them contained the insert in the desired orientation. The presence of the C-terminal of the anti-hBub1 ScFv insert in frame with the ECFP was positively determined by sequencing.

### **2.3.3 Characterization of anti-hBub1 ScFv**

The nucleotide sequence of the anti-hBub1 ScFv is given in Figure 16. The ScFv has 891 nucleotides encoding 296 amino acids including a flexible amino acid linker and a His-Tag polypeptide. Amino acid numbering and complementary determining regions (CDR) of the  $V_L$  and  $V_H$  domains were determined according to the method of Kabat [121] (Figure 16).

The similarity and identity determination showed a great agreement between the anti-hBub1 ScFv and specific mouse immunoglobulin light chain kappa variable domain (PDB ID 1IBG) and immunoglobulin heavy chain variable domain (PDB ID 1AY1). The  $V_L$  chains had an 88 % sequence identity and a 91 % sequence similarity while the  $V_H$  chains had an 84 % sequence identity and an 88 % sequence similarity. Overall % sequence identity and % sequence similarity were calculated using the macros available on the AAAA server [113].

		Anti-hBub1 ScFv - tags																																	
anti hBub1 ScFv		M	G	G	S	H	H	H	H	H	H	G	M	A	S	M	T	G	G	Q	Q	M	G	R	D	L	Y	D	D						
		atg	ggg	ggt	tct	cat	cat	cat	cat	cat	cat	ggt	atg	gct	agc	atg	act	ggt	gga	cag	caa	atg	ggt	cgg	gat	ctg	tac	gac	gat						
<b>Kabat VL Kappa</b>		Anti-hBub1 ScFv - tags																																	
anti hBub1 ScFv		D	D	K	D	P	G	S	R	D	Y	K	1	2	3	4	5	6	7	8	9	10	11	12	13	14	15	16	17						
		gac	gat	aag	gat	cct	ggc	tcg	agg	gac	tac	aaa	gat	att	gtg	atc	act	cag	tct	cct	gct	tcc	tta	gct	gta	tct	ctg	ggg	cag						
<b>Kabat VL kappa</b>		CDR L1																																	
anti hBub1 ScFv		18	19	20	21	22	23	24	25	26	27a	27b	27c	27d	27e	27f	29	30	31	32	33	34	35	36	37	38	39	40	41						
		R	A	T	I	S	Y	R	A	S	K	S	V	S	T	S	G	Y	S	Y	M	H	W	N	Q	Q	K	P	G						
		agg	gcc	acc	atc	tca	tac	agg	gcc	agc	aaa	agt	gtc	agt	aca	tct	ggc	tat	agt	tat	atg	cac	tgg	aac	caa	cag	aaa	cca	gga						
<b>Kabat VL kappa</b>		CDR L2																																	
anti hBub1 ScFv		42	43	44	45	46	47	48	49	50	51	52	53	54	55	56	57	58	59	60	61	62	63	64	65	66	67	68	69						
		Q	P	P	R	L	L	I	Y	L	V	S	N	L	E	S	G	V	P	A	R	F	S	G	S	G	S	G	T						
		cag	cca	ccc	aga	ctc	ctc	atc	tat	ctt	gta	tcc	aac	cta	gaa	tct	ggg	gtc	cct	gcc	agg	ttc	agt	ggc	agt	ggg	tct	ggg	aca						
<b>Kabat VL kappa</b>		CDR L3																																	
anti hBub1 ScFv		70	71	72	73	74	75	76	77	78	79	80	81	82	83	84	85	86	87	88	89	90	91	92	93	96	97	98							
		D	F	T	L	N	I	H	P	V	E	E	E	D	A	A	T	Y	Y	C	Q	H	I	R	E	P	Y	T	F						
		gac	ttc	acc	ctc	aac	atc	cat	cct	gtg	gag	gag	gag	gat	gct	gca	acc	tat	tac	tgt	cag	cac	att	agg	gag	cct	tac	acg	ttc						
<b>Kabat VL kappa</b>		Linker																																	
anti hBub1 ScFv		99	100	101	102	103	104	105	106	107	108	G	A	Q	K	K	G	T	G	T	G	N	P	A	T	G	K	G	T						
		gga	ggg	ggg	acc	aag	ctg	gag	ctg	aaa	cgt	gga	gct	cag	aag	aag	ggg	acc	ggg	acc	ggc	aac	ccc	gcc	aca	ggc	aag	ggg	act						
<b>Kabat VH</b>		Linker																																	
anti hBub1 ScFv		G	T	G	Q	E	G	T	S	A	E	1	2	3	4	5	6	7	8	9	10	11	12	13	14	15	16	17	18						
		ggc	acg	gga	cag	gag	ggt	acc	tct	gca	gag	gag	gtg	cag	gtg	gtg	gaa	tcg	gga	cct	ggc	ctg	gtg	aaa	cct	tct	cag	tct	ctg						
<b>Kabat VH</b>		CDR H1																																	
anti hBub1 ScFv		19	20	21	22	23	24	25	26	27	28	29	30	31	32	35b	36	37	38	39	40	41	42	43	44	45									
		S	L	T	C	T	V	T	G	Y	S	I	T	S	D	Y	A	W	N	W	I	R	Q	F	P	G	N	K	L						
		tcc	ctc	acc	tgc	act	gtc	act	ggc	tac	tca	atc	acc	agt	gat	tat	gcc	tgg	aac	tgg	atc	cgg	cag	ttt	cca	gga	aac	aag	ctg						
<b>Kabat VH</b>		CDR H2																																	
anti hBub1 ScFv		46	47	48	49	50	51	52	52a	54	55	56	57	58	59	60	61	62	63	64	65	66	67	68	69	70	71	72	73						
		E	W	M	G	Y	I	T	Y	S	G	N	T	N	Y	N	P	S	L	K	S	R	I	S	V	T	R	D	T						
		gag	tgg	atg	ggc	tac	ata	acc	tac	agt	ggt	aac	act	aat	tac	aac	cca	tct	ctc	aaa	agt	cga	atc	tct	gtc	act	cga	gac	aca						
<b>Kabat VH</b>		CDR H3																																	
anti hBub1 ScFv		74	75	76	77	78	79	80	81	82	82a	82b	82b	83	84	85	86	87	88	89	90	91	92	93	94	95	96	97	*						
		S	K	N	Q	F	F	L	Q	L	T	S	V	T	T	E	D	T	A	T	Y	Y	C	S	K	Y	G	N	F						
		tcc	aag	aac	cag	ttc	ttc	ctg	caa	ttg	act	tct	gtg	act	act	gag	gac	acg	gcc	act	tat	tac	tgt	tca	aaa	tat	ggt	aac	ttc						
<b>Kabat VH</b>		CDR H3																																	
anti hBub1 ScFv		*	*	*	101	102	103	104	105	106	107	108	109	110	111	112	113	Y	A	L	D	Y	W	G	Q	G	T	S	V	T	V	S	S	-	
		tat	gct	ctg	gac	tac	tgg	ggt	caa	gga	acc	tca	gtc	acc	gtc	tcc	tcg	taa																	

**Figure 16** Nucleotides and deduced amino acid sequences of anti-hBub1 ScFv. Amino acid numbering and complementary determining regions (CDR) of the V<sub>L</sub> (CDR L) and of the V<sub>H</sub> (CDR H) were determined.

The anti-hBub1 ScFv structure (Figure 17) modelled using the Swiss model server [114, 115] was based on the known crystal structure of a single chain Fv fragment [116]. The predicted structure of the ScFv highlights the presence of the binding pocket formed by the CDR amino acids.

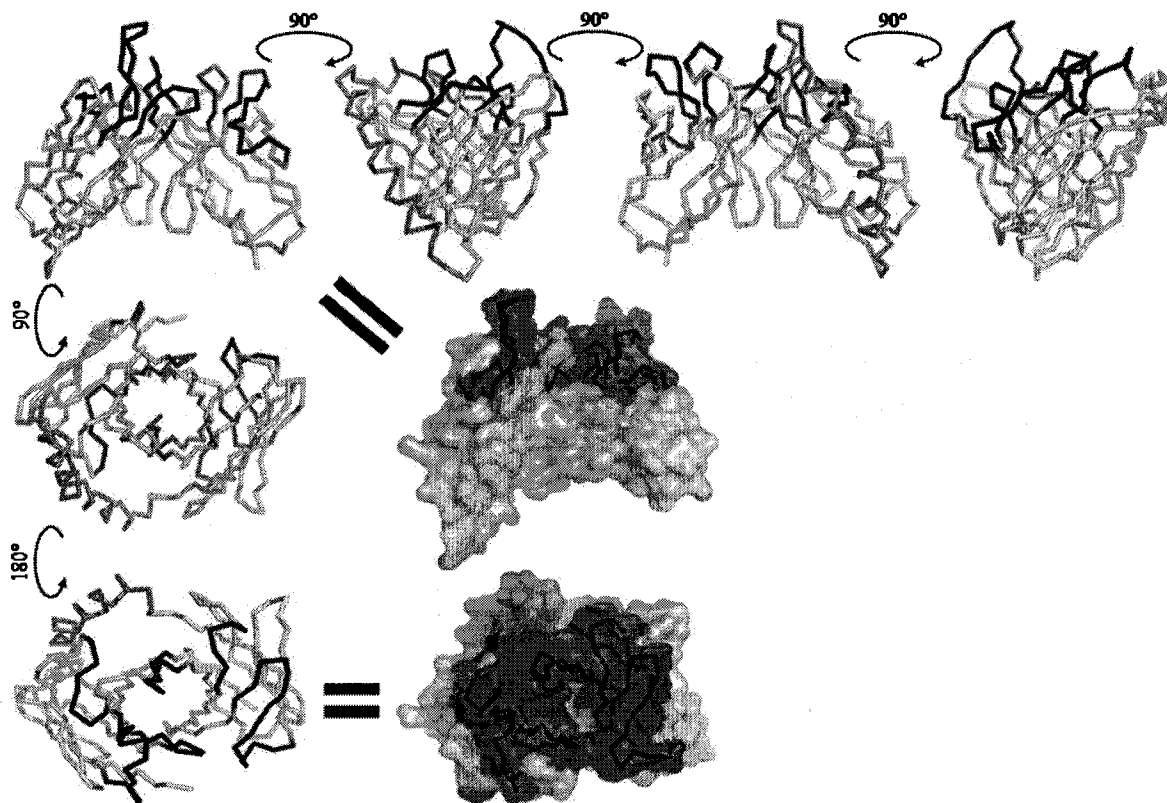


**Figure 17** Three dimensional predicted structure of anti-hBub1 ScFv. The structure of the ScFv is presented from 6 angles. On the first line, 4 images of the ScFv are presented, each corresponding to a rotation of 90° around a vertical axis, relative to the previous image. In the first column, 2 more different angles are illustrated, corresponding to the bottom and top views respectively. Finally, the surface representations of two of the illustrations are included. The light and heavy chain variable domains are in light grey, the linker in dark grey and the CDRs in black. The model is based on the known structure of a ScFv (PDB ID 1SVZ) and was performed with SwissModel. The figure was produced with the program Pymol [122].

### 2.3.4 Expression and purification of ScFv-anti hBub1

The pBAD/HisB vector (Invitrogen) contains the *araBAD* promoter providing tight, arabinose dose-dependent control of the protein expression. Expression of the anti-hBub1

ScFv, even after optimization, was quite low. The presence of the His-Tag allowed for fast purification of the protein with Ni-NTA, under native conditions. The full length anti-hBub1 ScFv protein has a computed molecular weight of 32292 Da and was thus expected to show at ~32 kDa on a SDS-PAGE gel. The purification on Ni-NTA agarose beads yielded a sample containing several bands including a faint band ~32 kDa and the band of a co-purified host protein of approximately 27 kDa, very likely SlyD, an *E. coli* protein that binds divalent metal ions [123] and often results in significant contamination of Ni-NTA purified His-tagged proteins. The purification by Ni-NTA chromatography, performed on a His Trap column, yielded a significantly more pure protein after elution with an imidazole gradient. A protein with an approximate MW of 30 kDa was eluted between 140-200 mM imidazole while a second protein with a MW of approximately 32 kDa was eluted between 200-245 mM imidazole (Figure 18A).

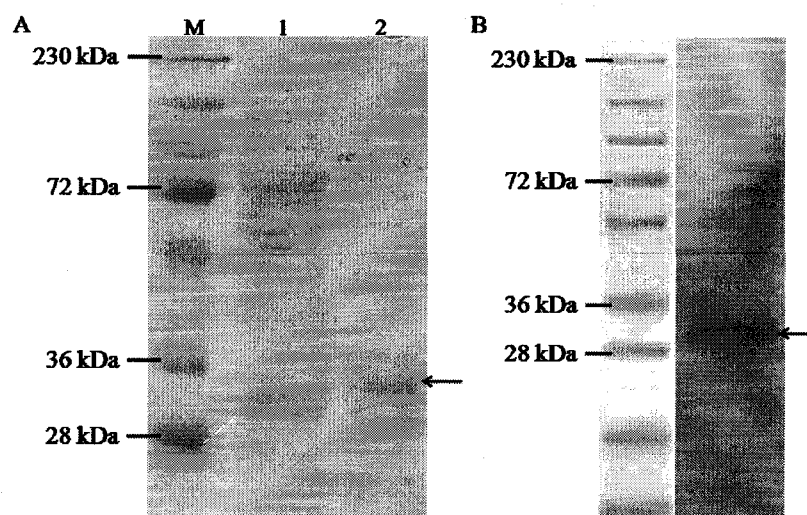


**Figure 18** SDS-PAGE and Western Blot of anti-hBub1 ScFv purified by Ni-NTA chromatography. *A.* SDS-PAGE of the samples obtained by elution with 140-200 mM imidazole (lane 1) and 200-245 mM imidazole (lane 2) presenting protein bands of apparent molecular weights 28-36 kDa. *B.* Western Blot of the sample obtained by elution with 200-245 mM imidazole presenting a protein band of apparent molecular weight ~32 kDa. M is the molecular weight marker and the arrows point out the bands of interest.

The Ni-NTA chromatography eluates containing the 32 kDa protein were analysed by Western Blot with an anti-His Tag antibody coupled to peroxidase and after reaction with the substrate, exposure and development of the light-sensitive film, a band of the

expected molecular weight was detected (Figure 18B). Therefore, purification of the anti-hBub1 ScFv seemed successful when performed on a His trap column with an imidazole gradient.

### **2.3.5 Expression of ECFP- anti-hBub1 ScFv ± NLS and EYFP-hBub1 in mammalian cells**

Expression of EYFP-hBub1, ECFP-anti-hBub1 ScFv-NLS and ECFP-anti-hBub1 ScFv was monitored using fluorescence microscopy. EYFP-hBub1 appeared to be easily expressed and even overexpressed in mammalian cells, and formation of fluorescent grains was observed. ECFP-anti-hBub1 ScFv-NLS appeared to be expressed in the nucleus but the resulting fluorescence was relatively dim.

Interactions between hBub1 and anti-hBub1 ScFv, if any, are anticipated to happen in the cell nucleus and be observable by FRET. One concern was that overexpression of the anti-hBub1 ScFv would result in a large excess of ECFP fluorescence in the nucleus and that this would prevent accurate measurement of FRET due to the bleedthrough into the weaker YFP channel (Figure 19). Thus, another vector expressing the ScFv fused to ECFP, but without cell nucleus targeting was used for ScFv expression. ECFP-anti-hBub1 ScFv was expressed and present everywhere in cells. However ECFP-anti-hBub1 ScFv was rather difficult to image due to low resulting CFP fluorescence.

The hBub1 protein is known to be involved in the spindle checkpoint function and to be mainly expressed and active in mammalian mitotic cells. Hence synchronization of the cells was carried out, in order to image exogenous hBub1 and anti-hBub1 ScFv expressed in mitotic cells. EYFP-hBub1 and ECFP-anti-hBub1 ScFv were expressed separately in synchronized cells and imaged, along with mCherry-PDGFR-TM to help identify the mitotic cells from the dead ones. EYFP-hBub1 was present in the cells, but did not appear to localize at the kinetochores as was anticipated [71]. It is plausible that no localization was discerned due to overexpression of the exogenous protein. As for ECFP-anti-hBub1 ScFv, very few to no cells exhibited ECFP fluorescence.

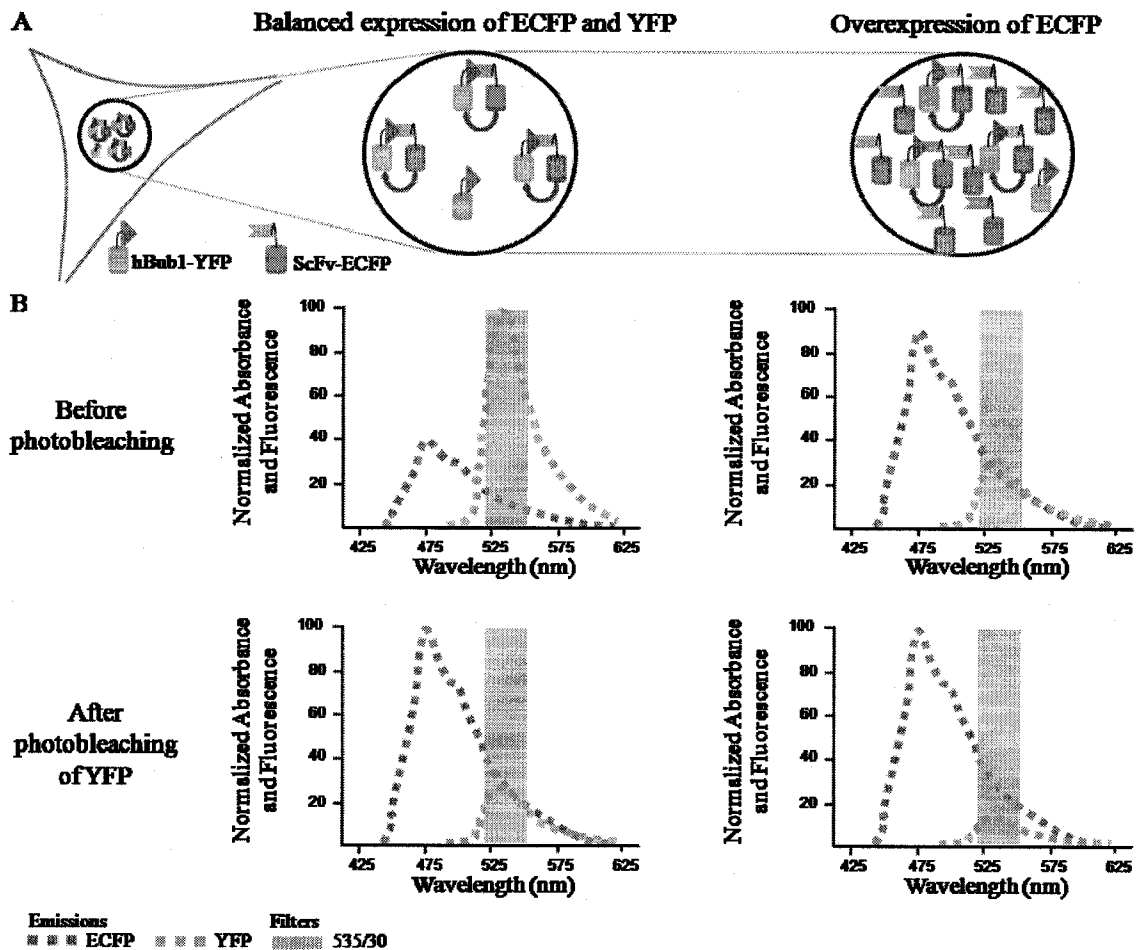


**Figure 19** Effect of overexpression of ECFP in HeLa cell nucleus on FRET measurements. *A.* Illustration of HeLa cell nuclei expressing and overexpressing ECFP. *B.* Representation of the corresponding excitation spectra caused by excitation at 436 nm, before and after YFP photobleaching. In the case of overexpressed ECFP, after photobleaching, the observed fluorescence is still moderate due to bleedthrough of ECFP in the YFP channel.

To try and understand why ECFP-anti-hBub1 ScFv fluorescence was so poorly demonstrated in mitotic cells, a timeline of coexpression with mCherry-PDGFR-TM was completed (Figure 20). Fluorescence from both mCherry and ECFP appeared between 5 and 9 hours after transfection, which roughly corresponds to the time necessary for expression and chromophore maturation of a FP. From 9 to 24 hours after transfection, mCherry fluorescence was easily detected and found in healthy looking cells. However, the ECFP fluorescence level was low after 9 hours, even lower after 17 hours and

somewhat difficult to distinguish from autofluorescence. At the 24h time point, no cell containing ECFP fluorescence was detected.

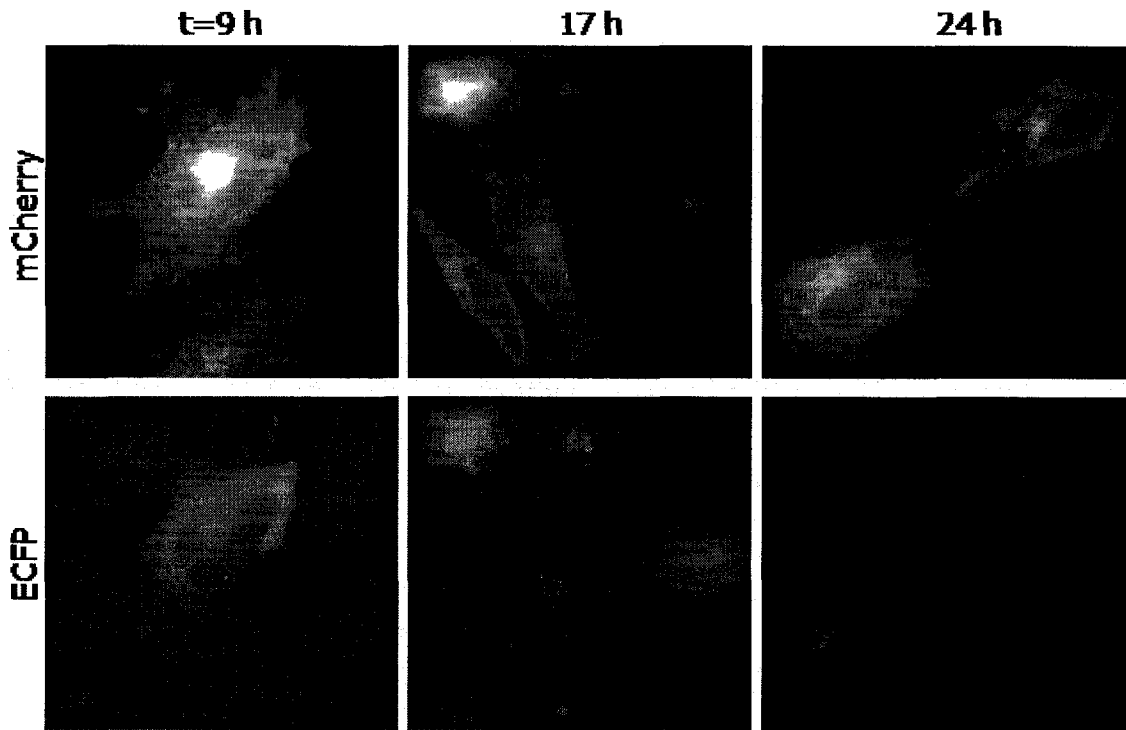


**Figure 20** Pictures of mCherry-PDGFR-TM and ECFP-ScFv expressing HeLa cells. HeLa cells expressing mCherry-PDGFR-TM and ECFP-ScFv, imaged for mCherry and ECFP fluorescence respectively, after 9h, 17h and 24h.

Furthermore, the cells presenting ECFP fluorescence in addition or not to mCherry were much smaller than the one displaying only mCherry after 17 hours. Finally, after 24 hours, many dead cells were seen, and the live cells only exhibited mCherry or no fluorescence.



## 2.4 DISCUSSION AND CONCLUSIONS

In this chapter we have described our attempts to create a new tool, a genetically encoded fusion of anti-hBub1-ScFv and a FP, for detection of hBub1 in mammalian cells.

The anti-hBub1 ScFv gene design followed a well-established multi-step procedure. The  $V_L$  and  $V_H$  were obtained separately and coupled successfully in a bacterial expression vector and a mammalian expression vector. After full sequence determination, the  $V_L$  and  $V_H$  chains found were plausible and the framework amino acids were in good agreement with the observed consensus from murine antibody sequences. After nucleic acid sequence translation, a comparison with well known antibody sequences indicated a strong homology with murine antibody light kappa chain variable domain and heavy chain variable domain. Those results allowed construction of a modeled structure that enabled visualisation of the binding pocket formed by the CDR amino acids. The representation will be useful to identify the interactions between the antibody and the antigen after binding characterization and determination of a potential epitope.

The protein was then expressed in bacterial cells and purification of the anti-hBub1 ScFv seemed successful when performed on a His trap column, with an imidazole gradient, as indicated by SDS-PAGE gel analysis and Western Blotting. However poor protein expression level was achieved and more protein would be required for better characterization of the protein and its binding.

When expressed in mammalian cells, ECFP-anti-hBub1 ScFv presented low fluorescence level compared to ECFP alone which could be due for example to improper folding of the anti-hBub1 ScFv or poor expression of the construct. In the particular case of ECFP-anti-hBub1 ScFv expression in mitotic cells, no expression at all was observable. Further characterization of the protein expression in HeLa cells was obtained through the expression timeline. The results seemed to point out a detrimental effect of the anti-hBub1 ScFv on the cells, leading to cell death. The absence of ECFP fluorescence after 24 hours in the timeline test explains the absence of ECFP fluorescence in mitotic cells, since the synchronised cells were imaged more than 24 hours after transfection.

**CHAPTER 3:**  
**DESIGN OF A BETA-LACTAMASE BASED LABELLING**  
**SYSTEM**

### 3.1 INTRODUCTION

As discussed in Section 1.1.4,  $\beta$ -lactamases have been used as catalytic reporters due to their versatility, their ability to catalyze the rapid hydrolysis of  $\beta$ -lactam substrates, and the possibility to design a large variety of substrates. However, the exact enzyme mechanism is still not very well established and various  $\beta$ -lactamase mutants have been prepared in an attempt to understand it and determine the role of specific residues. In particular, the Glu166Asn mutants of the TEM1  $\beta$ -lactamase as well as of other class A  $\beta$ -lactamases were investigated [124]. Whenever kinetic studies were performed, both acylation and deacylation rates appeared to be decreased by the mutation [124, 125], and a much higher impact on the deacylation step was observed. Interestingly, the TEM1 Glu166Asn mutant, when reacted with a  $\beta$ -lactam substrate, yields a very stable acyl-enzyme [126] adduct. This adduct has been observed in X-ray crystal structures of the enzyme [48] (Figure 21). The mechanism of formation of the acyl-enzyme from the Glu166Asn mutant  $\beta$ -lactamase has not yet been elucidated. It is believed that in the case of the replacement of the negatively charged Glu166 by a neutral asparagine, the catalytic acylation of the E166N mutant enzyme must rely on an alternative mechanism without the direct participation of Glu166.

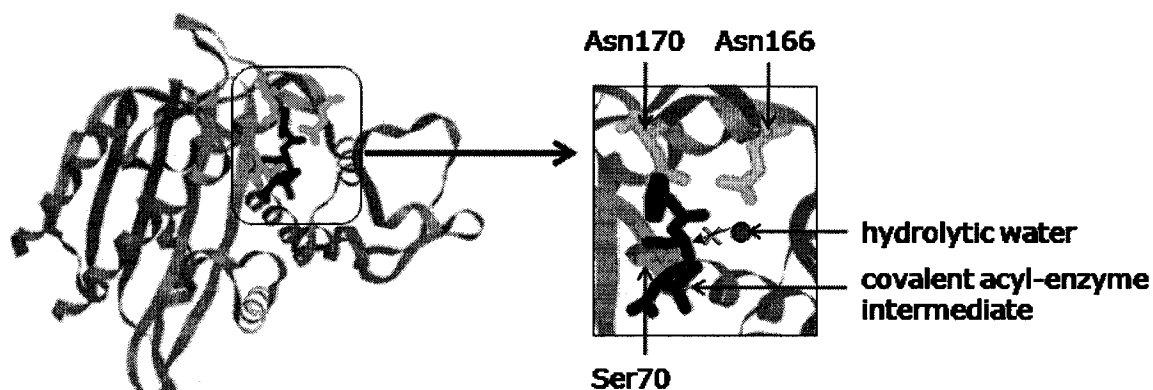


**Figure 21** Acyl-enzyme intermediate of TEM1  $\beta$ -lactamase. Shown is the three-dimensional structure of the acyl-enzyme intermediate of the E166N mutant of TEM1  $\beta$ -lactamase during  $\beta$ -lactam hydrolysis (PDB ID 1FQG). Penicillin G is covalently bound to the O of Ser70 in the acyl-enzyme.

Such deacylation impaired mutants, capable of a relatively fast acylation step and a slow deacylation step, are of great interest in the perspective of cell labelling through  $\beta$ -lactamase. Recently, a mutant  $\beta$ -lactamase was used in the design of a fluorescent biosensor for the detection of antibiotics [127], widening once again the scope of the applications for this enzyme. Furthermore, a hybrid system technique for bioorthogonal chemical labelling (1.1.3) using a mutant  $\beta$ -lactamase and a labelled substrate as an enzyme-inhibitor couple appears as an interesting labelling strategy for recombinant proteins expressed in live cells

As mentioned in 1.1.3, the availability of substrate analogues fused to appropriate labels is essential for bioorthogonal chemical labelling. In the case of mutant  $\beta$ -lactamase labelling, a variety of  $\beta$ -lactamase substrates such as the chromogenic substrates CENTA, nitrocefim and the fluorogenic substrates Bocillin 650/665 and Bocillin FL are commercially available. Furthermore it is possible to envisage the design of a large range of substrate analogues with, for example, longer wavelength for better tissue penetration, better spectral separation from cellular auto fluorescence or fused to a different kind of label.

In this chapter several  $\beta$ -lactamase substrates containing different functional group were used: two well characterized chromogenic substrates, CENTA and nitrocefim, a fluorogenic substrate, Bocillin FL, and a novel ketone cephalosporin substrate (Figure 22). CENTA is a chromogenic cephalosporin that is readily hydrolyzed by many  $\beta$ -lactamases including class A TEM1  $\beta$ -lactamases [128]. Light yellow CENTA ( $\lambda_{\max} = 346$  nm) releases a bright yellow chromophore ( $\lambda_{\max} = 405$  nm) upon hydrolysis, allowing for easy monitoring of the reaction. Nitrocefim, also known as 3-(2,4-dinitrostyryl)-(6R, 7R)-7-(2-thienylacetamido)-ceph-3-em-4-carboxylic acid E-isomer, is a yellow chromogenic cephalosporin based substrate ( $\lambda_{\max} = 390$  nm) that is quickly hydrolysed by many  $\beta$ -lactamases to form a red product ( $\lambda_{\max} = 486$  nm) [62, 129]. Bocillin FL is a commercially available fluorescent penicillin that has been demonstrated to bind to penicillin-binding proteins [64, 65]. It fluoresces at 511 nm upon excitation at 504 nm.

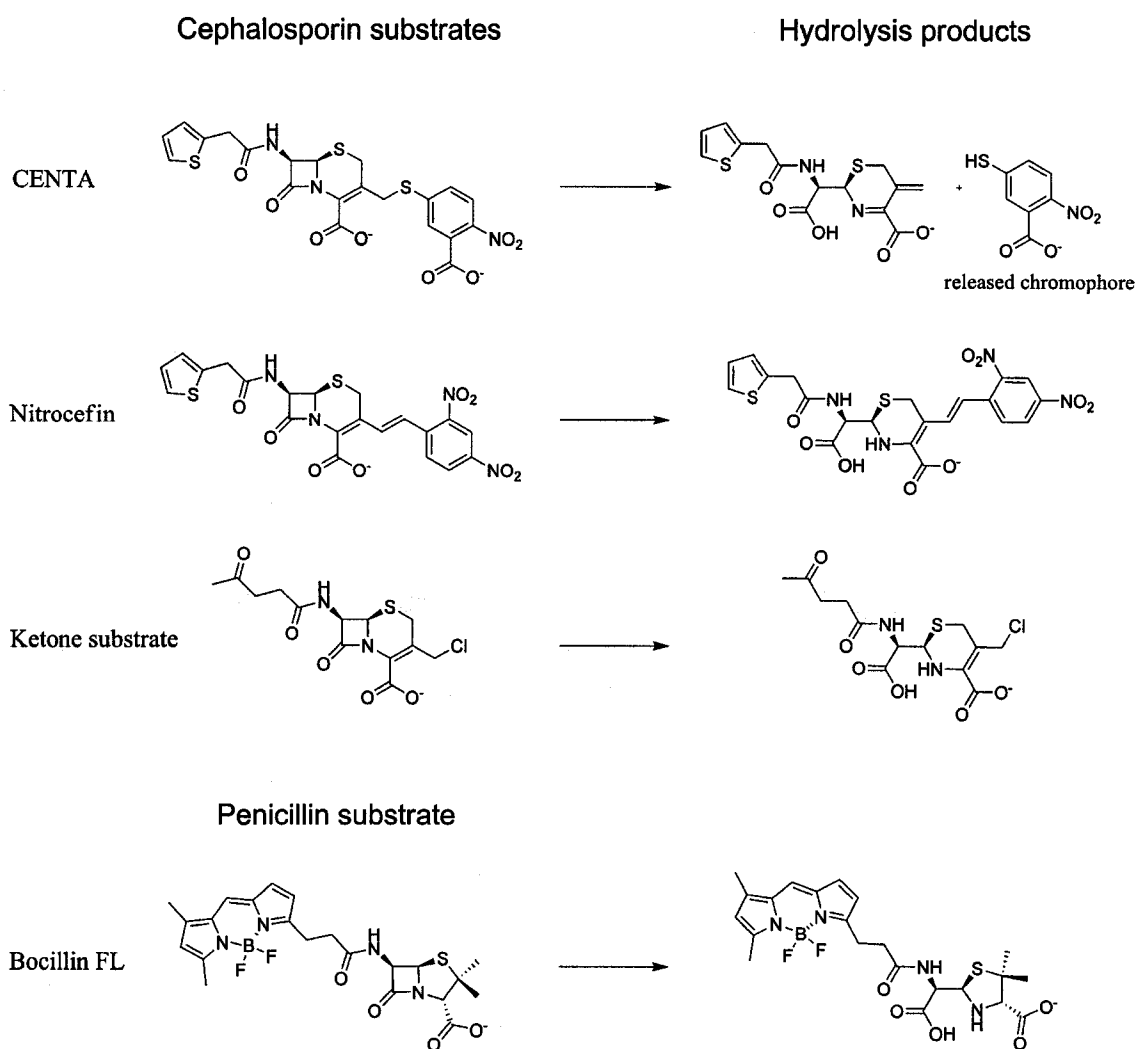


**Figure 22** Structure of the  $\beta$ -lactamase substrates used and of their hydrolysis products. CENTA, nitrocefin and the ketone substrate are cephalosporin substrates and Bocillin FL is a penicillin substrate

The ketone cephalosporin  $\beta$ -lactamase substrate, named (6R,7R)-3-(chloromethyl)-8-oxo-7-(4-oxopentanamido)-5-thia-1-azabicyclo[4.2.0]oct-2-ene-2-carboxylic acid, is not fluorescent and does not undergo any changes in absorbance upon hydrolysis. As a consequence, other compounds were tested to label the acyl-enzyme by bioorthogonal reaction with the ketone substrate. Ketones can be chemoselectively ligated with hydrazides under physiological conditions [130] through the formation of an acyl-hydrazone. Two hydrazide derivatives, Lucifer yellow CH and Biotin-XX-hydrazide, were used for conjugation with the ketone substrate (Figure 23).

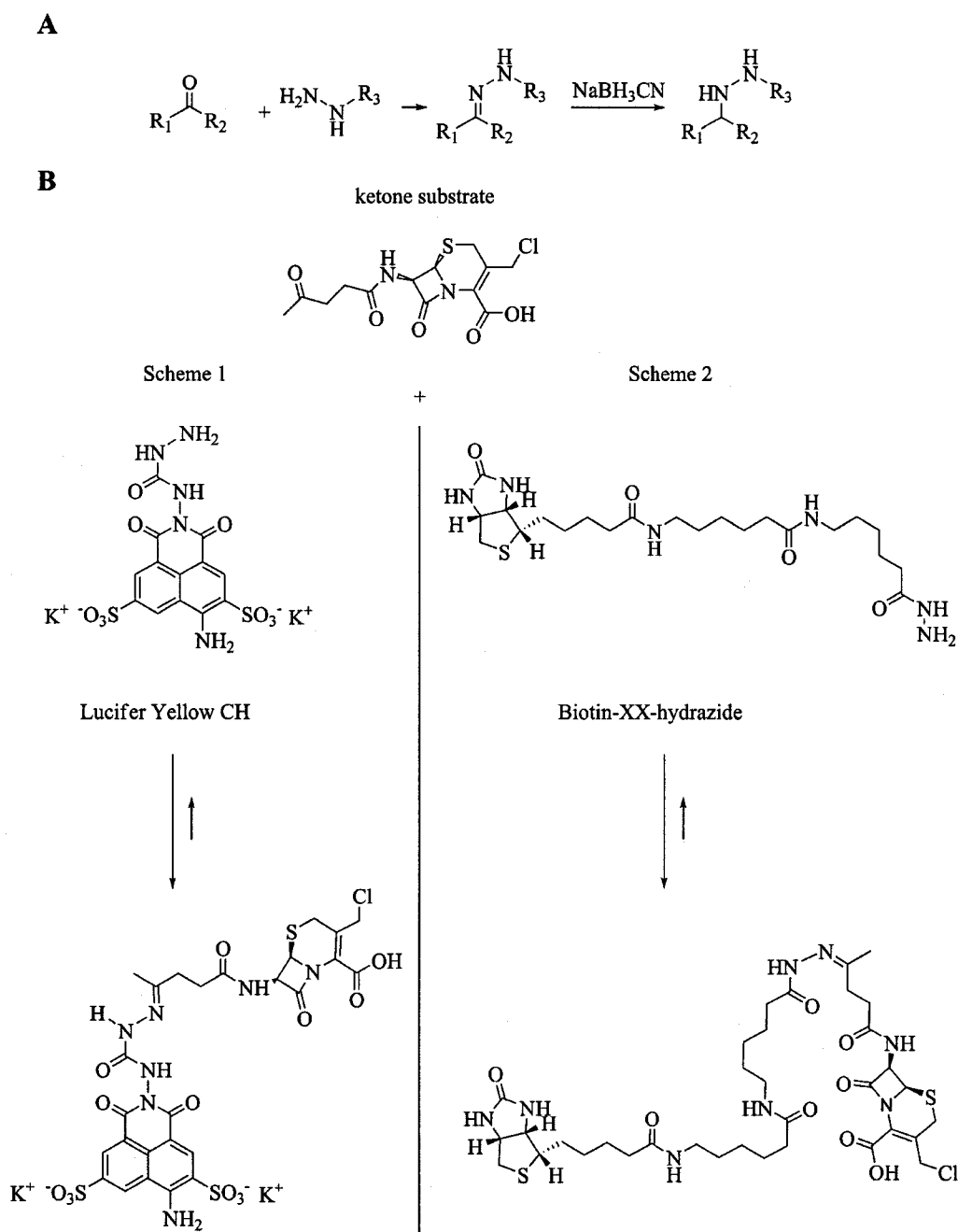


**Figure 23** Ligation of ketones with hydrazides. *A*. General scheme of the reaction of a ketone with a hydrazine to form a hydrazone and reduction by  $\text{NaBH}_3\text{CN}$ . *B*. Specific reaction of the ketone substrate with Lucifer yellow CH (*B*, Scheme 1) or with Biotin-XX-hydrazide (*B*, Scheme 2).

Lucifer Yellow CH is a well characterized fluorescent hydrazide derivative [131, 132] and can be detected directly at 528 nm upon excitation at 425 nm. However, Biotin-XX-hydrazide is a non fluorescent hydrazide derivative and must be detected indirectly, with

the fluorescent streptavidin-fluorescein for example. Streptavidin rapidly and effectively binds to biotin to form a complex with an exceptionally high affinity and stability [133]. Fluorescein is a commonly used fluorophore with an absorption maximum at 494 nm and emission maximum of 518 nm and can be chemically conjugated to streptavidin via primary amines. The hydrazide linkage is reversible, and sodium cyanoborohydride ( $\text{NaBH}_3\text{CN}$ ) can be added in order to reduce the hydrazone and bind irreversibly the ketone and Lucifer Yellow or Biotin Hydrazide.

In this chapter, progress toward the design of a new in situ labelling strategy for introducing a wide variety of labels into recombinant proteins expressed in live cells, based on the reaction of a deacylation impaired mutant of TEM1  $\beta$ -lactamase with several cephalosporin and penicillin based substrates are described. First a deacylation impaired mutant of a  $\beta$ -lactamase is made, expressed in bacteria and characterized. The mutant is then tested with various substrates in vitro. Finally, the mutant is expressed on the surface of mammalian cells and tested with substrates.

## **3.2 MATERIAL AND METHODS**

### **3.2.1 General material and methods**

General materials and methods were identical to those described in Section 2.2.1. The ketone substrate used for binding to E166N  $\beta$ -lactamase was a gift from Zhihua Yang, from the Department of Chemistry at the University of Alberta. The mCherry gene was a gift from the lab of Roger Y. Tsien, Department of Pharmacology, Department of Chemistry & Biochemistry, University of California, San Diego, USA.

### **3.2.2 Cloning and site-directed mutagenesis of TEM1 beta-lactamase**

The WT  $\beta$ -lactamase bacterial expression plasmid was created by PCR amplification of the TEM1  $\beta$ -lactamase gene lacking the export sequence, with a 5' primer encoding a NheI site and a 3' primer encoding a XhoI site. The PCR product was then purified,

digested and ligated into the pET28b vector (Novagen) that had been previously digested with the same restriction enzymes. The sequence of the WT  $\beta$ -lactamase was confirmed by sequencing.

Subsequent site-directed mutagenesis to introduce the Glu166Asn substitution was performed following the QuikChange® protocol (Stratagene). The primers used for mutagenesis were 5'- C CTT GAT CGT TGG **AAC** CCG GAG CTG AAT G - 3' and its complement, where the 2 mutated bases responsible for changing the position 166 codon (underlined) from glutamate to asparagine are in bold. The sequence of the mutant was confirmed by sequencing.

The WT  $\beta$ -lactamase fusion with platelet-derived growth factor receptor transmembrane domain (PDGFR-TM) mammalian expression plasmid (pDisplay-WT- $\beta$ -lactamase) was based on the pDisplay plasmid (Invitrogen). PCR amplification of the gene encoding WT  $\beta$ -lactamase was performed using a 5' primer encoding a BglII site and a 3' primer encoding a PstI restriction site. The purified and digested PCR product was ligated into the pDisplay vector (Invitrogen) that had been previously digested with the same restriction enzymes. To create the E166N  $\beta$ -lactamase-PDGFR-TM expression vector (pDisplay-E166N- $\beta$ -lactamase), an identical procedure was used. The sequences of both constructs were confirmed by sequencing.

A third plasmid, mCherry-PDGFR-TM mammalian expression vector was made following the same procedure, starting from mCherry DNA.

### **3.2.3 Expression, purification and mass spectrometry characterization of WT and mutant $\beta$ -lactamases**

Both WT and E166N  $\beta$ -lactamases were prepared in sufficient quantity for characterization, by transformation of *E. coli* strain BL21(DE3) with the pET28b vectors containing the genes of interest. A 1 mL Luria-Bertini media (LB) culture supplemented with kanamycin (25  $\mu$ g/mL) was inoculated with a single colony and allowed to grow overnight (37 °C and 225 rpm). The culture was then diluted into 1 litre of LB media



containing kanamycin (25 µg/mL) and allowed to grow for 3 h at 37 °C before induction with IPTG (1 mM). The culture was grown overnight at 25 °C and the cells were harvested by centrifugation. The inclusion bodies were solubilised in denaturing lysis buffer (100 mM NaH<sub>2</sub>PO<sub>4</sub>, 10 mM Tris-Cl and 8 M urea pH 8). Proteins were purified on Ni-NTA agarose beads (Qiagen), under denaturing conditions. Protein purity was assessed by SDS-PAGE.

First, the unfolded proteins were dialysed against 50 mM potassium phosphate buffer pH 6, for 3 h at room temperature, causing the protein to precipitate, and centrifuged at 8000 g for 15 min. Then the unfolded proteins were refolded as described previously [134]. Protein concentrations were assessed after refolding.

The approximate masses of both WT and E166N β-lactamase were determined by matrix-assisted laser desorption/ionization-time of flight (MALDI-TOF) mass spectrometry, on a Voyager Elite MALDI instrument (Applied Biosystems, formerly PE Biosystems). The proteins samples were in solution in 50 mM potassium phosphate (pH 7). The spots were obtained by a 2 layers technique with sinapinic acid as matrix. The first layer of sinapinic acid (8 mg/ml in 4:1 acetone:methanol) was spotted on a silver plate, and allowed to dry. The second layer was obtained by spotting a mixture of equal volumes of the samples and a solution of sinapinic acid (10 mg/mL in 1:1 acetonitrile: 0.1 % TFA in water).

A more accurate mass was determined for WT β-lactamase by electrospray ionization (ESI) mass spectrometry in positive ionisation mode. WT β-lactamase in solution in 50 mM ammonium acetate buffer pH 7 was analysed on a Mariner Biospectrometry Workstation (Applied Biosystems; formerly PE Biosystems), by the University of Alberta chemistry department Mass Spectrometry facility.

### 3.2.4 Preliminary kinetic characterization of WT and E166N $\beta$ -lactamases

The hydrolysis of the chromogenic  $\beta$ -lactamase substrates CENTA (Calbiochem) and nitrocefin (Calbiochem) were monitored in presence of both refolded enzymes, as preliminary activity based tests.

**Nitrocefin.** Nitrocefin, also known as 3-(2,4-dinitrostyryl)-(6R,7R)-7-(2-thienyl-acetamido)-ceph-3-em-4-carboxylic acid, E-isomer (Calbiochem) was used for preliminary kinetic characterization. Nitrocefin's hydrolysis was monitored by recording the increase in absorbance at 486 nm, with a DU800 UV/Visible spectrophotometer (Beckmann). Nitrocefin stock solution (0.5 mg/mL) was prepared by dissolution of 1 mg of nitrocefin in 100  $\mu$ L of dimethyl sulfoxide (DMSO) and addition of 1.9 mL of 100 mM sodium phosphate buffer pH 7. Aliquots were frozen at -20  $^{\circ}$ C. All experiments were performed using a similar procedure to the one described previously [62] in 50 mM sodium phosphate (pH 7) after incubation of enzymes and substrates at 37  $^{\circ}$ C, for 30 minutes.

The spectra of nitrocefin and hydrolysed nitrocefin were recorded respectively before and after hydrolysis of 150  $\mu$ M of nitrocefin with 23 nM of WT  $\beta$ -lactamase for 160 minutes at 37  $^{\circ}$ C. For the time course, the final concentration of nitrocefin ranged from 10 to 250  $\mu$ M and was hydrolysed at room temperature with 23 nM of WT enzyme.

In the case of E166N  $\beta$ -lactamase, a quick preliminary test was performed. Nitrocefin (100  $\mu$ M and 20  $\mu$ M final concentration) was hydrolysed with 20 nM and 70 nM of E166N  $\beta$ -lactamase, respectively, for 400 s and time courses were recorded.

**CENTA.** The preliminary kinetic experiments of both E166N and WT  $\beta$ -lactamases with CENTA (Calbiochem), were performed using a modification of a previously published procedure [61, 128]. All experiments were performed in 50 mM potassium phosphate (pH 7) after incubation of enzymes and substrate at 37  $^{\circ}$ C, for 30 minutes. The hydrolysis of CENTA was monitored by recording the absorbance variation at 405 nm on a DU800 UV/Visible spectrophotometer (Beckmann). CENTA stock solution was obtained by dissolution of CENTA (Calbiochem) into 50 mM potassium phosphate buffer pH 7. The

concentrations of CENTA ranged from 30 to 620  $\mu\text{M}$ , for final reaction volumes of 250  $\mu\text{L}$  for E166N and 500  $\mu\text{L}$  for WT  $\beta$ -lactamases. E166N and WT  $\beta$ -lactamases were used at final concentrations of 254 nM and 23 nM respectively. The time courses of CENTA hydrolysis were recorded.

Finally, a quick comparison of the reaction of WT and E166N  $\beta$ -lactamases at the same concentration with 150  $\mu\text{M}$  CENTA was performed. The time course of CENTA hydrolysis was recorded for WT and E166N  $\beta$ -lactamases used at a final concentration of 95 nM.

### **3.2.5 Characterization of the binding of E166N $\beta$ -lactamase to $\beta$ -lactam substrates**

**Gel displacement assay.** To test the labelling of the mutant  $\beta$ -lactamase with various substrates, gel displacement assays were performed.

A gel displacement assay was performed using Bocillin FL as  $\beta$ -lactamase substrate and a procedure adapted from Zhao *et al.* [64]. E166N  $\beta$ -lactamase (1.5  $\mu\text{g}/0.05$  nmol) was reacted with Bocillin FL penicillin (0.47  $\mu\text{g}/0.7$  nmol), sodium salt (Invitrogen) in PBS in a total volume of 13.5  $\mu\text{L}$  at 37  $^{\circ}\text{C}$  for 30 minutes. The same procedure was followed for WT  $\beta$ -lactamase and E166N  $\beta$ -lactamase pre-incubated with CENTA (2.4  $\mu\text{g}/4.5$  nmol and 5.8  $\mu\text{g}/10.8$  nmol) or the ketone substrate (2.2  $\mu\text{g}/6.3$  nmol and 5.5  $\mu\text{g}/15.9$  nmol). Samples were run on a 12 % SDS-PAGE gel after denaturation by boiling 3 minutes at 95  $^{\circ}\text{C}$  in presence of SDS gel loading buffer. To visualize the labelled  $\beta$ -lactamases, the gel was imaged with a custom built device. The gel is put under the light from a 175 W xenon arc lamp (Sutter) passed through a 470/40 nm bandpass filter (Chroma) and into a bifurcated fiber optic bundle (Newport). The light exiting the fibre optic bundle illuminates a 10 cm diameter area with an irradiance of approximately 0.04  $\text{mW}/\text{cm}^2$ . The gel was imaged after passing through a 510/20 nm bandpass filter (Chroma), with a monochrome Retiga 2000R 12-bit cooled CCD camera (QImaging) operated through the software Image Pro Plus 6 (Media Cybernetics). The gel was then stained with Silver Stain Plus Kit (BioRad).

Mixtures of E166N  $\beta$ -lactamase (2.4  $\mu$ g) and ketone substrate (0.6  $\mu$ g/1.7 nmol) were reacted with 2  $\mu$ g (3.8 nmol) of Lucifer Yellow CH potassium salt (Invitrogen), or 4.2  $\mu$ g (8.7 nmol) of Biotin-XX-hydrazide (6-((6-((biotinoyl)amino)hexanoyl)amino)hexanoic acid, hydrazide; Invitrogen) and 5  $\mu$ g (0.4 nmol) of streptavidin-fluorescein (Invitrogen) in presence or not of 0.08  $\mu$ mol of NaBH<sub>3</sub>CN. Samples were run on a 12.5% SDS-PAGE in presence of SDS gel loading buffer. To identify the labelled  $\beta$ -lactamase, the fluorescence was visualized as described above (excitation filters 436/20 for Lucifer Yellow and 500/20 for streptavidin-fluorescein, yellow goggles), and then stained with Coomassie blue.

The WT  $\beta$ -lactamase was reacted and analysed in the same conditions in order to get a negative control.

**Ni-NTA fast purification of the reacted enzyme.** To further characterize the E166N  $\beta$ -lactamase binding to Bocillin FL  $\beta$ -lactam substrate, reaction mixtures of E166N  $\beta$ -lactamase and substrate were purified on Ni-NTA.

The mutant and WT  $\beta$ -lactamases in 50 mM phosphate buffer pH 6 (3.4 nmol) were reacted in parallel with Bocillin FL in PBS buffer pH 7 (4.5 nmol) for 30 minutes at 37 °C in a total volume of 700  $\mu$ L. The mixtures were then incubated at 4 °C for 1 h, in presence of 40  $\mu$ L Ni-NTA agarose beads (Qiagen). The supernatants were removed after spinning (6000 rpm, 4 min). The beads were then washed with Ni-NTA wash buffer containing 20 mM imidazole and spinned down repeatedly until fluorescence in the supernatants was constant (1600  $\mu$ L of buffer, total). The proteins were then eluted with twice 200  $\mu$ L of Ni-NTA elution buffer containing 250 mM imidazole. The fluorescence was monitored at each step, with a Safire<sup>2</sup> quad-4 monochromator based microplate detection system (Tecan). Samples were excited at 490 nm and the corresponding emission spectra (500-550 nm) were recorded.

### **3.2.6 Expression and display of $\beta$ -lactamase on HeLa cell surface**

HeLa cells were grown on microscope coverslips and transfected with the vectors pDisplay-mCherry, pDisplay-E166N- $\beta$ -lactamase and pDisplay-WT- $\beta$ -lactamase. Alternatively, cells were cotransfected with pDisplay-WT- $\beta$ -lactamase or pDisplay-E166N- $\beta$ -lactamase in combination with pDisplay-mCherry.

Live HeLa cells transfected with pDisplay-mCherry were imaged using the appropriate bandpass filters, HQ 535/30 for excitation and HQ 610/75 for emission [110]. Another dish of cells was used for live cell immunofluorescence, 2 days after transfection. After washing with PBS, the cells were incubated with 25  $\mu$ L rabbit HA-Tag polyclonal antibody (Clontech), the primary antibody, at 2  $\mu$ g/mL for 5 minutes. After rinsing three times with PBS, 25  $\mu$ L of the secondary antibody Alexa Fluor® 488 Goat Anti-Rabbit highly cross-adsorbed antibody (Invitrogen) at 10  $\mu$ g/mL was added for 5 minutes. The cells were washed again three times with PBS and then imaged using the appropriate filters, HQ 500/20 and HQ 535/50 for excitation, and HQ 535/30 and HQ 610/75 for emission.

### **3.2.7 Labelling of HeLa cells with Bocillin FL**

HeLa cells were grown and cotransfected on microscope coverslips as described above in 3.2.6. Twenty hours after transfection, the cells were fixed with 4 % paraformaldehyde for 10 min, permeabilized with PBS + 0.5 % Triton X100 and incubated with 5  $\mu$ g of Bocillin FL in a total volume of 25  $\mu$ L, for 40 minutes at room temperature. The coverslips were washed once with PBS + 0.1 % Triton X100, repeatedly with PBS and mounted on microscope slides. The cells were imaged as described previously in 2.2.1 [110], using the appropriate filters, HQ 500/20 for excitation and HQ 535/30 for emission.

### 3.3 RESULTS

#### 3.3.1 Cloning and site-directed mutagenesis of TEM1 beta-lactamase

The shortened TEM1  $\beta$ -lactamase gene used is derived from the *E. Coli* TEM1 gene. The 69 nucleotides encoding the first 23 amino acids are deleted. This allows for cytoplasmic expression of  $\beta$ -lactamase in mammalian cells by removing the N-terminal region of the  $\beta$ -lactamase coding for the bacterial periplasmic signal sequence. The shortened gene was amplified by PCR and cloned into the pET28b vector (Novagen) in frame with both N and C-terminal His-Tag. The new gene will be named *WT-bla* hereafter. Site-directed mutagenesis was used to introduce the Glu166Asn mutation. The mutation was carried out in the *WT-bla* gene, by replacing the glutamic acid codon (GAA) by the asparagine codon (AAC) using the QuickChange® method (Stratagene) as summarized in Figure 24. The design of the primers and the choice of the cycling parameters followed the guidelines of the QuickChange® manual ([www.stratagene.com/manuals/200518.pdf](http://www.stratagene.com/manuals/200518.pdf)).

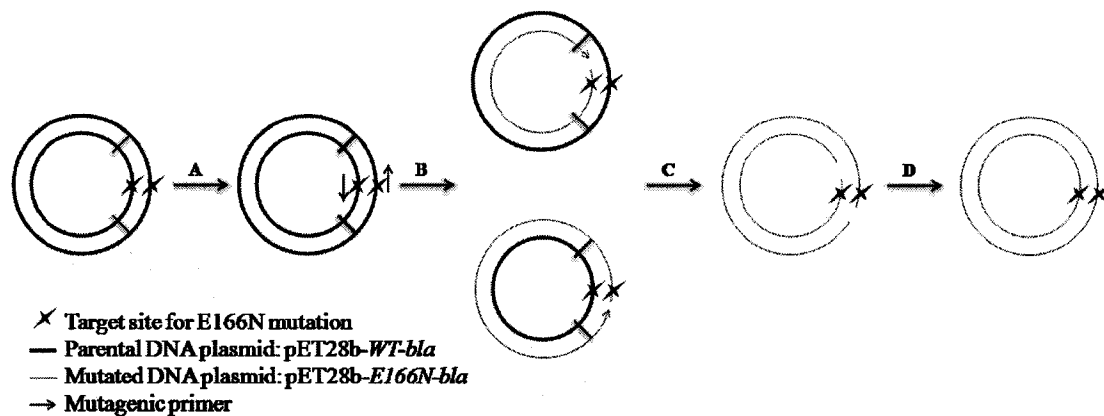


**Figure 24** Flow Chart of the QuickChange® method. During temperature cycling (*A*, *B*) the plasmid containing the gene of interest is denatured. The primers containing the desired mutation can then anneal (*A*) to the vector. Pfu DNA polymerase performs the extension and incorporation of the primers (*B*) to yield nicked circular strands. The methylated, parental DNA template is digested with Dpn1 (*C*). The nicked, circular mutated dsDNA is transformed in DH10B competent *E. Coli* and yields the mutated plasmid after miniprep (*D*).

Alignment of the DNA sequences of TEM1  $\beta$ -lactamase, *WT-bla* and *E166N-bla* (Figure 25) was performed using the ClustalW service online at the European Bioinformatics Institute [135].

The *WT-bla*, *E166N-bla* and mCherry genes were PCR amplified with the appropriate primers, and cloned in pDisplay in frame with an N-terminal Ig  $\kappa$  leader chain sequence, and a C-terminal PDGFR-TM domain. The primers encoded the removal of the stop codon at the end of all 3 genes to allow proper gene fusion with PDGFR-TM and proper localization of the protein after expression.

```

      10                               50
T   MSIQHFRVALIPFFAAFCLPVFAHPETLVKVKDAEDQLGARVGYIELDLNSGKILESFRP
W   MGSSHHHHHHSSGLVPRGSHMASHPETLVKVKDAEDQLGARVGYIELDLNSGKILESFRP
E   MGSSHHHHHHSSGLVPRGSHMASHPETLVKVKDAEDQLGARVGYIELDLNSGKILESFRP

                               100
T   EERFPMMSTFKVLLCGAVLSRIDAGQEQLGRRIHYSQNDLVEYSPVTEKHLTDGMTVREL
W   EERFPMMSTFKVLLCGAVLSRIDAGQEQLGRRIHYSQNDLVEYSPVTEKHLTDGMTVREL
E   EERFPMMSTFKVLLCGAVLSRIDAGQEQLGRRIHYSQNDLVEYSPVTEKHLTDGMTVREL

                               150
T   CSAAITMSDNTAANLLLTTIGGPKELTAFLHNMGDHVTRLDRWAPELNEAIPNDERDTTM
W   CSAAITMSDNTAANLLLTTIGGPKELTAFLHNMGDHVTRLDRWAPELNEAIPNDERDTTM
E   CSAAITMSDNTAANLLLTTIGGPKELTAFLHNMGDHVTRLDRWAPELNEAIPNDERDTTM

                               200
T   FVAMATTLRKLLTGELLTLASRQQLIDWMEADKVAGPLLRSALPAGWFIADKSGAGERGS
W   FVAMATTLRKLLTGELLTLASRQQLIDWMEADKVAGPLLRSALPAGWFIADKSGAGERGS
E   FVAMATTLRKLLTGELLTLASRQQLIDWMEADKVAGPLLRSALPAGWFIADKSGAGERGS

                               250                               290
T   RGIIAALGPDGKPSRIVVIYTTGSQATMDERNRQIAEIGASLIKHW
W   RGIIAALGPDGKPSRIVVIYTTGSQATMDERNRQIAEIGASLIKHWLEHHHHHHH
E   RGIIAALGPDGKPSRIVVIYTTGSQATMDERNRQIAEIGASLIKHWLEHHHHHHH

```

**Figure 25** Alignment of TEM1  $\beta$ -lactamase (T), WT  $\beta$ -lactamase (W), and E166N  $\beta$ -lactamase (E) sequences. The bacterial periplasmic signal sequence of TEM1 (underlined), is missing in WT and E166N  $\beta$ -lactamase. Amino acid 166, according to Ambler's numbering [41], corresponds to the Glu166Asn mutation.

The pDisplay-mCherry vector was prepared in order to get a control vector. It allowed for easy monitoring of transfection efficiency and expression through mCherry fluorescence.

mCherry, a monomeric red FP with an excitation maximum at 587 nm and an emission maximum at 610nm, was chosen because of its well described characteristics and spectral properties [14].

### 3.3.2 Expression, purification and mass spectrometry characterization of WT and mutant $\beta$ -lactamases

The *WT-bla* and *E166N-bla* gene were cloned in the pET28b vector (Novagen) which usually allows for very high expression levels of the recombinant protein in *E. Coli* under control of the T7 promoter.

Very high levels of expression were indeed attained for both WT and E166N  $\beta$ -lactamases and the proteins accumulated as inclusion bodies. The presence of the His-Tags allowed for fast purification of the protein with Ni-NTA, even under fully denaturing conditions. After loading on the Ni-NTA column, the proteins were eluted first with denaturing buffer at pH 5.9 and then at pH 3.1. The use of two different pHs for the elution buffer allowed for a better elution of the protein.

After purification, the unfolded proteins were precipitated out by dialysis against 50 mM potassium buffer pH 6 and recovered. Protein concentrations were kept low during resuspension of the proteins, E166N  $\beta$ -lactamase in particular, to minimize precipitation during the refolding step. Both unfolding and refolding steps were performed at room temperature. During refolding, some insoluble particles precipitated out and were removed by centrifugation. A second cycle of unfolding/refolding was performed with the recovered insoluble particles to maximise the yield of recovered protein.

The purity of both proteins was checked after Ni-NTA purification (Figure 26) and the concentrations of both proteins were determined after refolding (Table 1). The value of the extinction coefficient of  $\beta$ -lactamase at 280 nm,  $\epsilon_{280\text{nm}} = 28\,085\text{ M}^{-1}\cdot\text{cm}^{-1}$ , was calculated using the ExPaSy ProtParam tool [136] from the Swiss Institute of Bioinformatics (SIB) [137]. The computed extinction coefficient and the calculated molecular weights were used for the calculation of the protein concentrations.



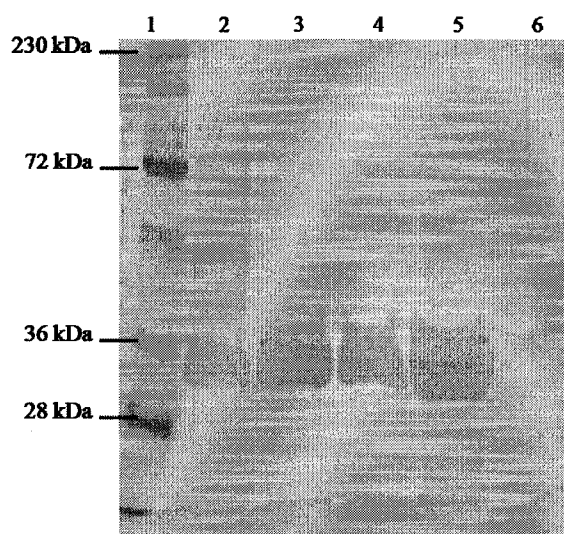


**Figure 26** E166N  $\beta$ -lactamase purification. 12.5 % SDS-PAGE gel electrophoresis of the samples of E166N  $\beta$ -lactamase during Ni-NTA purification. Lane 1 – PageRuler Prestained Protein Ladder Plus (Fermentas), lane 2 – Flow through (4  $\mu$ L), lanes 3/4 – eluates at pH 5.9 (10  $\mu$ L), lanes 5/6 – eluates at pH 3.1 (10  $\mu$ L).

**Table 1** Protein concentrations and total protein after refolding

$\beta$ -lactamase	Concentration mg/mL	Concentration $\mu$ M	Total protein mg	MW g/mol
E166N	0.16	4.9	4.8	32451.8
WT	0.15	4.6	1.5	32466.8

The approximate masses of WT and E166N  $\beta$ -lactamases were determined by MALDI-TOF. The masses recorded were 32357 Da and 32349 Da for WT and E166N  $\beta$ -lactamase respectively (Appendix C). Both masses were in relatively good agreement (3% error) with the calculated masses of 32466.8 Da and 32451.8 Da respectively. Interestingly, the MALDI signal strength was very different for WT and E166N  $\beta$ -lactamases samples, in solution in the same buffer, at similar concentrations in enzymes (0.15  $\mu$ g/mL) and identical laser intensity, making it more difficult to identify E166N  $\beta$ -lactamase molecular peaks.

A supposedly more accurate mass, 32332 Da, was determined for WT  $\beta$ -lactamase in solution in 50 mM ammonium acetate buffer pH 7, by ESI in positive ionization mode (Appendix C). The mass is relatively close from the value of the calculated mass (4% error). An accurate mass of E166N could not be determined, since dialysis of the enzyme against various ESI compatible solvents resulted in precipitation of the protein.

### 3.3.3 Preliminary kinetic characterization of WT and E166N $\beta$ -lactamases

An initial velocity kinetic analysis of E166N and WT  $\beta$ -lactamases was performed by determination of the initial rates of the enzymatic reaction at varying concentrations of CENTA and nitrocefin. A thorough discussion of the rules used to interpret initial velocity and product inhibition plots is provided in Appendix A.

**Nitrocefin.** Nitrocefin is a substrate that is quickly hydrolysed by many  $\beta$ -lactamases (see 3.1). The spectrum of nitrocefin before and after hydrolysis with WT  $\beta$ -lactamase was recorded and is shown in Figure 27. The wavelength of the absorption maximum shifts from 390 nm to 486 nm upon hydrolysis with WT  $\beta$ -lactamase as reported previously for other  $\beta$ -lactamases [62].

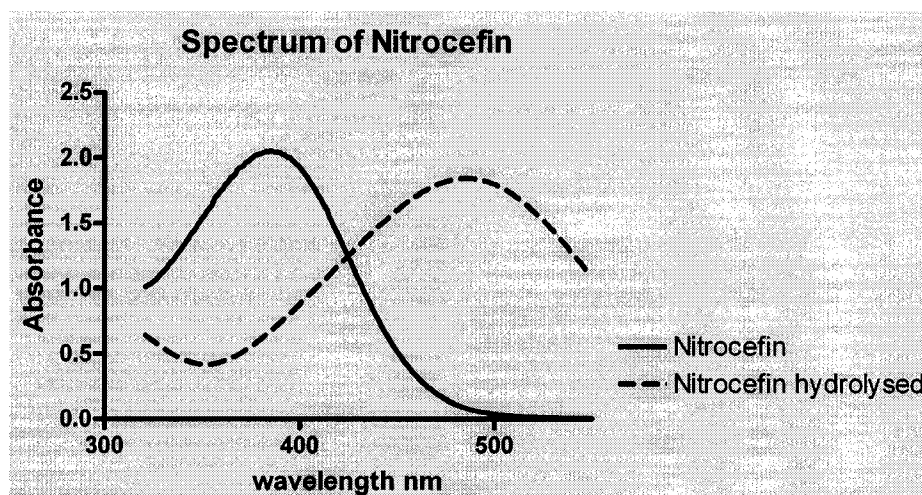


**Figure 27** Hydrolysis of nitrocefin. The change in absorbance spectra before and after hydrolysis allows for easy monitoring of  $\beta$ -lactamase activity. The yellow nitrocefin ( $\lambda_{\max} = 390$  nm) forms a red ( $\lambda_{\max} = 486$  nm) product upon hydrolysis.

Time courses of the hydrolysis of nitrocefin with WT  $\beta$ -lactamase were determined by continuously recording the absorbance at 486 nm. The concentration of hydrolysed nitrocefin (product) was calculated using the Beer-Lambert law and the value of the extinction coefficient variation  $\Delta\epsilon = 20500 \text{ M}^{-1}\cdot\text{cm}^{-1}$  at 486 nm. The formation of hydrolysis product was plotted in function of time for various substrate concentrations (Figure 28A).

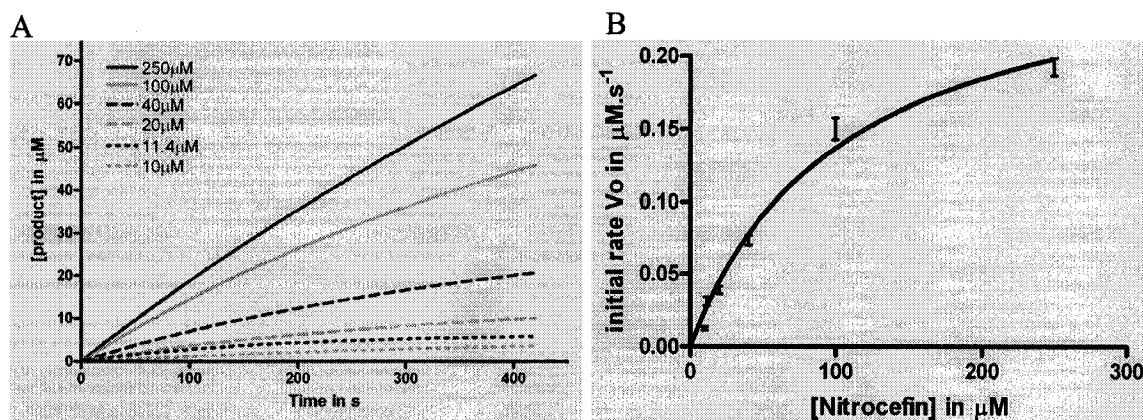


**Figure 28** Kinetics of nitrocefin hydrolysis with WT  $\beta$ -lactamase. *A.* Progress curves of the hydrolysis of 10 to 250  $\mu\text{M}$  of nitrocefin by 23 nM of WT  $\beta$ -lactamase. *B.* Michaelis – Menten plot for WT  $\beta$ -lactamase and the corresponding non linear regression. The fitted parameters are presented in Table 2.

WT  $\beta$ -lactamase initial rates ( $V_0$ ) were determined over 75 s for each concentration of substrate (4 replicates), averaged and plotted against the initial concentration of nitrocefin in a Michaelis-Menten plot (Figure 28B). The error bars represent the standard deviation obtained from 4 replicates. The  $k_{\text{cat}}$  and  $K_m$  values were derived from initial rates measurement by direct fitting on the hyperbolic equation by non linear regression and the acylation rate  $k_{\text{cat}}/K_m$  and deacylation rate  $k_{\text{cat}}$  were then recorded (Table 2).

The preliminary test of E166N  $\beta$ -lactamase with nitrocefin as substrate did not reveal any hydrolysis of the substrate. Under the experimental conditions used, the mixing dead-time was 5-10 s, time after which the absorbance started to be monitored, and any lag or burst that would be completed within a shorter time would not be detected. Therefore, the absence of observable change in absorbance at 486 nm could be due to fast burst kinetics taking place during this mixing-dead time. To overcome this problem, CENTA, a

substrate that exhibits slower acylation and deacylation rates in reaction with TEM1  $\beta$ -lactamase [128] was selected for further preliminary kinetic characterization.

**CENTA.** CENTA is a chromogenic cephalosporin that is readily hydrolyzed by class A TEM1  $\beta$ -lactamases (see 3.1). The kinetic analysis of WT and E166N  $\beta$ -lactamase with CENTA was performed in a similar manner to the one with nitrocefin.

Time courses of the hydrolysis of CENTA with WT and E166N  $\beta$ -lactamases were determined by continuously recording the absorbance at 405 nm. The concentration of product released upon hydrolysis of CENTA was calculated using the Beer-Lambert law and the value of the extinction coefficient variation  $\Delta\epsilon = 6400 \text{ M}^{-1}\cdot\text{cm}^{-1}$  at 405 nm [128]. The formation of hydrolysis product was plotted in function of time for various substrate concentrations (Figure 29).

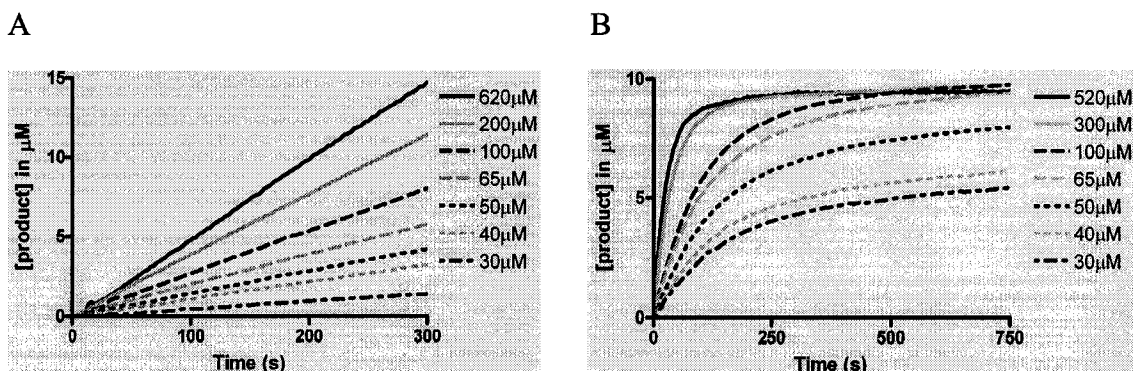


**Figure 29** Kinetics of CENTA hydrolysis with WT and E166N  $\beta$ -lactamase. Hydrolysis of CENTA by 23 nM of WT (A), and by 254 nM of E166N (B). Each curve is the average of 3 replicates (WT) or 4 replicates (E166N) at a given final concentration of CENTA.

The progress curves for the hydrolysis of CENTA with WT  $\beta$ -lactamase (Figure 29A) are very similar to the ones obtained for the hydrolysis of nitrocefin, and show a steady increase of the formation of hydrolysis product with time. WT  $\beta$ -lactamase initial rates were determined over 300 s for each concentration of substrate (3 replicates). They were then averaged and plotted against the initial concentrations of CENTA (Figure 30) and  $k_{\text{cat}}$  and  $K_{\text{m}}$  values were derived from initial rates measurement as described for

nitrocefin. The error bars represent the standard deviation obtained from 3 replicates. The acylation rate  $k_{\text{cat}}/K_m$  and deacylation rate  $k_{\text{cat}}$  were recorded (Table 2).

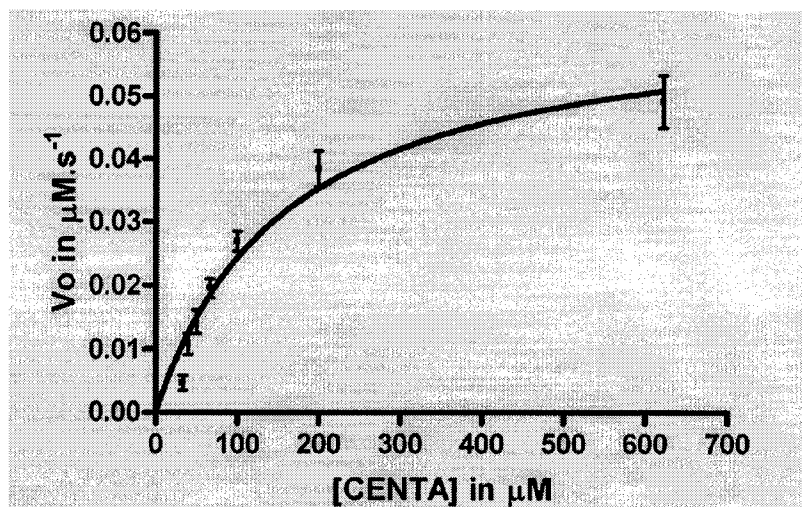


**Figure 30** Michaelis-Menten plot for WT  $\beta$ -lactamase. The initial rates ( $V_o$ ) were averaged and plotted against the initial concentration of CENTA and fitted on the hyperbolic equation by non linear regression. The error bars represent the standard deviation obtained from 3 replicates. The fitted parameters are presented in Table 2.

**Table 2** Kinetic parameters for interaction between WT  $\beta$ -lactamase and CENTA or nitrocefin

Substrate	WT			
	$V_{\text{max}}$ ( $\mu\text{M}^{-1}\cdot\text{s}^{-1}$ )	$K_m$ ( $\mu\text{M}$ )	$k_{\text{cat}}$ ( $\text{s}^{-1}$ )	$k_{\text{cat}}/K_m$ ( $\mu\text{M}^{-1}\cdot\text{s}^{-1}$ )
nitrocefin	0.27	105.1	12.20	0.116
CENTA	0.06	164.6	2.75	0.017

The results show a slightly faster acylation and deacylation of WT  $\beta$ -lactamase with nitrocefin than with CENTA, which corresponds to what has been reported for TEM1  $\beta$ -lactamase [128].

The progress curves for the hydrolysis of CENTA with E166N  $\beta$ -lactamase exhibit a burst followed by a linear phase (Figure 29B). The initial burst of product seen is much greater than the concentration of the enzyme, which is unexpected. The initial observed rates of hydrolysis ( $k_i^{\text{obs}}$ ) by E166N  $\beta$ -lactamase were determined over the time to reach a  $\Delta A_{405\text{nm}} = 0.015$  unit (i.e. [product] = 2.34  $\mu\text{M}$ ), which corresponds to the linear part of the burst, for each concentration of substrate (4 replicates). They were then averaged and plotted against the initial concentrations of CENTA and the irreversible inactivation constant  $k_i$ , inhibition constant  $K_i$ , and  $k_3$  value (Table 3) were derived from initial rates measurement as described in Appendix A. The second order rate of inactivation constant  $k_i/K_i$  was calculated.

**Table 3** Kinetic parameters for interaction between E166N  $\beta$ -lactamase and CENTA

Substrate	E166N			
	$K_i$ ( $\mu\text{M}$ )	$k_3$ ( $\mu\text{M}^{-1}\text{s}^{-1}$ )	$k_i$ ( $\mu\text{M}^{-1}\text{s}^{-1}$ )	$k_i/K_i$ ( $\text{s}^{-1}$ )
CENTA	540.3	$1.10^{-7}$	0.580	0.001

It is important to note that as mentioned earlier, under the experimental conditions used, the mixing dead-time was 5-10 s, and any lag or burst that would be completed within a shorter time could not be detected.

Finally, the progress curves of CENTA hydrolysis with WT and E166N  $\beta$ -lactamases at the same concentration (Figure 31) indicate a much more efficient hydrolysis in presence of the WT enzyme. Those results quickly summarize the kinetic differences observed between both enzymes.

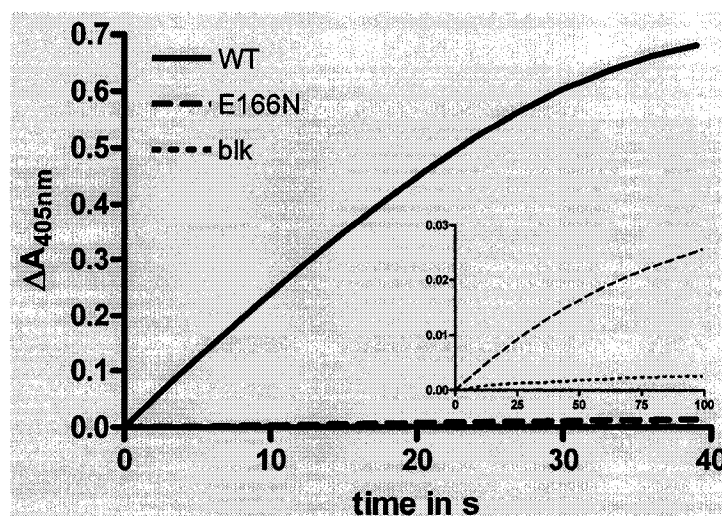


**Figure 31** Comparison of CENTA hydrolysis by WT and E166N  $\beta$ -lactamases. The solid line corresponds to the hydrolysis with WT  $\beta$ -lactamase, the long-dash line to the hydrolysis with E166N  $\beta$ -lactamase, whereas the short-dash line corresponds to auto hydrolysis of CENTA.

### 3.3.4 Characterization of the binding of E166N $\beta$ -lactamase to $\beta$ -lactam substrates by gel displacement assay

To determine the effectiveness of the various  $\beta$ -lactamase substrates for labelling and confirm the formation of the substrate labelled acyl-enzyme intermediate after reaction with the E166N mutant, binding assays were performed.

The gel displacement assay demonstrated fluorescent labelling of the E166N  $\beta$ -lactamase with Bocillin FL, and absence of such labelling of WT  $\beta$ -lactamase (Figure 32). The same gel displacement assay also tested for inhibition of the labelling by pre-incubation of the enzyme with CENTA or the ketone substrate at 2 different concentrations. A clear decrease in fluorescence was observed in both cases of pre-incubation of the mutant  $\beta$ -lactamase with CENTA or the ketone substrate. Those results suggested that CENTA and the ketone substrate both bind to the mutant  $\beta$ -lactamase during the pre-incubation, forming a stable acyl-enzyme, and preventing the enzyme to further react when Bocillin FL substrate was added.

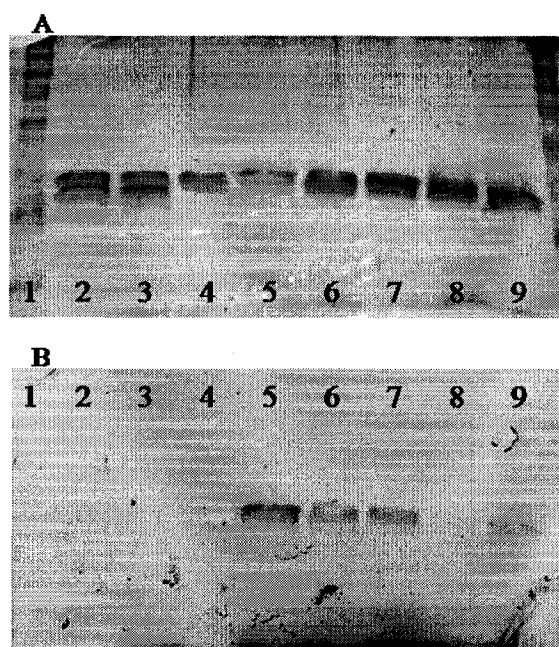


**Figure 32** Gel displacement assay of  $\beta$ -lactamase with Bocillin FL. Picture of the 12 % SDS-PAGE displacement assay gel, silver stained (A) and imaged by fluorescence (B) with the excitation filter 470/40 nm and the emission filter 510/20nm. Lanes 1&10 - protein ladder plus; lanes 2&3 - WT  $\beta$ -lactamase +/- Bocillin FL; lanes 4&5 - E166N  $\beta$ -lactamase +/- Bocillin FL; lanes 6&7 - E166N  $\beta$ -lactamase + Bocillin FL + CENTA (4.5 nmol /10.8 nmol); lanes 8&9 - E166N  $\beta$ -lactamase + Bocillin FL + ketone substrate (15.9 nmol/6.3 nmol).

To further characterize the binding of the mutant  $\beta$ -lactamase to the ketone substrate, another gel displacement assay was performed. A mixture of E166N  $\beta$ -lactamase and ketone substrate was reacted with either Lucifer Yellow CH potassium salt, or Biotin-XX-hydrazide and streptavidin-fluorescein in presence or absence of  $\text{NaBH}_3\text{CN}$ . The WT  $\beta$ -lactamase was reacted and analysed in the same conditions in order to get a negative control. After separation by SDS-PAGE, fluorescent imaging and staining, no obvious displacement was observed on the gel for any of the reaction mixtures. The linkage of the E166N  $\beta$ -lactamase to the reacted ketone substrate could not be verified.



### 3.3.5 Characterization of the binding of E166N $\beta$ -lactamase to $\beta$ -lactam substrates by Ni-NTA fast purification of the reacted enzyme

After determination of the binding effectiveness of E166N  $\beta$ -lactamase to Bocillin FL by gel displacement assay, the binding was further tested by tentative purification of the acyl-enzyme intermediate with Ni-NTA.

To monitor the presence of Bocillin FL in solution, fluorescence at 511 nm was recorded upon excitation at 490 nm with a fluorescent microplate reader. After reaction of 4.9  $\mu$ M E166N  $\beta$ -lactamase with 6.4  $\mu$ M of Bocillin FL, at 37 °C for 30 minutes, the reacted enzyme was purified by Ni-NTA through its 2 His-Tags. After binding of the enzyme to Ni-NTA at 4 °C, washing with 20 mM imidazole buffer was performed until fluorescence in the washes was constant. Elution was then performed with 250 mM imidazole buffer, and fluorescence in the eluate was recorded. The same experiment was done with WT  $\beta$ -lactamase, in parallel. The recorded fluorescence from each step was corrected for dilution and expressed as a percentage of the flow through fluorescence. The relative fluorescence of both enzymes at each step was plotted in a bar graph (Figure 33).

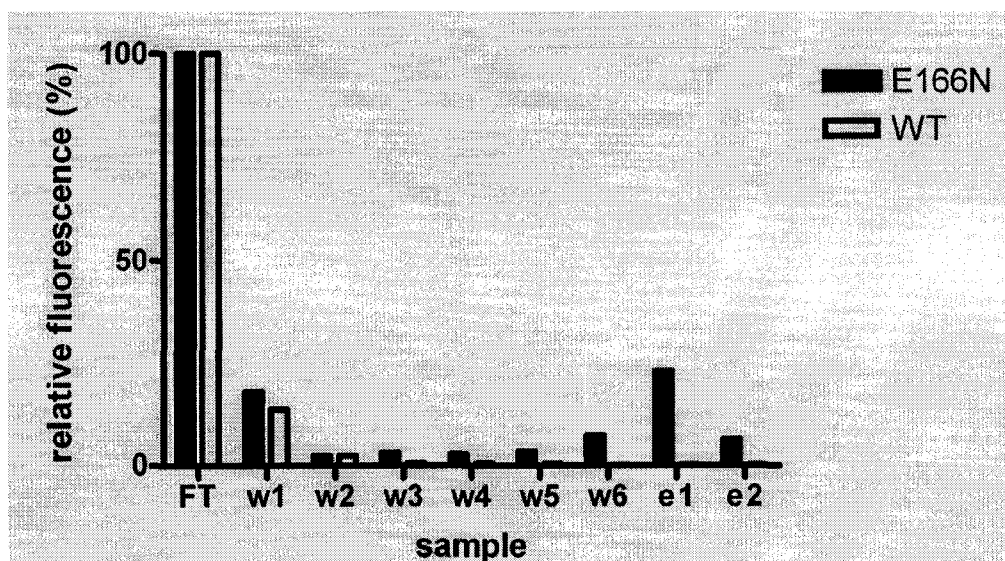


**Figure 33** Relative fluorescence of Bocillin FL-reacted  $\beta$ -lactamases purified with Ni-NTA. Fluorescence, expressed as a percentage of the initial fluorescence, is corrected for the dilution factors. Samples: FT - Flow through; w1 to w6 - wash1 to wash6; e1 and e2 - eluate1 and eluate2.

The fluorescence at 511 nm and thus the amount of Bocillin FL decreased dramatically during the first wash and stayed at low levels (<7.5 %) in the 5 following washes, in a similar pattern for both enzymes. The fluorescence in the first eluate increased to 22 % in the case of the mutant enzyme, whereas it stayed at a low level in the case of the WT enzyme. The difference in relative fluorescence in the washes between the E166N and WT  $\beta$ -lactamase can be explained by the stringency of the washes (20 mM of imidazole), where the imidazole competes with the enzyme on Ni-NTA. In the case of WT  $\beta$ -lactamase, only the enzyme was competed off Ni-NTA, whereas in the case of E166N, the enzyme and the linked Bocillin FL were both competed off Ni-NTA, accounting for the slight increase of relative fluorescence in the washings. The absence of fluorescence in the WT  $\beta$ -lactamase eluates, after reaction with Bocillin FL, binding to Ni-NTA and elution, demonstrated the absence of non specific binding between Bocillin FL, WT  $\beta$ -lactamase and Ni-NTA. The increase of relative fluorescence in the eluate, in the case of E166N  $\beta$ -lactamase supported the formation of a stable acyl-enzyme between the E166N  $\beta$ -lactamase and Bocillin FL, and gave an indication of the robustness of the labelling.

### **3.3.6 Expression and display of $\beta$ -lactamase on HeLa cell membrane**

mCherry was expressed on the membrane of HeLa cells using the pDisplay vector and the same transfection and expression protocols as for the  $\beta$ -lactamases. Imaging of mCherry-PDGFR-TM expressing cells allowed for verification of the transfection and expression efficiency and for easy determination of the expected expression pattern (Figure 34). As expected, the mCherry fluorescence was localised on the membrane, but also in the endoplasmic reticulum (ER) and Golgi apparatus. The murine Ig  $\kappa$ -chain leader sequence fused to the C-terminus of the protein directs mCherry to the secretory pathway [112], and allows the protein to travel through the ER and the Golgi. At the N-terminus, the platelet derived growth factor receptor (PDGFR) transmembrane domain acts as an anchor in the plasma membrane [138], allowing display of mCherry on the extracellular side.

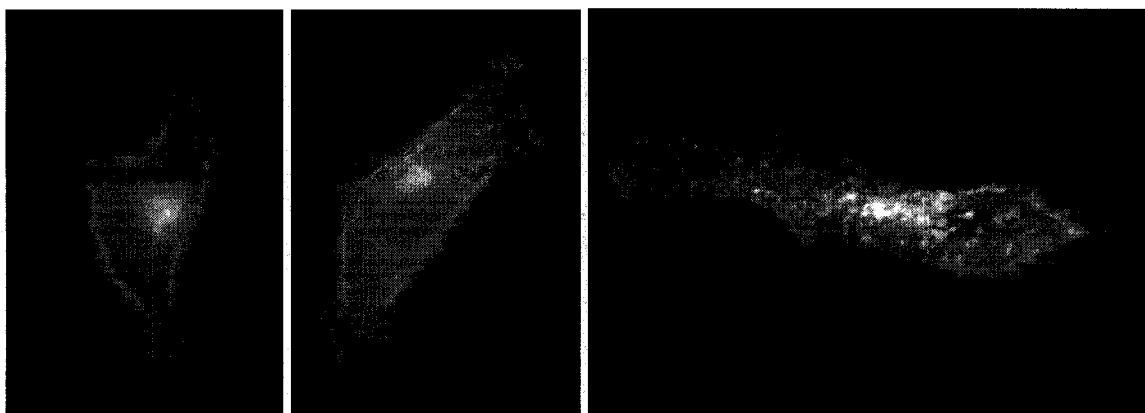


**Figure 34** HeLa cells transfected with pDisplay-mCherry. HeLa cells expressing mCherry-PDGFR-TM imaged at 610/75 nm after excitation at 535/50 nm.

Confirmation of the expression of the WT and E166N  $\beta$ -lactamases on the HeLa cells membrane was obtained through immunofluorescence. HeLa cells were grown on microscope coverslips, transfected with pDisplay-mCherry as control, pDisplay-E166N- $\beta$ -lactamase and pDisplay-WT- $\beta$ -lactamase. After treatment with an anti-HA antibody (primary antibody) and an anti-rabbit Alexa fluor 488 antibody (secondary antibody), the cells were imaged. The rabbit anti-HA antibody recognizes the Hemagglutinin A epitope tag (Tyr-Pro-Tyr-Asp-Val-Pro-Asp-Tyr-Ala), which is fused at the C-terminus of mCherry, WT  $\beta$ -lactamase or E166N  $\beta$ -lactamase. The anti-Rabbit Alexa fluor 488 antibody binds to the constant domain (Fc) of rabbit antibodies and in particular to the anti-HA antibody used.

The positive control protein mCherry-PDGFR-TM was expressed on the membrane of the HeLa cells as indicated by the mCherry fluorescence pattern (Figure 35A). The same pattern was seen when Alexa fluor 488 was imaged. The Alexa Fluor 488 fluorescence colocalize perfectly with the mCherry fluorescence and only a very light unspecific labelling was observed (Figure 35B). The HeLa cells transfected with pDisplay-E166N- $\beta$ -lactamase and pDisplay-WT- $\beta$ -lactamase presented a similar pattern, with Alexa Fluor 488 localized on the membrane of some of the cells (Figure 35C and D).

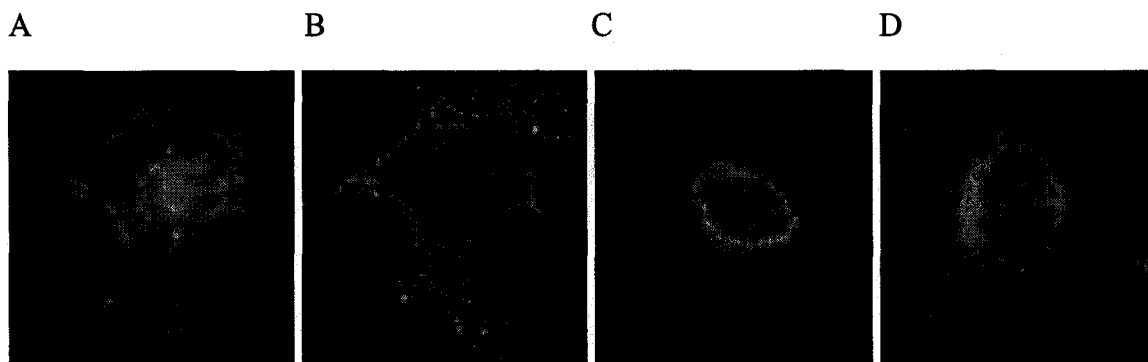


**Figure 35** HeLa cells displaying membrane-anchored mCherry, WT  $\beta$ -lactamase and E166N  $\beta$ -lactamase. mCherry-PDGFR-TM expressed in HeLa cell, imaged (A) at 610/75 nm after excitation at 535/50 nm (mCherry fluorescence) and (B) at 535/30 nm after excitation at 500/20 nm (Alexa Fluor 488 fluorescence). WT  $\beta$ -lactamase-PDGFR-TM (C) and E166N  $\beta$ -lactamase (D) expressed in HeLa cell and imaged at 535/30 nm after excitation at 500/20 nm (Alexa Fluor 488 fluorescence).

The immunostaining pattern obtained with anti-HA antibody indicated the presence of the Hemmagglutinin A epitope at the cell membrane of the transfected cells with all the tested plasmids. The colocalization of mCherry fluorescence and immunostaining in pDisplay-mCherry transfected cells allowed for a positive control of the immunostaining and identification of the non specific staining. This indicates that mCherry, WT and mutant  $\beta$ -lactamases are properly exported and expressed on the cell membrane.

### 3.3.7 Tentative labelling of HeLa cells with Bocillin FL

Labelling of E166N  $\beta$ -lactamase-expressing HeLa cells was attempted with Bocillin FL. The binding of E166N  $\beta$ -lactamase to Bocillin FL was demonstrated in vitro in 3.3.4 and 3.3.5. Therefore, Bocillin FL was chosen as substrate for tentative cell labelling.

HeLa cells were grown on coverslips and cotransfected with pDisplay-E166N- $\beta$ -lactamase and pDisplay-WT- $\beta$ -lactamase. After fixation, the cells were treated with Bocillin FL and imaged at 535/30 nm after excitation at 500/20 nm. All the cells presented an even Bocillin FL staining corresponding to the background, but unfortunately no specific labelling appeared on the cell membranes.

### 3.4 DISCUSSION AND CONCLUSIONS

The E166N mutant of the TEM1  $\beta$ -lactamase was prepared, expressed, purified and refolded. The masses of both proteins were determined by MALDI and ESI. An accurate mass of the mutant could not be obtained by ESI due to precipitation of the protein when dialysed against various buffers. In the exact same conditions, WT was highly soluble indicating a difference in stability between the proteins. The observed decreased stability of the E166N mutant may be due to an increased mobility of the  $\Omega$ -loop [125] that was reported for several TEM1 mutants [86].

Preliminary kinetic characterization of both proteins was then performed to check the activity of the protein as well as the effectiveness of the mutation. TEM1 and WT  $\beta$ -lactamase are very similar proteins and thus are expected to have kinetic parameters of the same order of magnitude, which was the case. In fact WT  $\beta$ -lactamase presented acylation  $k_{\text{cat}}/K_m$  and deacylation  $k_{\text{cat}}$  rates with CENTA and nitrocefin in relative good agreement with the values reported in the literature for TEM1  $\beta$ -lactamase [128, 129].

The mutant is expected to be deacylation impaired since identical mutants of other  $\beta$ -lactamases have been reported to show exceedingly low rates of deacylation compared to the WT  $\beta$ -lactamase [125]. The deacylation impairment hypothesis was tested by activity-based test of E166N enzymes with CENTA and nitrocefin. When tested with nitrocefin E166N  $\beta$ -lactamase apparently did not hydrolyse the substrate. A possible explanation for the absence of hydrolysis of nitrocefin with the mutant enzyme is that the initial burst happened during the mixing-dead-time and that once formed, the acyl-enzyme was very stable and no deacylation and enzyme turnover were observable. When tested with CENTA, E166N  $\beta$ -lactamase presented an exceedingly low deacylation rate ( $k_3$ ), much slower than the  $k_{\text{cat}}$  observed for the WT, in agreement with reported results for TEM1 E166N  $\beta$ -lactamase [48, 125, 126]. Those results confirmed the activity of the E166N  $\beta$ -lactamase and especially the presence of an extremely slow deacylation step, as anticipated. However, the observed progress curves exhibited an initial exponential phase followed by a slower steady-state linear phase, which often indicates a branched pathway where the initial acyl-enzyme is partially transformed into an inactive acyl-enzyme. An

unexpectedly large initial burst, several times the enzyme concentration, was observed. Such a burst usually indicates a product favoured compared to the inactive species, but the E166N TEM1  $\beta$ -lactamase has been shown to have a very slow deacylation, and to yield an inactive acyl-enzyme. Furthermore, the initial velocity and steady-state velocity obtained from such progress curves are both supposed to individually follow Michaelis-Menten kinetics, which was not the case here. Thus, the common branched pathway interpretation failed to explain the burst. A satisfying explanation could not be ascertained to account for the large burst.

The characterization of the binding of the mutant enzyme to  $\beta$ -lactam substrates by gel displacement assay strongly suggested that Bocillin FL was a good potential labelling substrate. In addition, the chromogenic substrate CENTA and the ketone substrate appeared to react with the enzyme and inactivate it for further hydrolysis. However, when reacted with the ketone substrate in combination with Lucifer Yellow CH or biotin-XX-hydrazide and streptavidin-fluorescein in presence or not of  $\text{NaBH}_3\text{CN}$ , the labelling of the enzyme could not be verified. Explanations for the absence of displacement on the gel with Lucifer Yellow CH include the absence of reaction between Lucifer Yellow and the substrate due to steric hindrance caused by the enzyme, and quenching of the Lucifer Yellow fluorescence by the protein environment [127]. In the case of biotin-XX-hydrazide, steric hindrance can still be a problem especially for the reaction between biotin and the bulky streptavidin tetramer.

The binding of the mutant enzyme to Bocillin FL was further characterized by Ni-NTA purification. The experiment enabled co-purification of the enzyme and fluorescent substrate after reaction, supporting the hypothesis of the formation of a stable acyl-enzyme between the enzyme and Bocillin FL and indicating a quite robust labelling of the enzyme.

The E166N  $\beta$ -lactamase-substrate system was intended as a live cell labelling technique, and thus test of the mutant *in vivo* was necessary. For convenience and to enable preliminary test with non cell-permeable substrates, the mutant was expressed on the cell surface. Cell surface expression and display were verified by immunofluorescence and the expected fluorescence pattern was imaged using mCherry as control. Both E166N and

WT  $\beta$ -lactamases were present on the cell membrane and thus the mutant enzyme should be available for labelling. Once the display of the enzyme on cell surface was established, labelling with the fluorescent substrate Bocillin FL was attempted. Unfortunately, fluorescence was observed indiscriminately in the cell and no specific cell surface labelling was present. It appeared that the bocillin FL substrate stained the cells arbitrarily. The absence of labelling could be caused by poor stability of the mutant E166N  $\beta$ -lactamase at 37 °C that would cause loss of its proper tertiary structure and prevent it from reacting with the substrate in vivo.

**CHAPTER 4:**  
**CONCLUSIONS AND FUTURE DIRECTIONS**



Recently, fluorescent live cell imaging has benefited from advances in molecular biology techniques with the development of genetically encoded labels. In parallel, advances in organic chemistry enabled development of new fluorescent dyes and of bioorthogonal chemical labels for use in hybrid systems. The objective of the work in this thesis was to present two very different approaches for the design of new hybrid fluorescent reporters. The first reporter is a single chain variable fragment antibody against the protein hBub1, which can be genetically fused to a FP for example, in a cross of the immunolabelling and genetically encoded FP techniques. The second reporter, based on a mutant  $\beta$ -lactamase, is a more general tool taking roots in bioorthogonal chemical labelling and the use of  $\beta$ -lactamase as catalytic reporter.

#### **4.1 SCFV FOR DETECTION OF HBUB1**

A single chain variable fragment antibody against a mitotic checkpoint protein was designed. Such a ScFv could potentially be used for detection of the antigen *in vivo*, after coupling to a fluorescent protein, for example, as introduced here.

In this work, the first steps of the design of the ScFv were presented. More experiments will be necessary for better understanding and characterization of this ScFv and improvement of the construct. Expression of the protein on a larger scale will be a preliminary requirement to further characterization of the protein and especially of its binding to hBub1 *in vivo*. The binding can be characterized with an indirect (cellular) ELISA using either purified hBub1 or mammalian cell lysate in combination with the ScFv and an anti-His tag antibody for example and compared to binding from the full length antibody. Identification of the specific epitope can be performed in a similar way by using the ScFv and various hBub1 fragments and analysing the bound fragments by mass spectrometry for example. Furthermore, engineering of the ScFv for better folding, stability, binding and specificity is often necessary prior to use in a more sophisticated environment and would certainly enable preparation of a more versatile antibody. Engineering for better binding and specificity is usually executed by error prone PCR followed by phage display or light chain shuffling affinity maturation [139]. ScFv

stability can also be improved by rational approaches such as CDR grafting or evolutionary approaches including rounds of diversification by error prone PCR followed by display based selection [140, 141]. Folding efficiency of the ScFv can sometimes be increased by mutation of key V<sub>H</sub> residues. Finally use of a different construct, based on an engineered ScFv, in HeLa cells to try and avoid cell death will be an important step to facilitate characterization of the protein and of its binding to hBub1 *in vivo*. FRET and co-immunoprecipitation are two tools commonly used for *in vivo* characterization of protein binding and could be used for the hBub1 and ScFv complex.

## 4.2 $\beta$ -LACTAMASE BASED LABELLING STRATEGY

A mutant  $\beta$ -lactamase based labelling strategy, in which the labelling of recombinantly expressed proteins with a wide variety of labels in live cells relies on the reaction between the deacylation impaired mutant of  $\beta$ -lactamase and various substrates, was also attempted.

The E166N  $\beta$ -lactamase, presenting an impaired deacylation, was tested with various cephalosporins and a penicillin substrate. Formation of a stable acyl-enzyme with Bocillin FL was suggested by the results of the gel displacement assay and of fast purification of the enzyme-Bocillin FL complex. However, inconclusive results were obtained in live cells.

The design of the mutant  $\beta$ -lactamase based labelling system relies on the ability of the enzyme to form a stable acyl-enzyme with a variety of substrates. Therefore, labelling of the enzyme with various substrates or substrate-tag combination will be useful to try. Such combinations include, but are not limited to, the ketone cephalosporin substrate in association with different bioorthogonal labels presenting a decreased steric hindrance. Especially two main directions for improvement of the chemical tagging, the development of a smaller bioorthogonal label and of a biotin-hydrazide label containing a long linker for reaction with streptavidin, should be tried. The design of new substrates bearing various functional groups is also of great interest and ketone cephalosporin based substrates bearing intrinsic functionalities other than the ketone, for example a

fluorophore, a biotin motif or a photosensitizing dye should be synthesized and tested. Other substrates that will open new possibilities are  $\beta$ -lactams coupled to quenched fluorophores, membrane permeable and near-IR substrates. Such substrates enable labelling without background fluorescence and inside mammalian cells respectively and would demonstrate the effectiveness and versatility of the method as a hybrid system for live cell imaging.

Furthermore, functional activity of the mutant  $\beta$ -lactamase expressed on cell surface should be tested to try and troubleshoot the absence of labelling observed with Bocillin FL. Additionally, engineering of the mutant enzyme for improved stability and decreased misfolding and aggregation by directed evolution will certainly increase the labelling ability of the enzyme in other environments.

## BIBLIOGRAPHY

1. Coons, A.H., et al., *The demonstration of pneumococcal antigen in tissues by the use of fluorescent antibody*. Journal Of Immunology, 1942. **45**(3): p. 159-170.
2. Giepmans, B.N., et al., *The fluorescent toolbox for assessing protein location and function*. Science, 2006. **312**(5771): p. 217-24.
3. Tsien, R.Y., *The green fluorescent protein*. Annual Review Of Biochemistry, 1998. **67**: p. 509-544.
4. Johnsson, N. and K. Johnsson, *A fusion of disciplines: chemical approaches to exploit fusion proteins for functional genomics*. Chembiochem, 2003. **4**(9): p. 803-10.
5. Kohler, G. and C. Milstein, *Continuous cultures of fused cells secreting antibody of predefined specificity*. Nature, 1975. **256**(5517): p. 495-7.
6. Tonegawa, S., *Somatic Generation Of Antibody Diversity*. Nature, 1983. **302**(5909): p. 575-581.
7. Kolodziej, P.A. and R.A. Young, *Epitope Tagging And Protein Surveillance*. Methods In Enzymology, 1991. **194**: p. 508-519.
8. Haugland, R.P. *The Handbook - A Guide to Fluorescent Probes and Labeling Technologies, 10th ed.* 2005 [Available from: <http://probes.invitrogen.com/handbook/>].
9. Kubista, M., B. Akerman, and B. Norden, *Characterization Of Interaction Between Dna And 4',6-Diamidino-2-Phenylindole By Optical Spectroscopy*. Biochemistry, 1987. **26**(14): p. 4545-4553.
10. Grynkiewicz, G., M. Poenie, and R.Y. Tsien, *A new generation of Ca<sup>2+</sup> indicators with greatly improved fluorescence properties*. J Biol Chem, 1985. **260**(6): p. 3440-50.
11. Minta, A., J.P.Y. Kao, and R.Y. Tsien, *Fluorescent Indicators For Cytosolic Calcium Based On Rhodamine And Fluorescein Chromophores*. Journal Of Biological Chemistry, 1989. **264**(14): p. 8171-8178.
12. Shimomura, O., F.H. Johnson, and Y. Saiga, *Extraction, Purification And Properties Of Aequorin, A Bioluminescent Protein From Luminous*

- Hydromedusan, Aequorea*. Journal Of Cellular And Comparative Physiology, 1962. **59**(3): p. 223-239.
13. Prasher, D.C., et al., *Primary Structure Of The Aequorea-Victoria Green-Fluorescent Protein*. Gene, 1992. **111**(2): p. 229-233.
  14. Shaner, N.C., P.A. Steinbach, and R.Y. Tsien, *A guide to choosing fluorescent proteins*. Nat Methods, 2005. **2**(12): p. 905-9.
  15. Lukyanov, K.A., et al., *Photoactivatable fluorescent proteins*. Nature Reviews Molecular Cell Biology, 2005. **6**(11): p. 885-891.
  16. Li, I.T., E. Pham, and K. Truong, *Protein biosensors based on the principle of fluorescence resonance energy transfer for monitoring cellular dynamics*. Biotechnology Letters, 2006. **28**(24): p. 1971-1982.
  17. Hu, C.D., Y. Chinenov, and T.K. Kerppola, *Visualization of interactions among bZip and Rel family proteins in living cells using bimolecular fluorescence complementation*. Molecular Cell, 2002. **9**(4): p. 789-798.
  18. Zacharias, D.A. and R.Y. Tsien, *Molecular biology and mutation of green fluorescent protein*. Methods Biochem Anal, 2006. **47**: p. 83-120.
  19. Heim, R., D.C. Prasher, and R.Y. Tsien, *Wavelength Mutations And Posttranslational Autoxidation Of Green Fluorescent Protein*. Proceedings Of The National Academy Of Sciences Of The United States Of America, 1994. **91**(26): p. 12501-12504.
  20. Cubitt, A.B., et al., *Understanding, Improving And Using Green Fluorescent Proteins*. Trends In Biochemical Sciences, 1995. **20**(11): p. 448-455.
  21. Lisenbee, C.S., S.K. Karnik, and R.N. Trelease, *Overexpression and mislocalization of a tail-anchored GFP redefines the identity of peroxisomal ER*. Traffic, 2003. **4**(7): p. 491-501.
  22. Zhang, J., et al., *Creating new fluorescent probes for cell biology*. Nat Rev Mol Cell Biol, 2002. **3**(12): p. 906-18.
  23. van Swieten, P.F., et al., *Bioorthogonal organic chemistry in living cells: novel strategies for labeling biomolecules*. Org Biomol Chem, 2005. **3**(1): p. 20-7.
  24. Gaietta, G., et al., *Multicolor and electron microscopic imaging of connexin trafficking*. Science, 2002. **296**(5567): p. 503-507.

25. Vivero-Pol, L., et al., *Multicolor Imaging of cell surface proteins*. Journal Of The American Chemical Society, 2005. **127**(37): p. 12770-12771.
26. Marek, K.W. and G.W. Davis, *Transgenically encoded protein photoinactivation (FIAsH-FALI): Acute inactivation of synaptotagmin I*. Neuron, 2002. **36**(5): p. 805-813.
27. Tour, O., et al., *Genetically targeted chromophore-assisted light inactivation*. Nature Biotechnology, 2003. **21**(12): p. 1505-1508.
28. Johnsson, N., N. George, and K. Johnsson, *Protein chemistry on the surface of living cells*. Chembiochem, 2005. **6**(1): p. 47-52.
29. Gronemeyer, T., G. Godin, and K. Johnsson, *Adding value to fusion proteins through covalent labelling*. Curr Opin Biotechnol, 2005. **16**(4): p. 453-8.
30. Miller, L.W. and V.W. Cornish, *Selective chemical labeling of proteins in living cells*. Curr Opin Chem Biol, 2005. **9**(1): p. 56-61.
31. Griffin, B.A., S.R. Adams, and R.Y. Tsien, *Specific covalent labeling of recombinant protein molecules inside live cells*. Science, 1998. **281**(5374): p. 269-72.
32. Martin, B.R., et al., *Mammalian cell-based optimization of the biarsenical-binding tetracysteine motif for improved fluorescence and affinity*. Nature Biotechnology, 2005. **23**(10): p. 1308-1314.
33. Nakanishi, J., et al., *Imaging of conformational changes of proteins with a new environment/sensitive fluorescent probe designed for site specific labeling of recombinant proteins in live cells*. Analytical Chemistry, 2001. **73**(13): p. 2920-2928.
34. Adams, S.R., et al., *New biarsenical Ligands and tetracysteine motifs for protein labeling in vitro and in vivo: Synthesis and biological applications*. Journal Of The American Chemical Society, 2002. **124**(21): p. 6063-6076.
35. Keppler, A., et al., *A general method for the covalent labeling of fusion proteins with small molecules in vivo*. Nat Biotechnol, 2003. **21**(1): p. 86-9.
36. An, G., K. Hidaka, and L. Siminovitch, *Expression of bacterial beta-galactosidase in animal cells*. Mol Cell Biol, 1982. **2**(12): p. 1628-32.

37. Gorman, C.M., L.F. Moffat, and B.H. Howard, *Recombinant Genomes Which Express Chloramphenicol Acetyltransferase In Mammalian-Cells*. *Molecular And Cellular Biology*, 1982. **2**(9): p. 1044-1051.
38. Campbell, R.E., *Realization of beta-lactamase as a versatile fluorogenic reporter*. *Trends Biotechnol*, 2004. **22**(5): p. 208-11.
39. Davies, J., *Inactivation Of Antibiotics And The Dissemination Of Resistance Genes*. *Science*, 1994. **264**(5157): p. 375-382.
40. Frere, J.M., *Beta-Lactamases And Bacterial-Resistance To Antibiotics*. *Molecular Microbiology*, 1995. **16**(3): p. 385-395.
41. Ambler, R.P., *The structure of beta-lactamases*. *Philos Trans R Soc Lond B Biol Sci*, 1980. **289**(1036): p. 321-31.
42. Ambler, R.P., et al., *A Standard Numbering Scheme For The Class-A Beta-Lactamases*. *Biochemical Journal*, 1991. **276**: p. 269-270.
43. Leung, Y.C., et al., *Site-directed mutagenesis of beta-lactamase I: role of Glu-166*. *Biochem J*, 1994. **299** (Pt 3): p. 671-8.
44. Matagne, A., J. Lamotte-Brasseur, and J.M. Frere, *Catalytic properties of class A beta-lactamases: efficiency and diversity*. *Biochem J*, 1998. **330** (Pt 2): p. 581-98.
45. Fonze, E., et al., *Tem1 Beta-Lactamase Structure Solved By Molecular Replacement And Refined Structure Of The S235a Mutant*. *Acta Crystallographica Section D-Biological Crystallography*, 1995. **51**: p. 682-694.
46. Jelsch, C., et al., *Beta-Lactamase Tem1 Of Escherichia-Coli - Crystal-Structure Determination At 2.5 A Resolution*. *Febs Letters*, 1992. **299**(2): p. 135-142.
47. Jelsch, C., et al., *Crystal-Structure Of Escherichia-Coli Tem1 Beta-Lactamase At 1.8-Angstrom Resolution*. *Proteins-Structure Function And Genetics*, 1993. **16**(4): p. 364-383.
48. Strynadka, N.C., et al., *Molecular structure of the acyl-enzyme intermediate in beta-lactam hydrolysis at 1.7 A resolution*. *Nature*, 1992. **359**(6397): p. 700-705.
49. Frere, J.M., Nguyen-Disteche, M., Coyette, J., Joris, B., *The Chemistry of  $\beta$ -lactams*, M.I. Page, Editor. 1992, Blackie Academic & Professional: London. p. pp.148-197.

50. Herzberg, O. and J. Moult, *Bacterial-Resistance To Beta-Lactam Antibiotics - Crystal-Structure Of Beta-Lactamase From Staphylococcus-Aurens Pc1 At 2.5-A Resolution*. Science, 1987. **236**(4802): p. 694-701.
51. Diaz, N., et al., *Insights into the acylation mechanism of class A beta-lactamases from molecular dynamics simulations of the TEM-1 enzyme complexed with benzylpenicillin*. J Am Chem Soc, 2003. **125**(3): p. 672-84.
52. Lamottebrasseur, J., et al., *Mechanism Of Acyl Transfer By The Class-A Serine Beta-Lactamase Of Streptomyces-Albus-G*. Biochemical Journal, 1991. **279**: p. 213-221.
53. Gibson, R.M., H. Christensen, and S.G. Waley, *Site-Directed Mutagenesis Of Beta-Lactamase-I - Single And Double Mutants Of Glu-166 And Lys-73*. Biochemical Journal, 1990. **272**(3): p. 613-619.
54. Minasov, G., X.J. Wang, and B.K. Shoichet, *An ultrahigh resolution structure of TEM-1 beta-lactamase suggests a role for Glu166 as the general base in acylation*. Journal Of The American Chemical Society, 2002. **124**(19): p. 5333-5340.
55. Broome-Smith, J.K., M. Tadayyon, and Y. Zhang, *Beta-lactamase as a probe of membrane protein assembly and protein export*. Mol Microbiol, 1990. **4**(10): p. 1637-44.
56. Zlokarnik, G., et al., *Quantitation of transcription and clonal selection of single living cells with beta-lactamase as reporter*. Science, 1998. **279**(5347): p. 84-8.
57. Spotts, J.M., R.E. Dolmetsch, and M.E. Greenberg, *Time-lapse imaging of a dynamic phosphorylation-dependent protein-protein interaction in mammalian cells*. Proc Natl Acad Sci U S A, 2002. **99**(23): p. 15142-7.
58. Wehrman, T., et al., *Protein-protein interactions monitored in mammalian cells via complementation of beta -lactamase enzyme fragments*. Proc Natl Acad Sci U S A, 2002. **99**(6): p. 3469-74.
59. Hasegawa, S., et al., *Imaging Tetrahymena ribozyme splicing activity in single live mammalian cells*. Proc Natl Acad Sci U S A, 2003. **100**(25): p. 14892-6.
60. Hasegawa, S., J.W. Choi, and J. Rao, *Single-cell detection of trans-splicing ribozyme in vivo activity*. J Am Chem Soc, 2004. **126**(23): p. 7158-9.



61. Jones, R.N., et al., *In vitro evaluation of CENTA, a new beta-lactamase-susceptible chromogenic cephalosporin reagent*. J Clin Microbiol, 1982. **15**(5): p. 954-8.
62. O'Callaghan, C.H., et al., *Novel method for detection of beta-lactamases by using a chromogenic cephalosporin substrate*. Antimicrob Agents Chemother, 1972. **1**(4): p. 283-8.
63. Xing, B., A. Khanamiryan, and J. Rao, *Cell-permeable near-infrared fluorogenic substrates for imaging beta-lactamase activity*. J Am Chem Soc, 2005. **127**(12): p. 4158-9.
64. Zhao, G., et al., *BOCILLIN FL, a sensitive and commercially available reagent for detection of penicillin-binding proteins*. Antimicrob Agents Chemother, 1999. **43**(5): p. 1124-8.
65. Gee, K.R., et al., *Fluorescent Bocillins: synthesis and application in the detection of penicillin-binding proteins*. Electrophoresis, 2001. **22**(5): p. 960-5.
66. Philippon, A., et al., *The diversity, structure and regulation of beta-lactamases*. Cell Mol Life Sci, 1998. **54**(4): p. 341-6.
67. Stokes, G.G., *On the Change of Refrangibility of Light*. Philosophical Transactions of the Royal Society of London, 1852. **142**: p. 463.
68. Minsky, M., *Memoir On Inventing The Confocal Scanning Microscope*. Scanning, 1988. **10**(4): p. 128-138.
69. Pangilinan, F., et al., *Mammalian BUB1 protein kinases: map positions and in vivo expression*. Genomics, 1997. **46**(3): p. 379-88.
70. Ouyang, B., et al., *Human Bub1: a putative spindle checkpoint kinase closely linked to cell proliferation*. Cell Growth Differ, 1998. **9**(10): p. 877-85.
71. Cahill, D.P., et al., *Mutations of mitotic checkpoint genes in human cancers*. Nature, 1998. **392**(6673): p. 300-3.
72. Rieder, C.L., et al., *Anaphase onset in vertebrate somatic cells is controlled by a checkpoint that monitors sister kinetochore attachment to the spindle*. J Cell Biol, 1994. **127**(5): p. 1301-10.
73. Jallepalli, P.V. and C. Lengauer, *Chromosome segregation and cancer: cutting through the mystery*. Nat Rev Cancer, 2001. **1**(2): p. 109-17.

74. Ohshima, K., et al., *Mutation analysis of mitotic checkpoint genes (hBUB1 and hBUBR1) and microsatellite instability in adult T-cell leukemia/lymphoma*. *Cancer Lett*, 2000. **158**(2): p. 141-50.
75. Ru, H.Y., et al., *hBUB1 defects in leukemia and lymphoma cells*. *Oncogene*, 2002. **21**(30): p. 4673-9.
76. Shigeishi, H., et al., *Correlation of human Bub1 expression with tumor-proliferating activity in salivary gland tumors*. *Oncol Rep*, 2006. **15**(4): p. 933-8.
77. Yuan, B., et al., *Increased expression of mitotic checkpoint genes in breast cancer cells with chromosomal instability*. *Clin Cancer Res*, 2006. **12**(2): p. 405-10.
78. Grabsch, H., et al., *Overexpression of the mitotic checkpoint genes BUB1, BUBR1, and BUB3 in gastric cancer--association with tumour cell proliferation*. *J Pathol*, 2003. **200**(1): p. 16-22.
79. Tang, Z., et al., *Human Bub1 protects centromeric sister-chromatid cohesion through Shugoshin during mitosis*. *Proc Natl Acad Sci U S A*, 2004. **101**(52): p. 18012-7.
80. Kitajima, T.S., et al., *Human Bub1 defines the persistent cohesion site along the mitotic chromosome by affecting Shugoshin localization*. *Curr Biol*, 2005. **15**(4): p. 353-9.
81. Taylor, S.S., et al., *Kinetochore localisation and phosphorylation of the mitotic checkpoint components Bub1 and BubR1 are differentially regulated by spindle events in human cells*. *J Cell Sci*, 2001. **114**(Pt 24): p. 4385-95.
82. Nicolaides, N.C., P.M. Sass, and L. Grasso, *Monoclonal antibodies: A morphing landscape for therapeutics*. *Drug Development Research*, 2006. **67**(10): p. 781-789.
83. Inbar, D., J. Hochman, and D. Givol, *Localization of antibody-combining sites within the variable portions of heavy and light chains*. *Proc Natl Acad Sci U S A*, 1972. **69**(9): p. 2659-62.
84. Skerra, A. and A. Pluckthun, *Assembly of a functional immunoglobulin Fv fragment in Escherichia coli*. *Science*, 1988. **240**(4855): p. 1038-41.
85. Bird, R.E., et al., *Single-chain antigen-binding proteins*. *Science*, 1988. **242**(4877): p. 423-6.

86. Palzkill, T., et al., *Evolution of antibiotic resistance: several different amino acid substitutions in an active site loop alter the substrate profile of beta-lactamase*. Mol Microbiol, 1994. **12**(2): p. 217-29.
87. Glockshuber, R., et al., *A comparison of strategies to stabilize immunoglobulin Fv-fragments*. Biochemistry, 1990. **29**(6): p. 1362-7.
88. Young, N.M., et al., *Thermal stabilization of a single-chain Fv antibody fragment by introduction of a disulphide bond*. FEBS Lett, 1995. **377**(2): p. 135-9.
89. Winter, G. and C. Milstein, *Man-made antibodies*. Nature, 1991. **349**(6307): p. 293-9.
90. Tsumoto, K., et al., *Effect Of The Order Of Antibody Variable Regions On The Expression Of The Single-Chain Hyhel10 Fv Fragment In Escherichia-Coli And The Thermodynamic Analysis Of Its Antigen-Binding Properties*. Biochemical And Biophysical Research Communications, 1994. **201**(2): p. 546-551.
91. Huston, J.S., et al., *Protein Engineering Of Single-Chain Fv Analogs And Fusion Proteins*. Methods In Enzymology, 1991. **203**: p. 46-&.
92. Whitlow, M., et al., *An improved linker for single-chain Fv with reduced aggregation and enhanced proteolytic stability*. Protein Eng, 1993. **6**(8): p. 989-95.
93. Turner, D.J., M.A. Ritter, and A.J. George, *Importance of the linker in expression of single-chain Fv antibody fragments: optimisation of peptide sequence using phage display technology*. J Immunol Methods, 1997. **205**(1): p. 43-54.
94. Huston, J.S., et al., *Protein engineering of antibody binding sites: recovery of specific activity in an anti-digoxin single-chain Fv analogue produced in Escherichia coli*. Proc Natl Acad Sci U S A, 1988. **85**(16): p. 5879-83.
95. Arndt, K.M., K.M. Muller, and A. Pluckthun, *Factors influencing the dimer to monomer transition of an antibody single-chain Fv fragment*. Biochemistry, 1998. **37**(37): p. 12918-26.
96. Atwell, J.L., et al., *scFv multimers of the anti-neuraminidase antibody NC10: length of the linker between VH and VL domains dictates precisely the transition between diabodies and triabodies*. Protein Eng, 1999. **12**(7): p. 597-604.

97. Hudson, P.J. and A.A. Kortt, *High avidity scFv multimers; diabodies and triabodies*. J Immunol Methods, 1999. **231**(1-2): p. 177-89.
98. Mohr, L., et al., *Antibody-directed therapy for human hepatocellular carcinoma*. Gastroenterology, 2004. **127**(5 Suppl 1): p. S225-31.
99. Cesco-Gaspere, M., F. Benvenuti, and O.R. Burrone, *BCL1 lymphoma protection induced by idiotype DNA vaccination is entirely dependent on anti-idiotypic antibodies*. Cancer Immunol Immunother, 2005. **54**(4): p. 351-8.
100. Hudson, P.J., *Recombinant antibody constructs in cancer therapy*. Curr Opin Immunol, 1999. **11**(5): p. 548-57.
101. Harris, B., *Exploiting antibody-based technologies to manage environmental pollution*. Trends Biotechnol, 1999. **17**(7): p. 290-6.
102. Colcher, D., et al., *Pharmacokinetics and biodistribution of genetically-engineered antibodies*. Quarterly Journal Of Nuclear Medicine, 1998. **42**(4): p. 225-241.
103. Shabat, D., et al., *Multiple event activation of a generic prodrug trigger by antibody catalysis*. Proceedings Of The National Academy Of Sciences Of The United States Of America, 1999. **96**(12): p. 6925-6930.
104. Reiter, Y. and I. Pastan, *Recombinant Fv immunotoxins and Fv fragments as novel agents for cancer therapy and diagnosis*. Trends In Biotechnology, 1998. **16**(12): p. 513-520.
105. Martin, F., et al., *Retrovirus targeting by tropism restriction to melanoma cells*. Journal Of Virology, 1999. **73**(8): p. 6923-6929.
106. Biocca, S., et al., *Redox State Of Single-Chain Fv Fragments Targeted To The Endoplasmic-Reticulum, Cytosol And Mitochondria*. Bio-Technology, 1995. **13**(10): p. 1110-1115.
107. Biocca, S. and A. Cattaneo, *Intracellular Immunization - Antibody Targeting To Subcellular Compartments*. Trends In Cell Biology, 1995. **5**(6): p. 248-252.
108. Williams, B.R. and Z. Zhu, *Intrabody-based approaches to cancer therapy: status and prospects*. Curr Med Chem, 2006. **13**(12): p. 1473-80.
109. Laemmli, U.K., *Cleavage of structural proteins during the assembly of the head of bacteriophage T4*. Nature, 1970. **227**(5259): p. 680-5.

110. Ai, H.W., et al., *Directed evolution of a monomeric, bright and photostable version of Clavularia cyan fluorescent protein: structural characterization and applications in fluorescence imaging*. *Biochem J*, 2006. **400**(3): p. 531-40.
111. Krebber, A., et al., *Reliable cloning of functional antibody variable domains from hybridomas and spleen cell repertoires employing a reengineered phage display system*. *J Immunol Methods*, 1997. **201**(1): p. 35-55.
112. Coloma, M.J., et al., *Novel vectors for the expression of antibody molecules using variable regions generated by polymerase chain reaction*. *J Immunol Methods*, 1992. **152**(1): p. 89-104.
113. Honegger, A. and A. Pluckthun, *Yet another numbering scheme for immunoglobulin variable domains: an automatic modeling and analysis tool*. *J Mol Biol*, 2001. **309**(3): p. 657-70.
114. Schwede, T., et al., *SWISS-MODEL: An automated protein homology-modeling server*. *Nucleic Acids Res*, 2003. **31**(13): p. 3381-5.
115. Guex, N. and M.C. Peitsch, *SWISS-MODEL and the Swiss-PdbViewer: an environment for comparative protein modeling*. *Electrophoresis*, 1997. **18**(15): p. 2714-23.
116. Rezacova, P., et al., *Crystal structure of a cross-reaction complex between an anti-HIV-1 protease antibody and an HIV-2 protease peptide*. *Journal Of Structural Biology*, 2005. **149**(3): p. 332-337.
117. Kalderon, D., et al., *A short amino acid sequence able to specify nuclear location*. *Cell*, 1984. **39**(3 Pt 2): p. 499-509.
118. Lanford, R.E., P. Kanda, and R.C. Kennedy, *Induction of nuclear transport with a synthetic peptide homologous to the SV40 T antigen transport signal*. *Cell*, 1986. **46**(4): p. 575-82.
119. Fischer-Fantuzzi, L. and C. Vesco, *Cell-dependent efficiency of reiterated nuclear signals in a mutant simian virus 40 oncoprotein targeted to the nucleus*. *Mol Cell Biol*, 1988. **8**(12): p. 5495-503.
120. Kozak, M., *An Analysis Of 5'-Noncoding Sequences From 699 Vertebrate Messenger-Rnas*. *Nucleic Acids Research*, 1987. **15**(20): p. 8125-8148.

121. Kabat EA, W.T., Perry H, Gottesman K, Foeller C, *Sequences of Proteins of Immunological Interest, 5th edit.* 1991: NIH Publication no.91-3242 U.S. Department of Health and Human Services.
122. DeLano, W.L. *The PyMOL Molecular Graphics System.* 2002 [Available from: <http://www.pymol.org>].
123. Wulfig, C., J. Lombardero, and A. Pluckthun, *An Escherichia-Coli Protein Consisting Of A Domain Homologous To Fk506-Binding Proteins (Fkbp) And A New Metal-Binding Motif.* Journal Of Biological Chemistry, 1994. **269**(4): p. 2895-2901.
124. Matagne, A. and J.M. Frere, *Contribution Of Mutant Analysis To The Understanding Of Enzyme Catalysis - The Case Of Class-A Beta-Lactamases.* Biochimica Et Biophysica Acta-Protein Structure And Molecular Enzymology, 1995. **1246**(2): p. 109-127.
125. Guillaume, G., et al., *Site-directed mutagenesis of glutamate 166 in two beta-lactamases. Kinetic and molecular modeling studies.* J Biol Chem, 1997. **272**(9): p. 5438-44.
126. Adachi, H., T. Ohta, and H. Matsuzawa, *Site-directed mutants, at position 166, of RTEM-1 beta-lactamase that form a stable acyl-enzyme intermediate with penicillin.* J Biol Chem, 1991. **266**(5): p. 3186-91.
127. Chan, P.H., et al., *Rational design of a novel fluorescent biosensor for beta-lactam antibiotics from a class A beta-lactamase.* J Am Chem Soc, 2004. **126**(13): p. 4074-5.
128. Bebrone, C., et al., *CENTA as a chromogenic substrate for studying beta-lactamases.* Antimicrob Agents Chemother, 2001. **45**(6): p. 1868-71.
129. Raquet, X., et al., *TEM beta-lactamase mutants hydrolysing third-generation cephalosporins. A kinetic and molecular modelling analysis.* J Mol Biol, 1994. **244**(5): p. 625-39.
130. Mahal, L.K., K.J. Yarema, and C.R. Bertozzi, *Engineering chemical reactivity on cell surfaces through oligosaccharide biosynthesis.* Science, 1997. **276**(5315): p. 1125-8.

131. Stewart, W.W., *Functional Connections Between Cells As Revealed By Dye-Coupling With A Highly Fluorescent Naphthalimide Tracer*. Cell, 1978. **14**(3): p. 741-759.
132. Stewart, W.W., *Lucifer dyes--highly fluorescent dyes for biological tracing*. Nature, 1981. **292**(5818): p. 17-21.
133. Wilchek, M. and E.A. Bayer, *Introduction To Avidin-Biotin Technology*. Methods In Enzymology, 1990. **184**: p. 5-13.
134. Himmel, M.E., et al., *Biocatalyst design for stability and specificity*. ACS symposium series. 516. 1993, Washington, DC: American Chemical Society.
135. Chenna, R., et al., *Multiple sequence alignment with the Clustal series of programs*. Nucleic Acids Res, 2003. **31**(13): p. 3497-500.
136. Gasteiger E., H.C., Gattiker A., Duvaud S., Wilkins M.R., Appel R.D., Bairoch A., *Protein Identification and Analysis Tools on the ExPASy Server*, in *The Proteomics Protocols Handbook*, J.M. Walker, Editor. 2005, Humana Press.
137. Gasteiger, E., et al., *ExPASy: The proteomics server for in-depth protein knowledge and analysis*. Nucleic Acids Res, 2003. **31**(13): p. 3784-8.
138. Gronwald, R.G., et al., *Cloning and expression of a cDNA coding for the human platelet-derived growth factor receptor: evidence for more than one receptor class*. Proc Natl Acad Sci U S A, 1988. **85**(10): p. 3435-9.
139. Lu, D., et al., *Tailoring in vitro selection for a picomolar affinity human antibody directed against vascular endothelial growth factor receptor 2 for enhanced neutralizing activity*. Journal Of Biological Chemistry, 2003. **278**(44): p. 43496-43507.
140. Worn, A. and A. Pluckthun, *Stability engineering of antibody single-chain Fv fragments*. Journal Of Molecular Biology, 2001. **305**(5): p. 989-1010.
141. Ewert, S., A. Honegger, and A. Pluckthun, *Stability improvement of antibodies for extracellular and intracellular applications: CDR grafting to stable frameworks and structure-based framework engineering*. Methods, 2004. **34**(2): p. 184-199.

**APPENDIX A :**  
**THEORETICAL TREATMENT OF ENZYME KINETICS**



## A.1 RATE EQUATION FOR A SIMPLE ENZYME MECHANISM

The  $\beta$ -lactamase enzyme (E) follows single substrate enzyme kinetics, and a brief derivation of the Michaelis-Menten rate equation for this simple mechanism is necessary. The basic steady state model (Briggs-Haldane) for enzyme kinetics has the enzyme (E) and the substrate (S) in a fast equilibrium between the free species (E + S) and the non-covalent Henri-Michaelis complex (E.S). The complex (E.S) is irreversibly transformed into the covalent acyl-enzyme (ES). Catalytic turnover of the ES complex occurs in the rate determining step ( $k_3$ ). The kinetic model is represented in Figure 36.

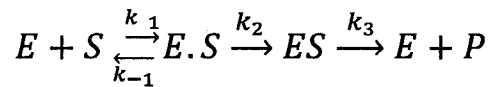


**Figure 36** Interaction between a serine  $\beta$ -lactamase (E) and a substrate (S)

The Michaelis-Menten kinetic model assumes that several conditions are met:

- Initial velocity conditions so  $[S] \approx [S]_0$ , with  $[S]_0$  the initial concentration of substrate
- No product present so  $k_3$  is effectively irreversible
- $[S] \gg [E]_0$ , with  $[E]_0$  the total concentration of enzyme, both bound and free
- No allosteric or cooperative effects
- The derivation of Michaelis Menten is performed by applying the steady-state approximation to both  $[E.S]$  and  $[ES]$  (i.e.  $d[E.S]/dt=0$  and  $d[ES]/dt=0$ ). Furthermore, the enzyme exists in solution as E, E.S, or ES, so that at any time, the total enzyme concentration is equal to the sum of these concentrations (Equation 1).

### Equation 1

$$[E]_0 = [E] + [E.S] + [ES]$$

The initial rate of formation of product can be obtained, as given in the following equation:

**Equation 2**

$$v_0 = k_3[ES] = \frac{[S][E]_0}{[S] \left( \frac{1}{k_3} + \frac{1}{k_2} \right) + \frac{(k_{-1} + k_2)}{k_1} \frac{1}{k_2}}$$

The following substitutions (Equation 3) can be made.

**Equation 3**

$$k_{cat} = \frac{k_2 k_3}{k_2 + k_3}, K' = \frac{k_{-1} + k_2}{k_1} \text{ and } K_m = \frac{K' \cdot k_3}{k_2 + k_3}$$

Finally, the maximum initial rate of reaction  $V_{max}$  can be described by the following expression (Equation 4) to yield the standard form of the Michaelis-Menten equation (Equation 5).

**Equation 4**

$$V_{max} = k_{cat}[E]_0$$

**Equation 5**

$$v_0 = \frac{V_{max}[S]}{[S] + K_m}$$

The constant  $K_m$  is the Michaelis constant and is equal to the substrate concentration at half the maximal velocity ( $V_{max}$ ) of the enzyme reaction.

$V_{max}$  is the maximal velocity for the enzyme reaction. The value of  $k_{cat}$  is commonly referred to as the turnover number, or the number of moles of product formed per unit time per mole of enzyme.

Michaelis-Menten parameters,  $K_m$  and  $k_{cat}$  can be experimentally determined using a best fit curve to a direct plot of the data  $v_0$  against  $[S]$  i.e. a direct non linear regression of the hyperbolic equation.

In the case of  $\beta$ -lactamase,  $k_{cat}$  corresponds to the deacylation rate, whereas the acylation is described by  $k_{cat}/K_m$ .

## A.2 IRREVERSIBLE INACTIVATION OF THE MUTANT $\beta$ -LACTAMASE

Irreversible inactivation of a mutant enzyme by a substrate can be represented schematically by the following model:

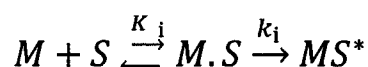


**Figure 37** Scheme of irreversible inactivation of a mutant enzyme (M) by a substrate (S).

The substrate (S) can reversibly bind to the free mutant enzyme (M) to form the non-covalent Henri-Michaelis complex (M.S), with the inhibition constant  $K_i$ . The complex (M.S) is irreversibly transformed into the inactivated covalent acyl-enzyme ( $MS^*$ ), the slower step, with the irreversible inactivation constant  $k_i$ . It is assumed that  $[S]$  is much greater than  $[M]$  and is therefore constant. The derivation of the rate equation describing the observed rate of inactivation is straightforward.

**Equation 6**

$$k_i^{obs} = k_i[M.S] = \frac{k_i[S]}{[S] + K_i}$$

The observed rate of inactivation,  $k_i^{obs}$ , is the first order rate constant obtained from a plot of the time-dependent inactivation of the mutant enzyme in the presence of the substrate.

A direct plot of  $k_i^{obs}$  against  $[S]$  should obey typical saturation kinetics and the values for  $k_i$  and  $K_i$  can be extracted from this curve.

In the case where the inactivated acyl-enzyme  $MS^*$  is unstable and can regenerate free enzyme, the scheme from Figure 37 becomes:

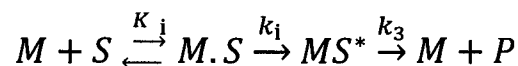


**Figure 38** Scheme of reversible inactivation of a mutant enzyme (M) with a substrate (S).

Equation 6 describing the observed rate of inactivation becomes:

**Equation 7**

$$k_i^{obs} = k_3 + \frac{k_i[S]}{[S] + K_i}$$

In the case of E166N  $\beta$ -lactamase, where  $k_3$  is small,  $k_3$  will be assimilated with the deacylation rate, while  $k_i/K_i$  corresponds to the second order rate of inactivation.

**APPENDIX B :**  
**PRIMERS FOR HEAVY AND LIGHT CHAIN**  
**AMPLIFICATION AND CLONING**

This appendix describes and lists the primers used for assembling mouse ScFv fragments in the orientation  $V_L$ -Linker- $V_H$  in the pBAD based vector.

The  $V_L$  DNA was obtained by PCR amplification using a set of primers annealing to the Leader Sequence described by Coloma *et al.* [112], LS-LB mix, and a set annealing to the light chain constant region, adapted from Krebber *et al.* [111], CLLF mix. In the following primers, the **bold** sequence corresponds to the ribosome binding sequence identified by Kozak. The underlined sequence corresponds to the introduced restriction site EcoR1 (LS-LB1-5).

	5'	3'	d	$\mu$ L mix
LS-LB1	<b>ggg</b> <u>gat</u> <b>atccacc</b> ATGGAGACAGACACACTCCTGCTAT		1	3
LS-LB2	<b>ggg</b> <u>gat</u> <b>atccacc</b> ATGGATTTTCAAGTGCAGATTTTCAG		1	3
LS-LB3	<b>ggg</b> <u>gat</u> <b>atccacc</b> ATGGAGWCACAKWCTCAGGTCTTTRTA		16	12
LS-LB4	<b>ggg</b> <u>gat</u> <b>atccacc</b> ATGKCCCCWRCTCAGYTYCTKGT		64	15
LS-LB5	<b>ggg</b> <u>gat</u> <b>atccacc</b> ATGAAGTTGCCTGTTAGGCTGTTG		1	3
LB- $\lambda$	gccatggcggactacaaaGATGCTGTTGTGACTCAGGAATC		1	1.8
CLLF1	ccagatccactggtcgagccaccACGTTTKATTTCCAGCTTGG		2	19
CLLF4	ccagatccactggtcgagccaccACGTTTTATTTCCAACCTTTG		1	9.5
CLLF5	ccagatccactggtcgagccaccACGTTTCAGCTCCAGCTTGG		1	9.5
CLLF $\lambda$	ccagatccactggtcgagccaccACCTAGGACAGTCAGTTTGG		1	2

The DNA was then reamplified with the same backward primer set, CLLF mix and a set of primers annealing to the Framework Region 1 (FR1) of the light chain, adapted from Krebber *et al.* [111], LB mix. The underlined sequence corresponds to the introduced restriction sites, Sfi1 (ScBack).

	5'	3'	d	μL mix
Seback	ttactcgcggcccagccggccatggcggactacaaaG			
LB1	gccatggcggactacaaaGAYATCCAGCTGACTCAGCC		2	2
LB2	gccatggcggactacaaaGAYATTGTTCTCWCCCAGTC		4	2
LB3	gccatggcggactacaaaGAYATTGTGMTMACTCAGTC		8	3
LB4	gccatggcggactacaaaGAYATTGTGYTRACACAGTC		8	3
LB5	gccatggcggactacaaaGAYATTGTRATGACMCAGTC		8	3
LB6	gccatggcggactacaaaGAYATTMAGATRAMCCAGTC		16	4
LB7	gccatggcggactacaaaGAYATTCAGATGAYDCAGTC		12	4
LB8	gccatggcggactacaaaGAYATYCAGATGACACAGAC		4	2
LB9	gccatggcggactacaaaGAYATTGTTCTCAWCCAGTC		4	2
LB10	gccatggcggactacaaaGAYATTGWGCTSACCCAATC		8	3
LB11	gccatggcggactacaaaGAYATTSTRATGACCCARTC		16	4
LB12	gccatggcggactacaaaGAYRTTKTGATGACCCARAC		16	4
LB13	gccatggcggactacaaaGAYATTGTGATGACBCAGKC		12	4
LB14	gccatggcggactacaaaGAYATTGTGATAACYCAGGA		4	2
LB15	gccatggcggactacaaaGAYATTGTGATGACCCAGWT		4	2
LB16	gccatggcggactacaaaGAYATTGTGATGACACAACC		2	2
LB17	gccatggcggactacaaaGAYATTTTGCTGACTCAGTC		2	2
LBλ	gccatggcggactacaaaGATGCTGTTGTGACTCAGGAATC		1	2.4

The V<sub>H</sub> DNA was made by PCR amplification with a set of primers annealing to the end of the heavy chain, Not-HF mix, and a set annealing to the heavy chain constant region, adapted from Krebber *et al.* [111], CLHB mix. The underlined sequence corresponds to the introduced restriction site, Not1 in Not-HF1-4.

	5'	3'	d	μL mix
CLHB1	caggagaaggtagcaca <u>aaaggggtcc</u> GAKGTRMAGCTTCAGGAGTC		8	3
CLHB2	caggagaaggtagcaca <u>aaaggggtcc</u> GAGGTBCAGCTBCAGCAGTC		9	3
CLHB3	caggagaaggtagcaca <u>aaaggggtcc</u> CAGGTGCAGCTGAAGSARTC		4	2
CLHB4	caggagaaggtagcaca <u>aaaggggtcc</u> GAGGTCCARCTGCAACARTC		4	2
CLHB5	caggagaaggtagcaca <u>aaaggggtcc</u> CAGGTYCAGCTBCAGCARTC		12	4
CLHB6	caggagaaggtagcaca <u>aaaggggtcc</u> CAGGTYCARCTGCAGCARTC		8	3
CLHB7	caggagaaggtagcaca <u>aaaggggtcc</u> CAGGTCCACGTGAAGCARTC		2	2
CLHB8	caggagaaggtagcaca <u>aaaggggtcc</u> GAGGTGAASSTGGTGGARTC		8	3
CLHB9	caggagaaggtagcaca <u>aaaggggtcc</u> GAVGTGAWGSTGGTGGAGTC		12	4
CLHB10	caggagaaggtagcaca <u>aaaggggtcc</u> GAGGTGCAGSTGGTGGARTC		4	2
CLHB11	caggagaaggtagcaca <u>aaaggggtcc</u> GAKGTGCAMCTGGTGGARTC		8	3
CLHB12	caggagaaggtagcaca <u>aaaggggtcc</u> GAGGTGAAGCTGATGGARTC		2	2
CLHB13	caggagaaggtagcaca <u>aaaggggtcc</u> GAGGTGCARCTTGTTGARTC		4	2
CLHB14	caggagaaggtagcaca <u>aaaggggtcc</u> GARGTRAAGCTTCTCGARTC		8	3
CLHB15	caggagaaggtagcaca <u>aaaggggtcc</u> GAAGTGAARSTTGAGGARTC		8	3
CLHB16	caggagaaggtagcaca <u>aaaggggtcc</u> CAGGTTACTCTRAAASARTC		8	3
CLHB17	caggagaaggtagcaca <u>aaaggggtcc</u> CAGGTCCAACVTCAGCARCC		6	3
CLHB18	caggagaaggtagcaca <u>aaaggggtcc</u> GATGTGAACTTGGAASARTC		4	2



CLHB19	caggagaaggtagcacaaggggtccGAGGTGAAGGTCATCGARTC	2	2
Not-HF1	gaattc <u>gcggccgc</u> CGAGGAAACGGTGACCGTGGT	1	2
Not-HF2	gaattc <u>gcggccgc</u> CGAGGAGACTGTGAGAGTGGT	1	2
Not-HF3	gaattc <u>gcggccgc</u> CGCAGAGACAGTGACCAGAGT	1	2
Not-HF4	gaattc <u>gcggccgc</u> CGAGGAGACGGTGACTGAGGT	1	2

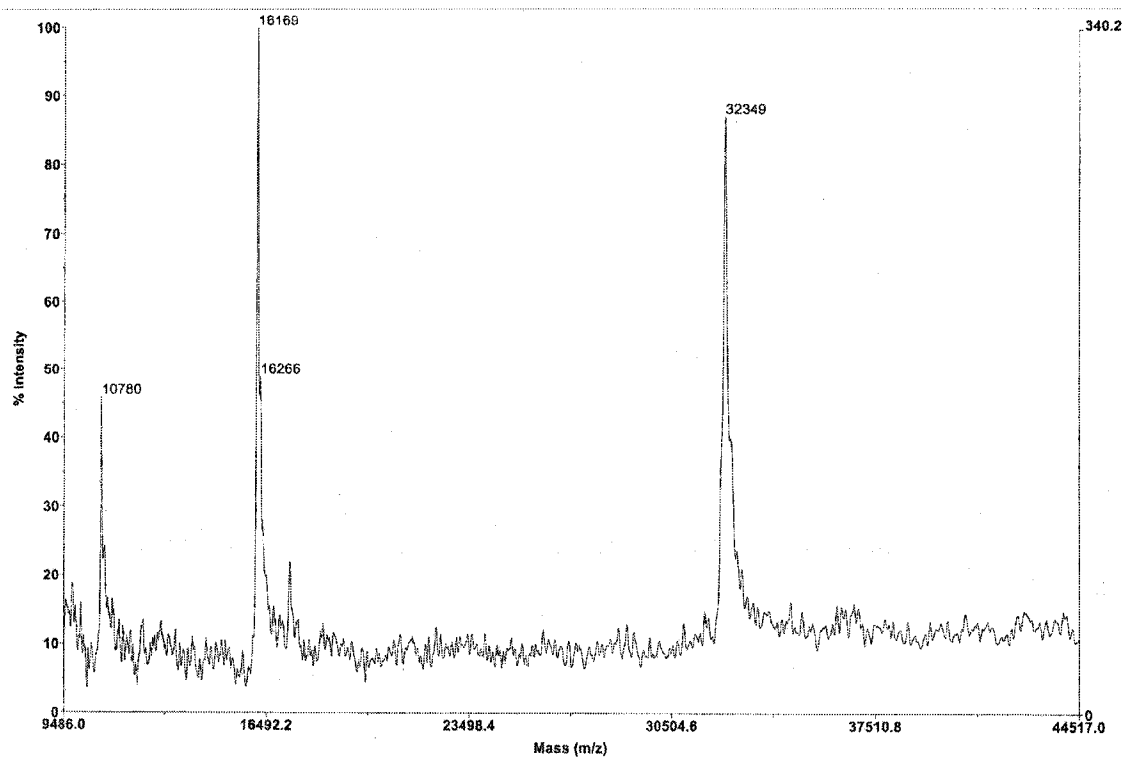
The necessary primers for PCR amplification of the  $V_L$  and  $V_H$  DNA and insertion in pBAD436 were LB-pBAD and LF-pBAD mixes for the light chain and HF-pBAD and HB-pBAD mixes for the heavy chain. The underlined sequences correspond to the introduced restriction sites: EcoR1 in HF4-pBAD, Pst1 in HB5/6/10-pBAD, Sac1 in LF1/5-pBAD and Xho1 in LB3/4-pBAD.

	5'	3'	d	$\mu$ L mix
LB3-pBAD	ttactcgcctc <u>gcgggactacaaa</u> GAYATTGTGMTMACTCAGTC		8	3
LB4-pBAD	ttactcgcctc <u>gcgggactacaaa</u> GAYATTGTGYTRACACAGTC		8	3
LF1-pBAD	gcgagtaactgagctccACGTTTKATTTCCAGCTTGG		2	1
LF5-pBAD	gcgagtaactgagctccACGTTTCAGCTCCAGCTTGG		1	1
HB5-pBAD	ttactcgcggccct <u>gcagag</u> CAGGTYCAGCTBCAGCARTC		12	4
HB6-pBAD	ttactcgcggccct <u>gcagag</u> CAGGTYCARCTGCAGCARTC		8	3
HB10-pBAD	ttactcgcggccct <u>gcagag</u> GAGGTGCAGSTGGTGGARTC		4	2
HF4-pBAD	gcgagtaaga <u>aattcgctta</u> CGAGGAGACGGTGACTGAGGT		1	1

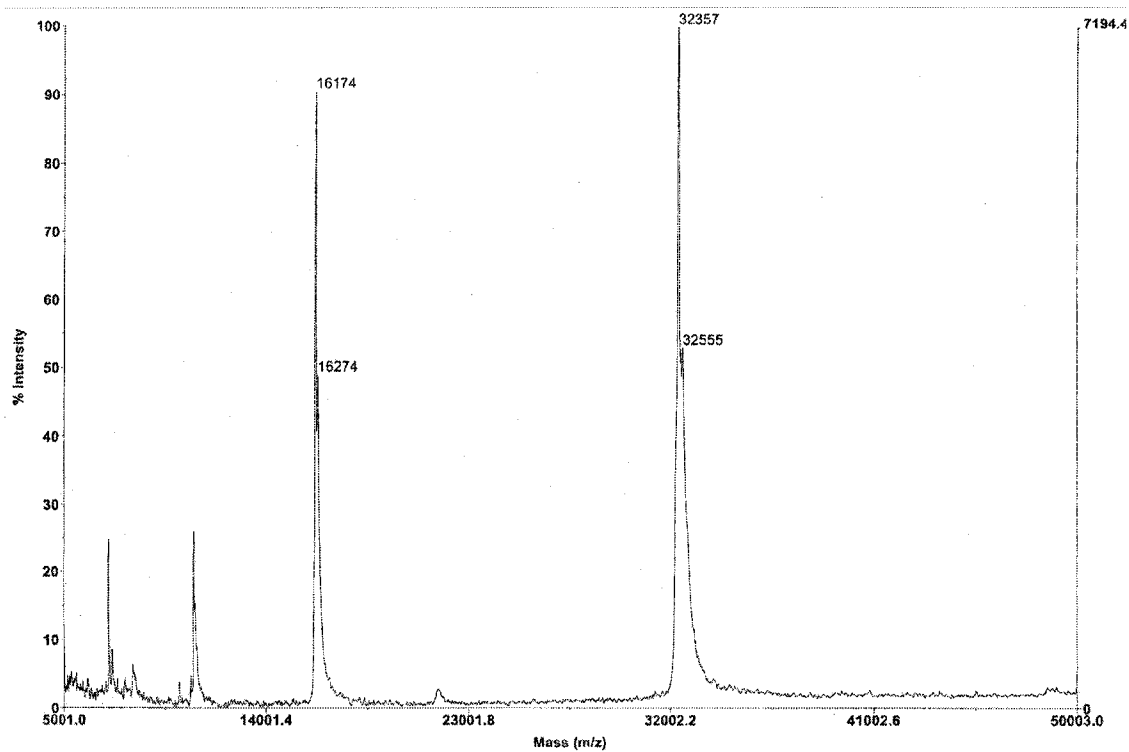
In the previous list of primers, the IUPAC nomenclature of mixed bases (R = A or G; Y = C or T; M = A or C; K = G or T; S = C or G; W = A or T; H = A or C or T; B = C or G or T; V = A or C or G; D = A or G or T) is used for all the sequences. The column “d” is listing the d-fold generation encoded in each primer. The column “ $\mu\text{L}$  mix” indicates the volume of each primer used in the mix. The CAPITALIZED sequences correspond to the parts annealing to the  $V_H$  or  $V_L$ .

**APPENDIX C :**  
**MALDI AND ESI MASS SPECTRA OF WT AND E166N**  
**BETA-LACTAMASE**

MALDI-TOF mass spectra of E166N  $\beta$ -lactamase in 50 mM potassium phosphate buffer



MALDI-TOF mass spectra of WT  $\beta$ -lactamase in 50 mM potassium phosphate buffer pH 7



ESI in positive ionisation mode mass spectra of WT  $\beta$ -lactamase in 50 mM ammonium acetate buffer pH7

